Università degli Studi di Milano

Department of Pharmacological and Biomolecular Sciences

PhD School of Biochemical Sciences

XXIX Cycle

The RNA binding protein Zc3h10 couples mitochondrial function and iron metabolism

Matteo Audano

Student ID: R10502

Tutor: Professor Nico Mitro

Coordinator: Professor Sandro Sonnino

A.A. 2015/2016

A mia moglie,

per avermi incoraggiato a concretizzare i miei sogni.

E ad esserne parte.

"Il sapere è come una sfera, più è grande,

più sarà vasta la superficie di contatto con l'ignoto"

Wolfgang Goethe

Summary

1. Introduction

1.1 Energy metabolism

Metabolism is the set of enzyme-driven reactions that sustain and maintain all living organisms. Metabolism is usually divided into two complementary subsets of reactions: anabolism and catabolism. The former comprehends those reactions that use ATP, coming from catabolism, and little units like amino acids, sugars and fatty acids to build macromolecules. On the other hand, catabolism is the set of those reactions necessary to gain ATP from the breakdown of macromolecules. ATP is obtained by the oxidation of energetic substrates and the subsequent reduction of nicotinamide adenine dinucleotide (NAD^+) and flavin adenine dinucleotide (FADH) cofactors. In eukaryotic cells, the breakdown of small energetic substrates takes place in three highly regulated metabolic pathways: glycolysis, β-oxidation, amino acid degradation and TCA cycle. Glycolysis is a ten-steps cytoplasmic pathway necessary for the conversion of glucose to pyruvate. The net yield of glycolytic reactions is two molecules of pyruvate, two ATP, two NADH and two H_2O from one molecule of glucose. In addition to ATP, glycolysis provides the intermediates necessary for the synthesis of other molecules as purines, pyrimidines and amino acids. Under aerobic conditions, the main fate of pyruvate is to be converted into acetyl-CoA and entry the tricarboxylic acid pathway (TCA cycle) in the mitochondria. The TCA cycle is a sequence of eight different reactions that yields three NADH, one GTP, one $FADH_2$, three H^+ and two CO_2 for each molecule of pyruvate. In addition, the cycle provides precursors of certain amino acids as well as the reducing agent NADH that is used in oxidoreductive biochemical reactions. Its central importance to many biochemical pathways suggests that TCA cycle was one of the earliest established components of cellular metabolism. The acetyl-CoA can also originate from the breakdown of fatty acids by β-oxidation. Even fatty acids with even-numbered chains of carbon atoms are shuttled into mitochondria and covalently bound to Coenzyme A, then β-oxidation repeatedly cleaves two carbons in form of acetyl-CoA that enters into the TCA cycle. All the reducing potential given by the oxidation of energetic substrates fuels the electrons transport chain, enabling the synthesis of ATP in the mitochondria by the oxidative phosphorylation (OXPHOS) (Fig 1.1).

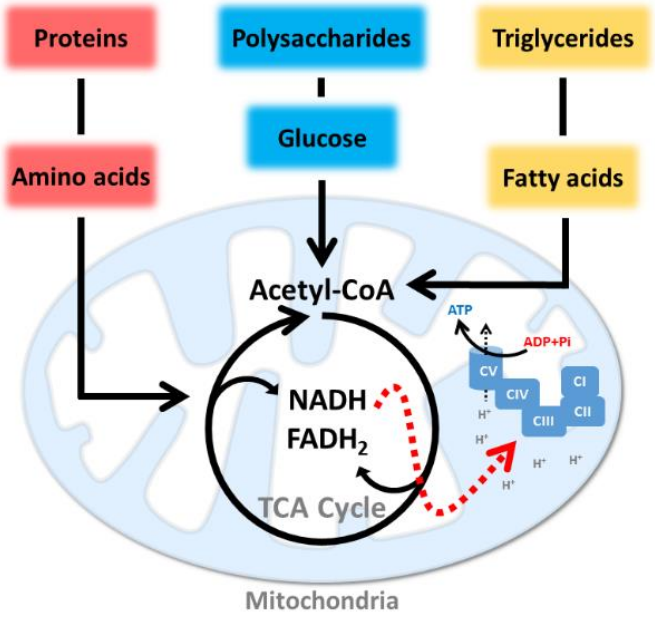

Fig. 1.1 General overview of catabolic reactions in energy metabolism. Macromolecules like proteins, polysaccharides and triglycerides are broken in smaller energetic substrates. Glucose and fatty acids are converted to acetyl-CoA while amino acids are used in the TCA cycle trough anaplerotic reactions. Reducing cofactors generated by glycolysis, β-oxidation and TCA cycle transfer electrons to the electron transport chain enabling the production of ATP from ADP and inorganic phosphate by oxidative phosphorylation.

1.2 Mitochondria

The ability to generate chemical energy inside the cell represent the evolutionary push that likely led eukaryotic organisms to be the dominant living systems. Nowadays, mitochondria are widely recognized as the crossroads of the eukaryotic cell evolution. Beyond the energy metabolism pathways described above, these incredibly sophisticated structures are the primary site of heme synthesis, iron sulfur clusters (ISCs) biosynthetic pathway, apoptosis, calcium homeostasis and many other cellular processes.

Originating from an α-protobacterion, mitochondria maintain many features of their ancient relatives as they possess their own genome (mtDNA) and a limited translation machinery. They vary from 1 to 10 μm of diameter and consist of an outer (OMM) and an inner (IMM) mitochondrial membrane. The OMM and the IMM define two different compartments: the intermembrane space, where the proton gradient necessary for the OXPHOS activity is generated, and the inner matrix, the site of the main mitochondrial reactions. The area of the IMM is greater than the OMM one due to the presence of specific invaginations, called cristae, that include the OXPHOS complexes and the ATP synthase. The mitochondrial aqueous compartments are separated from cytoplasm. For this reason, import and export of small

organic molecules and ions across IMM and OMM are controlled by specific transporters and carriers, whose activity is finely regulated by external cues like energy deprivation and stress (Harbauer et al., 2014; Qiu et al., 2013; Wenz et al., 2014)

1.2.1 Mitochondria dynamics

Mitochondria are organized in an intricate and extended network. Mitochondrial framework is shaped by continuous events of fusion and fission, orchestrated by different proteins located in the IMM and the OMM belonging to the GTPases superfamily. Mitofusin1 and 2 (Mfn1 and 2), Optic atrophy 1 (Opa1) are the main regulators of mitochondrial fusion events (Chen et al., 2005; Chen et al., 2003; Rahn et al., 2013). On the other hand, Dynamin-related protein 1 (Drp1) and Fission 1 (Fis1) are involved in mitochondrial fission (Chan, 2012; Friedman and Nunnari, 2014). Mitochondrial fusion and fission events not only merge the mitochondrial IMM and OMM but also mixes mitochondria matrices and redistributes mtDNA haplotypes among different organelles (D.C., 2010; Jourdain and Martinou, 2010).

Mitochondrial fusion and fission events rapidly respond to external cues. Energy demand increases mitochondrial fusion bringing to the formation of hyperfused and tubular mitochondria. In line with this, physical exercise, cold exposure and nutrient withdrawal increase mitochondrial fusion to maximize energy production and increase mitochondrial mass (Wai and Langer, 2016). On the contrary, mitochondrial fission is associated with mitochondrial degradation (a physiological process known as mitophagy) and quality control, cell division and apoptosis (Mao and Klionsky, 2013; Mitra, 2013; Youle and Karbowski, 2005). Recent findings suggest that mitochondria shape is finely regulated also during cell reprogramming and differentiation. Stem cells are proliferative, low-energy demanding cells that mostly live in hypoxic niches (Mohyeldin et al., 2010). In this regard, new data show that during cell reprogramming to iPS there is a shift toward a more glycolytic metabolism and rounded, cristae-poor mitochondria, while cell differentiation needs hyperfused, cristae-rich and tubular organelles to support oxidative metabolism and great energy demand (Wanet et al., 2015; Xu et al., 2013b; Zhang et al., 2016b). Furthermore, mitochondrial dynamics are regulated by the interaction with other cellular compartments like endoplasmic reticulum (ER), Golgi apparatus and cytoskeleton (Olga Martins de Brito, 2008; Reja et al., 2009; Yang et al., 2013). For instance, phosphorylated Drp1 is shuttled from the cytoplasm to the ER-mitochondria interaction points where it starts mitochondrial fission (Friedman et al., 2011) while mitochondria-cytoskeleton interactions are fundamental for mammalian cells cytokinesis and mitochondrial OXPHOS activity (Knowles et al., 2002; Kuznetsov et al., 2013).

1.2.2 Mitochondrial DNA

In addition to their shape and dynamicity, mitochondria inherited a little genome from their ancestors, the mtDNA (Fig. 1.2). Unlike nuclear DNA (nDNA), mtDNA copy number can largely vary between different cell types and different tissue. For instance, in highly metabolic tissues, as skeletal muscle, liver and adipose tissue, mtDNA can reach 10.000 copies per cell, whereas in other tissues the mitochondrial density is lower due to a little energy demand (Mootha et al., 2003a). mtDNA encodes for only 13 proteins, all belonging to the electron transport chain complexes, 2 rRNAs (mt-rRNA) and 22 tRNAs (mt-tRNA)(Kelly and Scarpulla, 2004). mtDNA is a 16.568 bp in humans, circular, double stranded genome, where the two strands show different percentage of guanine (G) and cytosine (C) (Patananan et al., 2016). Due to the different composition, the mtDNA strands are defined as heavy strand (HS, enriched in G) and light strand (LS, enriched in C). The components of the mtDNA replication and transcription machinery are completely encoded by the nDNA, as well as the greatest part of mitochondrial proteome. Among the others, the mitochondrial transcription factor A (Tfam) is one of the most important regulators of mitochondrial function, controlling mtDNA replication and transcription (Patti and Corvera, 2010). The mtDNA also contains a non-coding region, called D-loop, necessary for binding of Tfam and the regulation of mtDNA transcription and replication. In contrast to the limited coding capacity of mitochondria, the set of mitochondrial proteins encoded by the nuclear genome accounts for 1500 genes, as recently emerged from an extensive analysis of the mitochondrial proteome (Pagliarini et al., 2008). The great disparity between mitochondria-encoded proteins and the mitoproteome highlights the unquestionable relationship between mitochondria and nucleus. Nevertheless, at present, a comprehensive view of the signaling pathways operating between the two organelles is still incomplete.

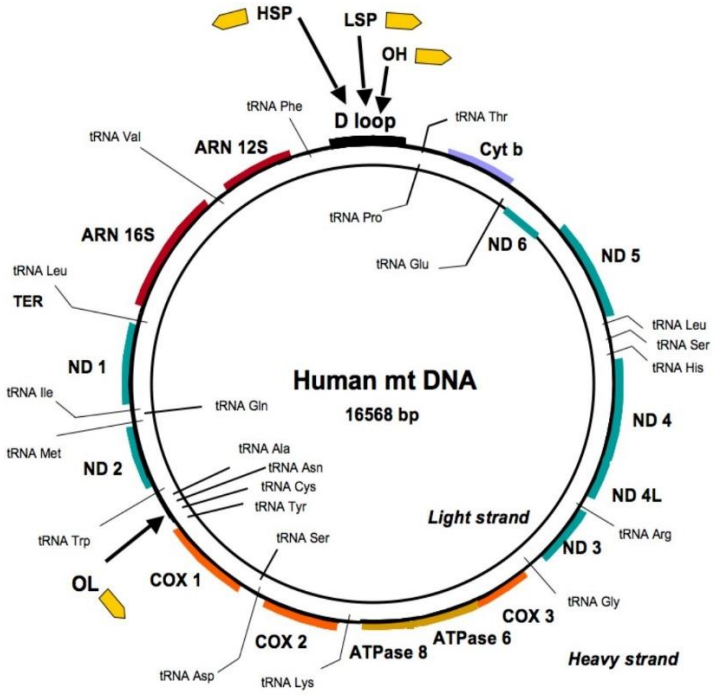

Fig. 1.2 Mitochondrial DNA (mtDNA) structure. Schematic representation of the human mitochondrial genome. Genomic organization and structural features of human mtDNA are depicted in a circular genomic map showing heavy (outer) and light (inner) strands. Protein coding and rRNA genes are interspersed with 22 tRNA genes. The D-loop regulatory region contains the L- and H-strand promoters (LSP, HSP1, and HSP2), along with the origin of H-strand replication (OH). On contrast, the origin of L-strand replication (OL) is displaced by approximately two-thirds of the genome. Protein coding genes include the following: cytochrome oxidase (COX) subunits 1, 2, and 3; NADH dehydrogenase (ND) subunits 1, 2, 3, 4, 4L, 5, and 6; ATP synthase subunits 6 and 8 (ATPase 6 and 8); cytochrome b (Cyt b). ND6 and the 8 tRNA genes transcribed from the L-strand as template are labeled on the inside of the genomic map, whereas the remaining protein coding and RNA genes transcribed from the H-strand as template are labeled on the outside (Themitoblog.wordpress.com/tag/dna/).

MtDNA integrity is maintained primarily by the mtDNA replication machinery. In fact, the mitochondria specific DNA polymerase PolG and Twinkle helicase possess exonuclease activity as well, and continuously proof-reads the mtDNA strand that is replicated (Kaguni, 2004). MtDNA mutations play a central role in stem cell commitment and differentiation. The non-random segregation of mitochondria in stem cells has been observed in a recent research where mitochondria were shown to segregate asymmetrically in human stem-like cells during asymmetric cell division (Katajisto et al., 2015). The daughter cells that received mostly young mitochondria maintained stem cell mitochondrial pool, while those cells that retained most of the aged mitochondria were committed to differentiation. Further, when asymmetric segregation of mitochondria was inhibited by blocking Drp1 activity, the progeny lost its stem cell features suggesting that this asymmetric segregation of mitochondria is required to maintain stemness

(Katajisto et al., 2015). In contrast, excessive mtDNA mutations compromise cell differentiation blocking mtDNA replication and the following mitochondrial mass growth (Dickinson et al., 2013; Wang et al., 2011). In line with this, recent results also demonstrated that mitochondrial fusion safeguards mtDNA health, preserving mtDNA copy number and blunting mtDNA mutation rate in skeletal muscle and brain (Amati-Bonneau et al., 2007; Chen et al., 2010).

1.2.3 Regulation of mitochondrial function at the transcriptional level

Many nuclear encoded factors are involved in mtDNA expression and maintenance, sustaining the tight crosstalk between the nucleus and the mitochondria. Thanks to new experimental approaches and the increasing number of mouse models, the regulation of mtDNA replication and transcription is now largely described. The expression of Tfam is mainly regulated by Pgc-1α (Bonawitz et al., 2006; Patti and Corvera, 2010; Wu et al., 1999), which interacts with and co-activates among the others the transcription factor nuclear respiratory factor 1 (Nrf1). It is worthwhile to mention that Pgc-1α controls the expression of many other mitochondrial genes through different transcription factors and nuclear receptors such as Nrf2, Pparα, and the estrogen related receptor α (Errα) (Scarpulla et al., 2012). Pgc-1α is highly sensitive to environmental conditions, representing one of the most outstanding links between external cues and nuclear transcription. Pgc-1α expression is deeply influenced by cold, physical exercise and cell energy status (Akimoto et al., 2005; Handschin et al., 2007; Oliveira et al., 2004). In addition, its activity is deeply affected by post-transcriptional modifications such as phosphorylation by AMP-activated protein kinase (Jager et al., 2007), acetylation by Sirt1 (Lagouge et al., 2006), or direct interaction with other proteins such as the mammalian target of rapamycin (mTOR) or the transcriptional repressor Yy1 (Yin Yang-1) (Blättler et al., 2012; Cunningham et al., 2007).

nDNA transcription and replication are two distinct processes controlled by different machineries. In contrast, mtDNA transcription and replication are intimately dependent on each other and are carried out basically by the same large protein complex. The activity of the mitochondrial transcription complex is initiated by three transcription factors: Tfam, transcription factor B1 mitochondrial (Tfb1m) and transcription factor 2B mitochondrial (Tfb2m). Their presence is necessary to activate the bacteriophage-related mitochondrial RNA polymerase (Polrmt) on heavy strand promoter (HSP) and the light strand promoter (LSP) in the D-loop, the only untranscribed region of mtDNA (Yakubovskaya et al., 2014). In this way, the transcription complex starts its activity along the HS and LS in a bidirectional way (Bonawitz et al., 2006). In addition to the transcription initiation complex, mtDNA need other factors as the Twinkle helicase, the mitochondrial DNA polymerase Polg and the single stranded DNA binding protein,

mitochondrial Ssbp1, which together constitute the mtDNA replication machinery (Bonawitz et al., 2006; Milenkovic et al., 2013; Rajala et al., 2014; Shutt et al., 2011).

Tfam is the main mediator of a great variety of molecular cues directed to mitochondria (Kang et al., 2007). Tfam is a highly conserved protein with a molecular weight of about of 25 kDa and its ability to bind DNA is due to the presence of two distinct high mobility group (HMG) boxes (Kanki et al., 2004). The essential role of Tfam is demonstrated by the fact that its ubiquitous deletion in mouse brings to complete impairment of embryonic mitochondrial content and subsequent death at E10.5 (Silva et al., 2000). Recent findings indicate that Tfam control of mtDNA transcription and replication is not given just by its ability to coat the HSP and LSP. In fact, Tfam is the main component of mitochondrial nucleoprotein complexes called nucleoids, bound to the IMM in which it seems to have a histone-like function in mtDNA packaging and spatial organization (Bogenhagen, 2012; Kukat and Larsson, 2013). In line with this, Tfam:mtDNA ratios represent another important regulatory mechanism of mtDNA replication and transcription, as well as Tfam dimerization degree and the number of Tfam molecules bound to the HSP and LSP. Specifically, in a monomeric form, Tfam binds LSP within the D-loop thus allowing transcription of a short sequence that acts as a primer for HS replication. However, when dimer/monomer ratio increases, HS transcription starts while its replication halts. mtDNA transcription is interrupted when the Tfam:mtDNA ratio is very high (Fig. 1.3). Thus, mtDNA transcription and replication are finely tuned by the levels of Tfam, its degree of dimerization, and by the Tfam:mtDNA ratio. Furthermore, Tfam is able to bind mtDNA also at aspecific sites outside the D-loop. In this way, the random dimerization between Tfam molecules associated at distal position causes packaging of mtDNA and blocks the assembling of the transcription initiation complex (Ngo et al., 2014). These models were recently verified experimentally in in vitro reconstituted nucleoids (Farge et al., 2014).

Given its essential role in governing mtDNA transcription and replication, Tfam accessibility to mtDNA is tightly monitored. To this end, degradation of unnecessary and/or misfolded proteins is guaranteed by a quality control machinery containing typical proteases (Matsushima and Kaguni, 2012). Specifically, mitochondrial levels of Tfam are regulated by the AAA+ Lon protease (LonP) in a phosphorylation-dependent manner (Lu et al., 2013).

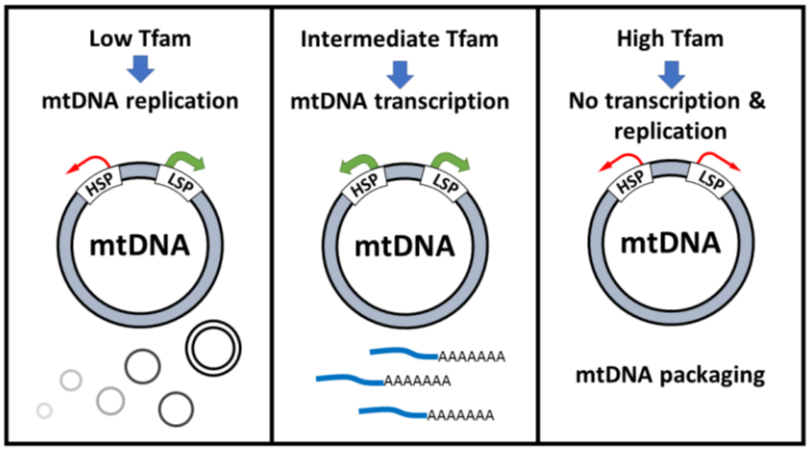

Fig. 1.3 Tfam levels modulate mtDNA replication and transcription. At low concentration levels, Tfam binds to the LSP, predominantly in monomeric form, and promotes mtDNA replication (left panel). Increased expression and/or stability of Tfam protein leads to its dimerization, a condition that facilitates mtDNA transcription (middle panel). Very high levels of Tfam lead to its binding at many aspecific sites along the mtDNA; this event causes higher compaction of the mitochondrial genome and turns off of its replication/transcription (right panel) (Audano et al., 2014).

1.2.4 Oxidative phosphorylation

The oxidative phosphorylation is made up by five large complexes (complexes I to V) with 90 individual genes products. The first four complexes represent the electron transport chain (ETC) whose activity is usually coupled to the ATP synthase or complex V. The proteins that constitute the different complexes are encoded from both nuclear and mitochondrial DNAs, exception for the complex II that is completely nuclear encoded. In Table 1 the number of subunits for each complex that are nucleus or mitochondria encoded are reported (Scarpulla, 2008b).

	Complex I	**Complex II**	**Complex III**	**Complex IV**	**Complex V**
mtDNA	*7*	*0*	*1*	*3*	*2*
nDNA	*39*	*4*	*10*	*10*	*14*

Table 1 Number of genes belonging to oxidative phosphorylation and their encoding genome.

The ETC transfers electrons from donors (NADH at complex I, $FADH_2$ at complex II) to a final acceptor, molecular oxygen, forming H_2O at complex IV. Two electrons (reducing equivalents from hydrogen) are transferred from NADH + H^+ to the OXPHOS complex NADH dehydrogenase (complex I) or from $FADH_2$ to the succinate dehydrogenase (SDH, complex II) to reduce ubiquinone (coenzyme Q10, CoQ) into ubiquinol $CoQH_2$. The electrons from CoQH2 are transferred successively to complex III (bc1 complex), cytochrome c and complex IV

(cytochrome c oxidase, COX), and finally to oxygen ($1⁄2O_2$) to give H_2O. The energy that is freed during the electrons' flow is used to pump protons out through complexes I, III, and IV creating a proton electrochemical gradient across the mitochondrial inner membrane. The energy contained in the proton electrochemical gradient generated by the ETC is then coupled to ATP production as protons flow back into the matrix through the mitochondrial ATPase (Fig. 1.4). Matrix ATP is then exchanged for cytosolic ADP by the inner membrane adenine nucleotide translocators. The high electronegative potential produced by the proton gradient also forces the rapid entry of Ca^{2+} into the mitochondrial matrix, protecting its concentration in the cytoplasm. In the mitochondrial matrix, Ca^{2+} can stimulate flux through the TCA cycle by rising dehydrogenase activities (Rimessi et al., 2008). The exit of Ca^{2+} from the matrix is driven by electroneutral exchange with Na^+ or H^+. The efficiency by which dietary reducing equivalents are converted to ATP by OXPHOS is known as the coupling efficiency (D.C., 2010). This is determined by the efficiency by which protons are pumped out of the matrix by complexes I, III, and IV and the efficiency by which proton flux through complex V is converted to ATP (D.C., 2010). The uncoupler compounds like 2,4-dinitrophenol (DNP) or carbonyl cyanide chlorophenylhydrazone (CCCP) and the nDNA-encoded UCP1, 2 and 3 render the mitochondrial inner membrane leaky for protons, by-passing complex V and dissipating the electrochemical energy potential as heat (Busiello et al., 2015).

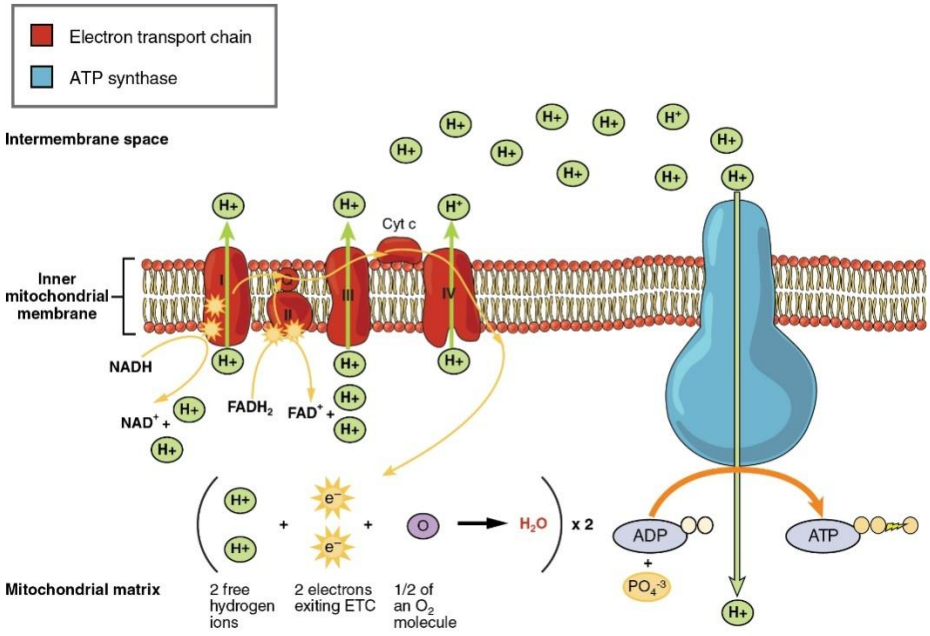

Fig. 1.4 Mammalian oxidative phosphorylation (OXPHOS) system. Depicted are the four respiratory complexes (I–IV), electron carriers coenzyme Q and cytochrome c and the ATP synthase complex. Arrows at complexes I, III, and IV

illustrate the proton pumping to the intermembrane space (www.boundless.com/biology/textbooks/boundless-biology-textbook/cellular-respiration-7/oxidative-phosphorylation-76/electron-transport-chain-362-11588/).

Electron transport chain complexes are usually represented in textbooks as independent entities that randomly flow in the IMM. Despite this common assumption, recent studies indicate that ETC is made up by quaternary structures named supercomplexes (RSC), in which complex I interacts with complex III and complex III binds to complex IV (Lapuente-Brun et al., 2013). Supercomplexes facilitate electron transfer through the ETC, reduce reactive oxygen species (ROS) formation from CI and make the system more responsive to metabolic cues (Genova and Lenaz, 2013). For instance, mitochondrial reprogramming during differentiation is characterized by supermolecular organization of CIV and by increased supercomplexes formation (Chen et al., 2008; Hofmann et al., 2012). In this context, RSC establishment is also dependent on mitochondrial cristae shape regulated by Opa1 activity, corroborating the idea that mitochondrial shape and morphology deeply impact ETC activity and efficiency (Cogliati et al., 2013).

1.2.5 Mitochondria and iron metabolism

Iron metabolism is a set of reactions that control iron homeostasis at both systemic and cellular level. This metal is fundamental in both eukaryotic and bacterial cells since is required for the synthesis of iron-sulfur (Fe-S) clusters and heme prosthetic groups, both synthesized in mitochondria, participating to a large number of intracellular redox reactions (Rouault and Tong, 2005).

Systemic iron levels are mainly controlled by its absorption by enterocytes in the intestine, the spleen recycling rate of macrophages and its turnover in the liver. Iron fluxes through different organs and tissues are mainly regulated by hepcidin and the only characterized iron exporter ferroportin. Hepcidin is a hormone released by the liver that acts as negative regulator of ferroportin mediated iron absorption in gut and spleen (Ganz, 2013). On the other hand, cellular iron levels are controlled mainly by the presence of specific iron regulatory proteins and transporters (Ganz, 2013; Wang and Pantopoulos, 2011). The major amount of iron found in human diet, in form of ferritin, heme group and ferric ion, is absorbed by enterocytes by the divalent metal-ion transporter 1 (Dmt1/ Solute Carrier Family 11 Member 2, Slc11a2) and by a still unknown heme transporter. Inside the enterocyte, iron can be stocked in the cytoplasm bound to ferritin or can be exported into the bloodstream and transported by transferrin (Tf) that, thanks to its interaction with transferrin receptor 1 (TfR1), delivers iron to peripheral tissues (Wang and Pantopoulos, 2011). In erythrocytes, iron is internalized after TfR1 endocytosis, reduced by the ferric iron reductase Steap3 and directly transferred to mitochondria by Dmt1 in a

"kiss and run" fashion (Richardson et al., 2010). In other peripheral tissues (i.e. skeletal muscle, liver and macrophages), the widely accepted hypothesis is that ferrous iron is imported into mitochondria after creating a labile pool in the cytoplasm (Richardson et al., 2010).

Mitochondrial iron import is carried out by specific transporters at the IMM that are differentially expressed in many cell types. For instance, erythrocytes mainly express Slc25a37 (mitoferrin 1), while mitoferrin 2 is ubiquitously expressed (Chen et al., 2009; Paradkar et al., 2008). Recent results also suggest that mitochondrial iron import in mammalian cells could be regulated directly by Dmt1, that unlikely to Slc25a37 is localized on the OMM (Wolff et al., 2014).However, the role of mitochondrial Dmt1 needs to be fully understood.

Once in mitochondria, iron can be used to synthesize heme groups and iron sulfur clusters (ISC) proteins. All organisms start to synthesize the tetrapyrrol porphyrin ring of heme groups from 5-aminolevulinic acid (ALA) (Barupala et al., 2016; Severance and Hamza, 2009). Most eukaryotes synthesize ALA in mitochondria by condensing succinyl-CoA and glycine by ALA synthase (Alas) activity. Mammals express a housekeeping (Alas1) and an erythroid-specific (Alas2) isoform of this enzyme. Finally, after several reactions, ferrochelatase inserts Fe^{2+} into protoporphyrin IX. Newly synthesized heme is then exported from mitochondria to the cytosol for incorporation into hemeproteins (Barupala et al., 2016).

The assembly and repair of ISCs is mediated by a complex pathway (Fig 1.5). The cysteine desulfurase nitrogen fixation homologue 1 (Nfs1), by interacting with desulfurase-interacting protein 11 (Isd11), generates elemental sulfur, while the iron-binding protein frataxin (Fxn) acts as ferrous iron donor (Sheftel et al., 2010). The mitochondrial proteins Isu1/2 (also known as Iscu) and Isa1/2 (also known as Isca1/2) provide a scaffold for the first steps of ISCs biosynthesis. The mitochondrial proteins Grxl5 and the transporter Abcb7 participate to ISCs biogenesis, even if in a still unknown manner. The biogenesis of cytosolic ISC proteins requires mitochondria-derived ISC precursors, which are processed by a dedicated cytosolic ISCs assembly (CIA) machinery (Paul and Lill, 2015).

Iron sulfur cluster proteins take part to fundamental processes in all organisms as they allow the proper function of mitochondrial ETC and TCA cycle but also nDNA replication, repair and mRNA translation (Khoshnevis et al., 2010; Sheftel et al., 2010; Veatch et al., 2009). In this context, recent evidences show that iron is a necessary component of cell cycle regulation and stem cell biology, rising new interest on its role in cancer stem cell (CSC) proliferation and cell development. Iron exposure increases cell proliferation, migration and invasiveness of glioblastoma cell lines (Chanvorachote and Luanpitpong, 2016; Schonberg et al., 2015), while other studies indicate that iron is necessary for proper mitochondrial development during adipogenesis, supporting the possibility that mitochondria can function as cell cycle clock

controlling iron homeostasis and ISCs biogenesis (Moreno-Navarrete et al., 2014; Moreno et al., 2015). New data suggest that skeletal muscle of obese subjects are characterized by iron overload (Moreno-Navarrete et al., 2016), as well as skeletal muscle atrophy and muscular strength loss in humans, suggesting an iron-dependent regulatory circuit for skeletal muscle regeneration and development in adulthood (Mochel et al., 2008; Reardon and Allen, 2009). Moreover, iron overload has been associated with metabolic disorders, as type 2 diabetes (T2D) (Rajpathak et al., 2008), global mitochondrial dysfunctions (Cameron et al., 2011; Navarro-Sastre et al., 2011) and neurodegenerative disorders as amyotrophic lateral sclerosis (ALS) (Faes and Callewaert, 2011; Hartig et al., 2011; Zhou et al., 2001). However, despite the great amount of data available in literature from decades, the molecular mechanism that controls iron homeostasis still need to be fully understood. Complete understanding of the relationship between metals and mitochondria through new methodologies and approaches will improve our knowledge about mitochondria biology and will give us more chances to identify and tackle iron-related pathologies.

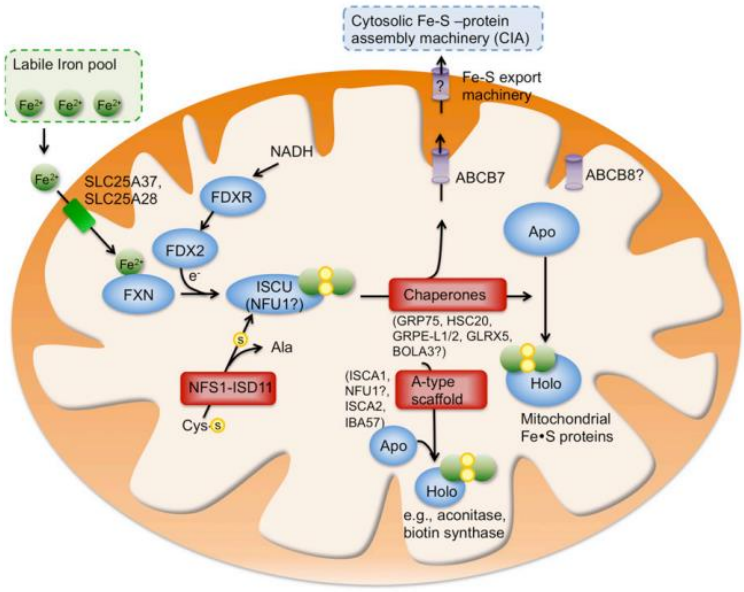

Fig. 1.5 Iron sulfur cluster biosynthetic pathway. ISCs are synthesized in the mitochondria where ferrous iron (Fe^{2+}) is imported by mitoferrin 1 and 2 (Slc25a37 and Slc25a28) in a potential-dependent manner, with the proton motive force (PMF) as a source of energy. The first step of ISC synthesis is the removal of sulfur from cysteine, while iron is internalized in the iron sulfur clusters thanks to the activity of frataxin, ferrodoxin reductase (Fdxr), ferrodoxin (Fdx2) and the scaffold protein Iscu. Finally, apoproteins (the recipient proteins) are converted to holoproteins by different chaperones as the ATP-dependent Hsp70 chaperone (Grp75), the DnaJ-like co-chaperone (Hsc20), the nucleotide exchange factor 1 (GrpE-L1/2) and the monothiol glutaredoxin 5 (Glrx5). Proteins of the aconitase family and radical

SAM proteins, as biotin synthase,specifically need Isca1, Isca2 and Iba57 for the complete maturation of their ISCs. Assembly of respiratory complex I also requires the P-loop NTPase Nubpl (Xu et al., 2013a).

Nowadays, one of the most characterized mechanism that control iron homeostasis is the regulation of mRNA stability of transcripts involved in iron metabolism and utilization, also referred to as IRP/IRE regulatory network. Iron responsive element (IRE) is a specific motif found in the 5'UTR or 3'UTR of iron related genes as FTH1, FTL, TFRC, ALAS2, Sdhb, ACO2, Hao1, SLC11A2 (encoding DMT1), NDUFS1, SLC40A1 (encoding the ferroportin), CDC42BPA, CDC14A and EPAS1. In low iron condition, 5'UTR IRE is bound by ACO1 and ACO1 in low iron concentration and reduce translation rate of these gene. On the contrary, iron overload leads to the upregulation of 3' UTR IRE genes stability and translation.

1.2.6 Mitochondrial diseases

In the last 20 years, mitochondrial dysfunction has been recognized as an important promoter of human pathologies. Mitochondrial defects play a direct role in certain well-defined neuromuscular diseases and are also thought to contribute indirectly to many degenerative diseases (Scarpulla, 2008a). Mutations in mitochondrial genes for respiratory proteins and translational RNAs, particularly tRNAs, appear in a wide range of clinical conditions, most of which affect the neuromuscular system (DiMauro et al., 2006; Schon et al., 2012; Wallace, 2005). MtDNA mutations are maternally inherited, while a subset of mitochondrial diseases exhibits a Mendelian inheritance pattern, typical of nuclear gene defects (Suomalainen and Isohanni, 2010). Furthermore, dispersed and somatic lesions in mtDNA or, more generally, mitochondrial dysfunctions can accumulate over time and may be involved in a causative fashion in human pathologies, including neurodegenerative diseases and metabolic disorders like type I and type II diabetes (Dufour and Larsson, 2004; Lowell and Shulman, 2005; Ramadasan-Nair et al., 2013).

1.2.7 MtDNA-related diseases

- ***Leber's hereditary optic neuropathy (LHON).***

LHON is the most common mitochondrial DNA (mtDNA)-related disorder, causing subacute loss of central vision predominantly in young men. LHON is usually due to homoplasmic mutations in one of three genes encoding complex I subunits (ND4, ND1 and ND6) (Edward J. Novotny et al., 1986; Holt et al., 1990).

- ***Leigh's syndrome.***

This disease is more commonly due to nuclear DNA (nDNA) mutations than to mtDNA mutations (Lake et al., 2015). The mutations are most frequently in subunits of complex I or in assembly factors of complex IV. Despite the striking variety of specific etiologies, Leigh's syndrome has common clinical features (developmental delay or regression, respiratory abnormalities, recurrent vomiting, nystagmus, ataxia, dystonia and early death).

- ***Mitochondrial encephalomyopathy, lactic acidosis and stroke-like episodes (MELAS).***

This is a multisystem disorder in which brain, muscle and the endocrine system are predominantly involved and is often fatal already in childhood (Kaufmann et al., 2011). Unique to MELAS are the transient stroke-like episodes, which are most often due to infarcts in the temporal and occipital lobes and are associated with hemiplegia and cortical blindness. Although we still do not understand the cause, their occurrence highlights the fact that MELAS is also an angiopathy, making it almost unique among the mitochondrial diseases (Tay et al., 2006). Although the most common causal mutation is m.3243A→G in tRNALeu (UUR), more than a dozen other mutations have been associated with MELAS, affecting both tRNA and protein-coding genes.

- ***Myoclonus epilepsy and ragged red fibers (MERRF).***

For unknown reasons, MERRF is due almost exclusively to mutations in tRNALys. It is associated with a rather different set of signs and symptoms from the other diseases, often including cervical lipomas as well as myoclonus and epilepsy (Chong et al., 2003). As in MELAS, the pathogenic cause seems to be a post-transcriptional failure to modify the tRNAs with taurine, thereby affecting translational efficiency (Suzuki and Nagao, 2011). Moreover, in MERRF and MELAS, there is mitochondrial proliferation not only in muscle (that is, the ragged red fibers (RRFs)) but also in blood vessels (strongly SDH-positive vessels (SSVs)) (Hasegawa et al., 1993).

- ***Neuropathy, ataxia and retinitis pigmentosa, and maternally inherited Leigh's syndrome (NARP and MILS, respectively).***

These are two possible clinical outcomes of mutations at the same nucleotide (m.8993T→G or, less frequently, m.8993T→C) (Duno et al., 2012). In the family in which these were originally identified, three adults had one or more of the acronymic features, whereas a maternally related child had severe developmental delay, pyramidal signs, retinitis pigmentosa, ataxia and cerebellar and brainstem atrophy, features that are characteristic of Leigh's syndrome.

- ***Reversible respiratory chain deficiency.***

Although it is rare, mutation in another tRNA — a homoplasmic m.14674T→C mutation causes a highly unusual disorder, namely a 'reversible' form of OXPHOS deficiency in which infants are severely ill but, if sustained vigorously during the perinatal period, recover full mitochondrial function spontaneously within 2 years (Horvath et al., 2009).

- ***Random deletions of mtDNA.***

Kearns–Sayre syndrome (KSS) is defined by the onset before age 20 of ophthalmoplegia (paralysis of the muscles that move the eyeballs), ptosis (droopy eyelids), pigmentary retinopathy and at least one of the following: complete heart block, cerebrospinal fluid protein levels above 100 mg dL^{-1} and cerebellar ataxia. In this multi-systemic disorder, partially deleted mtDNAs (Δ-mtDNAs) are present in all examined tissues (implying that the deletion event occurred in the germ line or soon after fertilization). In chronic progressive external ophthalmoplegia (CPEO) (Moraes et al., 1989) – a peculiar form of myopathy with the defining features of ophthalmoplegia and ptosis - Δ-mtDNAs are found only in muscle (implying that the deletion event occurred after fertilization in the muscle lineage of mesoderm). In Pearson's syndrome (Pearson et al., 1979), which is characterized by sideroblastic anemia and exocrine pancreas dysfunction, Δ-mtDNAs are initially abundant in hematopoietic cells. Patients with Pearson's syndrome who survive their anemia often develop KSS as teenagers: as the Δ-mtDNA load declines in blood (a rapidly dividing tissue), the Δ-mtDNA load increases in more terminally differentiated tissues (for example, in the muscles or brain). This phenomenon demonstrates two other features of mitochondrial genetics: first, the different thresholds for dysfunction in different tissues and the autonomy of mitochondrial division (and mtDNA replication), even in completely differentiated cells.

1.2.8 Mendelian hereditary mitochondrial diseases

Mendelian mitochondrial diseases are due to mutations of several mitochondrial genes that are encoded by nuclear DNA. These alterations are typically divided into two subclasses of pathologies: first, mutations that affect electron transport chain genes, and second, alteration of nuclear genes indirectly associated to OXPHOS (i.e. iron metabolism and mitochondria dynamics).

- ***Structural components of the respiratory chain.***

Complex I (Leigh's syndrome, Leukodystrophy, myoclonus).

Complex II (Leigh's Syndrome, Hereditary Paragangliomas).

Synthesis of coenzyme Q (Ataxia, myoglobinuria, seizures).

- ***Factors controlling OXPHOS or mtDNA metabolism.***

SURF1 (Leigh's Syndrome).
SCO1 (infantile encephalomyopathy).
SCO2 (infantile cardiomyopathy).
COX10 (infantile encephalomyopathy).
COX15 (cardiomyopathy).
DGUOK (mitochondrial DNA-depletion syndrome, hepatocerebral form).
TK2 (mitochondrial DNA-depletion syndrome, myopathy).
POLG1 (progressive external ophthalmoplegia, Alpes syndrome).
BCSI disorder (infantile encephalomyopathy, tubulopathy, hepatopathy).
Twinkle helicase.
Thymidine Phosphorylase (Mitochondrial Neuro-Gastro-Intestinal Encephalomyopathy, MNGIE).

- ***Factors indirectly correlated to OXPHOS.***

OPA1 (dominant optic atrophy)
Frataxin (Freidreich's Ataxia)
Paraplegin (hereditary spastic paraplegia)
Tim 8/9 transporters (X-linked deafness-dystonia syndrome)

1.2.8 Mitochondrial dysfunction related pathologies

- ***Neurodegenerative disorders.***

1. Parkinson's disease (PD).

PD is the most common movement disorder and is characterized primarily by the loss of dopaminergic neurons in the substantia nigra pars compacta leading to a dopamine deficit in the striatum. The consequent dysregulation of basal ganglia circuitries explains the most prominent motor symptoms, including rigidity, resting tremor and postural instability. Little is known about the etiopathogenesis of PD. Accumulating evidence suggests that PD-associated genes directly or indirectly affect mitochondrial integrity, for example the MTPT compound (1-methyl-4-phenyl-1,2,3,6-tetrahydropyridine), an ETC complex I inhibitor, was found to induce Parkinson in humans (Davis et al., 1979; Langston et al., 1999). The most common sporadic form of PD seems to be an intricate multifactorial disorder with variable influences by environmental cues and genetic susceptibility. A major breakthrough in PD research was the identification of genes that are responsible for monogenic familial forms. Mutations in the genes encoding α-synuclein

and leucine rich repeat kinase 2 (LRRK2) are accountable for autosomal dominant forms of PD, apparently by a gain-of-function process. Increased α-synuclein expression as well as α-synuclein deficiency may be associated with mitochondrial irregularities like ultrastructural abnormalities, impaired complex IV activity, reduced complex I/III activity and oxidation of mitochondria-associated metabolic proteins (Parihar et al., 2009; Song et al., 2004; Tabrizi et al., 2000).

Loss-of-function mutations in the genes encoding parkin and PINK1 mediate autosomal recessive PD. Sporadic and monogenic forms share important clinical, pathological and biochemical characters, notably the progressive demise of dopaminergic neurons in the substantia nigra (Winklhofer and Haass, 2009). Mitochondrial analyses carried out on tissues from parkin-mutant patients proved an important reduction in complex I activity both in patients with parkin mutations and sporadic PD patients, whereas complex IV activity was only impaired in sporadic PD patients (Mortiboys et al., 2008). Another report show how parkin mutant fibroblasts are characterized by a significant decrease in mtDNA copy number and an increased vulnerability to oxidative stress-induced mtDNA impairment (Rothfuss et al., 2009). The consequences of PINK1 deficiency on mitochondrial function and morphology are multidimensional, including decreases in mitochondrial membrane potential, complexes I and IV activities, ATP production and abnormal ultrastructural mitochondrial morphology (Gautier et al., 2008; Gegg et al., 2009; Wood-Kaczmar et al., 2008).

2. Alzheimer's disease (AD).

AD is the most common cause of dementia in elderly people. Epidemiologic studies show that ADonset has a prevalence of 7-10% in >65 years and 50-60% among >85 years old subjects (Martin, 2012). The greatest number of AD cases are due to sporadic events, even though mutations in amyloid precursor protein (APP) have been reported to be associated with some familial episodes. APP is highly expressed in the brain and it is able to bind to the outer mitochondrial membrane, specifically to the OMM transporter 40 (TOMM40) and IMM transporter 23 (TIMM23). When overexpressed in cultured cells, APP inhibits mitochondria import machinery resulting in bioenergetic dysfunctions (Anandatheerthavarada et al., 2003). In postmortem human brain samples, APP variants were found to be associated with mitochondria from the AD brain but not mitochondria from control brain (Caspersen et al., 2005; Devi et al., 2006). High mitochondrial APP levels mirror deficiencies in respiratory chain subunit levels and activity and enhanced ROS production (Devi et al., 2006). In addition, APP transgenic mouse model present Aβ was also found to be associated with mitochondria isolated from cerebral cortex (Manczak et al., 2006).

3. Amyotrophic lateral sclerosis (ALS).

The etiology of motor neuron degeneration in ALS need to be better understood, even though it is believed that ALS is a multifactorial and multisystem pathology. A number of studies in humans and animal models suggest that mitochondria are involved in the progression of the neurodegenerative process. Specifically, mitochondria morphology and physiology have been demonstrated to be affected already in the early phases of ALS onset (Bruijn et al., 2004; Manfredi and Xu, 2005). Approximately 10–20% of the cases are familial whereas the majority of them are sporadic. Among the familial cases, the most common disease-causing mutations are found in the copper–zinc superoxide dismutase (SOD1) gene (Rosen, 1993). In G93A Sod1 transgenic mice, cytosolic release of mitochondrial cytochrome c was observed and levels of pro-apoptotic proteins Bad and Bax were upregulated. On the other hand, anti-apoptotic proteins Bcl-2, Bcl-xL and XIAP were decreased (Guegan et al., 2001). Data suggest that mutant Sod1 can also sequester anti-apoptotic protein Bcl-2, reduce mitochondrial membrane potential, and trigger cytochrome c release from mitochondria (Pasinelli et al., 2004). In addition, caspase-1 and caspase-3 were found to be sequentially activated in motor neurons and astrocytes in G93A Sod1 mice, as well as in G37R SOD1 and G85R Sod1 mice (Li et al., 2000; Pasinelli et al., 2000).

- ***Type 1 and type 2 diabetes.***

Mitochondrial dysfunction as a contributing factor in the onset of type 2 diabetes (T2D) represent a hot-topic in preclinical and clinical research (Patti and Corvera, 2010). Although the primary cause of this disease is unknown, it is clear that insulin resistance plays an early role in its pathogenesis and that defects in insulin secretion by pancreatic β cells are instrumental in the subsequent progression to hyperglycemia. Indeed, several lines of evidence indicate that insulin resistance is an early feature of T2D. Petersen et al. found that in comparison with matched young controls, healthy lean elderly subjects had severe insulin resistance in muscle, as well as significantly higher levels of triglycerides in both muscle and liver (Petersen et al., 2004). These changes were accompanied by decreases in both mitochondrial oxidative activity and mitochondrial adenosine triphosphate (ATP) synthesis. These data support the hypothesis that insulin resistance in human skeletal muscle arises from defects in mitochondrial fatty acid oxidation, which in turn lead to increases in intracellular fatty acid metabolites (fatty Acyl-CoA and diacylglycerol) that disrupt insulin signaling (Lowell and Shulman, 2005). Insulin resistance in healthy aged individuals with no family history has been correlated with a decline in mitochondrial oxidative phosphorylation (Petersen et al., 2004). The expression of a number of genes involved in oxidative metabolism is reduced in diabetic subjects as well as in those predisposed to diabetes because of family history (Mootha et al., 2003b; Patti et al., 2003). In

addition, in comparison with insulin-sensitive controls, the insulin resistant subjects were found to have a lower ratio of type I to type II muscle fibers. Alternatively, the reduction in mitochondrial oxidative phosphorylation activity in insulin-resistant individuals could be due not to mitochondrial loss but rather to a defect in mitochondrial function, hypothesis supported by muscle biopsy studies (Kelley et al., 2002; Vondra et al., 1977).

Because obese individuals have also been shown to have smaller mitochondria with reduced bioenergetic capacity compared with lean controls (Kelley et al., 2002), the mitochondrial abnormalities in these subjects might be related to obesity rather than to insulin resistance. Although insulin secretion is also modulated by a number of stimuli that operate outside this pathway, it is clear that oxidative mitochondrial metabolism is central to glucose-stimulated insulin secretion (Maechler and Wollheim, 2001). The critical role of mitochondria is evident from the rare hereditary disorders in which diabetes with β cell dysfunction has been traced to specific mutations in the mitochondrial genome (Maassen et al., 2004; Maechler and Wollheim, 2001). Given the central role of mitochondria in glucose sensing, it is possible that decreased mitochondrial function in β cells might predispose individuals to develop β cell dysfunction and T2D. These associations of mitochondrial dysfunction with human degenerative disease raise the basic question of how mammalian cells control mitochondrial biogenesis. It has become increasingly apparent that transcriptional mechanisms contribute to the biogenesis of mitochondria including the expression of the respiratory apparatus.

1.3 RNA metabolism and RNA binding proteins

Till 15 years ago, RNA was considered a set of macromolecules that served as a template, in the form of mRNA, or scaffold and structural molecules, in the form of tRNA and rRNA, for protein synthesis. The intensifying development of large scale genomic next generation sequencing (NGS) and modern protein mass spectrometry technologies helped researchers to shed light on the large number of mechanism that control RNA metabolism after genomic transcription (Hafner et al., 2010a, b; Konig et al., 2012; Mann, 2006). Post-transcriptional gene regulation is carried out by a complex machinery made up by RNA binding proteins (RBPs) and non-coding RNA sequences (ncRNAs), also referred to as RNA operon (Kapranov et al., 2007; Rinn and Chang, 2012). The interest in this multi-step process is raised in the last few years given its regulatory activity of fundamental pathways as energy metabolism, cell cycle and cell differentiation, to name a few, but also for the potential as future therapeutic target of its components.

1.3.1 mRNA splicing

Pre-mRNA (messenger RNA) splicing is the process of removing introns from pre-mRNA and ligating together exons to produce a mature mRNA, which is the template for protein translation. Pre-mRNA splicing is the second regulatory step of mRNA metabolism and expression after RNA transcription, in fact more than 90% of human genes undergoes alternative splicing (AS) events (Scotti and Swanson, 2015). In eukaryotes, introns represent almost 95% of pre-mRNA sequence and the removal of these large sequences is completed by the splicing machinery in almost all cases before the mRNA can be transferred out of the nucleus (Mattick and Gagen, 2001). Given the great importance of this process and the large number of proteins and non-coding RNAs that take part to it, it is not surprising that almost 15% of human diseases are characterized by splicing mis-regulation. Among the others, the most important are retinitis pigmentosa, myotonic dystrophy, spinal muscular atrophy, and chronic lymphocytic leukaemia and myelodysplasia (Scotti and Swanson, 2015). Defects in pre-mRNA splicing can be divided into four different categories, based on two criteria. First, the mutation could affect gene expression by disrupting a splicing cis-element, or in trans on multiple genes by disrupting a splicing machinery member. Second, the mutation could cause aberrant splicing (expression of unnatural mRNAs) or aberrant splicing misregulation (the inappropriate expression of natural mRNAs) (Faustino and Cooper, 2003).

Pre-mRNA splicing is catalyzed by the spliceosome, a huge nuclear ribonucleoprotein (RNP) complex that contains five small nuclear RNAs (snRNAs, U1, U2, U4, U5 and U6) that interact in a step-wise manner with more than 170 proteins, of which the most part are RBPs with specific RNA recognition motifs (RRM) (Zhang et al., 2013). Through AS events, pre-mRNAs can be processed to produce “mRNA isoforms” with diverse stability and/or coding potential. This enables the eukaryotic cell to control proteins synthesis in a quantitative way and to synthesize different proteins with qualitatively distinct functions and guaranteeing a high efficient extension of gene expression machinery (Nilsen and Graveley, 2010). On the other hand, the depth of the complexity of the RNA operon have yet to be fully understood. A major challenge is given by the presence of multiple possible interactions involved in the control of AS and the great specificity of all these interactions. For instance, a single RBP can bind different RRMs and, vice versa, a single RRM can be recognized by different RBPs or different isomers. Further, the distance of a RRM from a regulated exon controls the positive and the negative mechanism of action of a specific RBP. So far, different *in silico* models have been developed trying to predict alternative splicing outcomes, but the wide cellular composition of tissues and the great variability of possible interactions between RBPs and RRMs described above represent an important limitation to these kind of studies (Min et al., 2015). Making the whole process more complicated

is that spliceosome assembly seems to be finely regulated by the specific localization of RRM in respect to exons and introns. In fact, AS is typically controlled by numerous cis-regulatory RNA elements that serve as both splicing enhancers or silencers. On the basis of their locations and activities, these splicing regulatory elements (SRE) are classified in four different categories: exonic splicing enhancers (ESE), intronic splicing enhancers (ISE), exonic splicing silencers (ESS) or intronic splicing silencers (ISS) (Matlin et al., 2005; Wang and Burge, 2008). In addition, human introns, which consist of hundreds of kb (~5kb on average), contain numerous 'decoy' splice sites (that is, sequences that have a similar degree of consensus matching to authentic sites) (Sun and Chasin, 2000). Despite these prevalent decoy sites, splicing occurs with high fidelity as well, suggesting the existence of additional regulatory circuits to intronic-exonic sequence signals, maybe directed by non-coding RNAs.

Splicing events seems to be horizontally involved in many biological processes. Certainly, the most relevant is cell differentiation, even though recent studies start to highlight the importance of splicing events in cell cycle regulation and energy metabolism as well (Liu et al., 2012; Ravi et al., 2015). Given its impact on energy metabolism and the fine regulation of its differentiation in both embryonal stages and adulthood, skeletal muscle is one of those tissues whose physiology is highly regulated by RNA splicing events (Cardinali et al., 2016; Wei et al., 2015). In addition, AS is necessary for the proper commitment of skeletal muscle precursors to the proper differentiated phenotype, as striated muscle, smooth muscle and cardiac muscle (Gils et al., 2013; Yang et al., 2014).

1.3.2 Nuclear export and cytosolic fate of mRNA

After processing passages, mRNA is ready to be exported to the cytoplasm where it will be used as a template for protein synthesis. Until few years ago, mRNA export was considered one of the few constitutive steps of mRNA pathway to ribosomes, but it is now widely recognized that mRNA can be transferred from the nucleus to cytoplasm in both aspecific or specific fashion (Wickramasinghe and Laskey, 2015). mRNA nuclear export is controlled by the nuclear pore complexes (NPCs), which interact with the RNA export factors NXF1/p15 complex through a phenylalanine-glycine (FG) domain and the transcription-export complexes TREX and TREX2 (Bachi et al., 2000; Wickramasinghe et al., 2009). The formation of nuclear ribonucleoprotein complexes for mRNA export is thought to happen in specific nuclei loci, the nuclear speckles. This notion could suggest that the formation of nuclear export complexes already occurs during mRNA splicing and processing. As a proofof this, the selective deletion of NXF1 leads to polyA mRNA accumulation in this structures, as well as TREX2 scaffold protein germinal centre-

associated nuclear protein (GANP) knock-out (Wickramasinghe et al., 2014; Wickramasinghe et al., 2009). Once in the cytoplasm, mRNA is released from the RNP complex by the collaboration of the ATP dependent RNA helicase DBP5 and its cofactors, the mRNA export factor nucleoporin GLE1, small signalling molecule inositol hexakisphosphate (InsP6) and cytoplasmic nuclear pore complex protein NUP214 (von Moeller et al., 2009). Several studies suggest that cytoplasmic remodelling of mRNPs by NUP214 is crucial in imposing mRNA export directionality and setting up mRNA for translation (Hodge et al., 2011; Weirich et al., 2006). Evidences show that mRNA export in mammals can be a selective process. Diverse biological processes, including DNA repair, maintenance of stemness, gene expression, stress responses and cell differentiation can be regulated by selective mRNA export, and the large part of this selectivity seems to be mediated by components of the TREX and TREX2 complexes (Wang et al., 2013; Wickramasinghe et al., 2014).

Once in the cytoplasm, mRNA is bound by translation initiation factors and translated into proteins. Nevertheless, due to its great impact on translation rate, mRNA cytosolic half-life is finely regulated by the activity of a large number of RBPs and non-coding RNAs (Gong and Maquat, 2011; Valencia-Sanchez et al., 2006). mRNA degradation is in competition with mRNA translation, since the mRNA that is not engaged by ribosomes is sequestered to specific structures, also referred to as P-bodies and stress granules, where it is degraded (Decker and Parker, 2012). A large amount of data indicates that posttranscriptional regulation of mRNA half-life is necessary for the proper response to many cellular cues such as inflammation, energy metabolism and cell differentiation. Like the other members of this family, RBPs involved in mRNA degradation show a great affinity to specific mRNA sequences. The best-known *cis*-element is AU-rich elements (AREs) localized in the 3′UTR that is bound by at least four ARE-binding proteins (ARE-BPs). These proteins include HuR, ARE RNA binding protein 1 (AUF1), KH-type splicing regulatory protein (KSRP) and Tristetraprolin (TTP; also known as Zfp36). While HuR stabilizes ARE-containing mRNAs, other decay enzymes catalyze ARE-mediated mRNA decay (Uehata and Akira, 2013). In this context, one of the most posttrascriptionally regulated processes is the intracellular iron homeostasis. TTP is induced by iron deficiency and required for the survival of mammalian cells in low-iron conditions (Bayeva et al., 2012). TTP binds to AU-rich elements (AREs) in the 3'UTR of their target mRNA, recruiting DExD/H-box helicase 1 (Dhh1) RNA helicase, mRNA de-capping, and degradation (Pedro-Segura et al., 2008). Among the main targets of TTP there are genes coding for proteins that need iron for their function such as lipoic acid synthase (Lias), but also enzymes belonging to TCA cycle including citrate synthase 1, mitochondrial aconitase 1, α-ketoglutarate dehydrogenase, succinate dehydrogenase 2 and 4 subunits, and mitochondrial fumarase 1. Moreover, TTP binds to the

mRNAs encoding some electron transport chain (ETC) subunits, including cytochrome C oxidase and ubiquinol cytochrome C reductase are degraded by TTP (Bayeva et al., 2013).

1.4 Skeletal muscle

Skeletal muscle is a highly dynamic tissue that represent almost 50% of total body weight in human adults. Human body accounts for 650 different skeletal muscles that, along with skeleton, control and sustain body movements. Nevertheless, skeletal muscle is involved in several systemic processes that do not concern only motility. In fact, it is now well known that skeletal muscle is fundamental for energy metabolism homeostasis and represent an important endocrine tissue producing molecules, .referred to as myokines (Pedersen and Febbraio, 2012). Furthermore, skeletal muscle is responsible for 85% of postprandial insulin dependent glucose uptake from the blood stream and it is responsible for ≈30% of the resting metabolic rate in adult humans (DeFronzo et al., 1981; Zurlo et al., 1990). It serves as an important stock site for glycogen as well, with an accumulation capacity ≈4 folds higher than the liver, while physical exercise can induce muscular glucose uptake in an insulin independent manner rising the expression and the translocation to the plasma membrane of the glucose transporter Glut4, increasing up to 100 fold the energy substrates utilization (Richter and Hargreaves, 2013).

Skeletal muscle is also referred to as striated muscle and it is one of the three muscle types present in mammals, the others being cardiac muscle and smooth muscle. Unlike cardiac muscle and smooth muscle, skeletal muscle responds to voluntary stimuli of somatic nervous system. Skeletal muscle fibers, that consist of many multinucleated muscular cells, also referred to as myotubes, are surrounded by a tiny layer of connective tissue, the endomysium, while myofibers are enclosed in the perimysium and single muscles are surrounded by the epimysium, respectively(Turrina et al., 2013). Microscopically, skeletal muscle is organized by cytoskeleton structures mainly made up by myosin and actin, which are arranged in repetitive units, named sarcomere. The interactions of myosin and actin are responsible of skeletal muscle contraction.

Mammalian skeletal muscle is a heterogeneous set of fibers types characterized by the expression of different myosin heavy chain (MyHC) isoforms and by diverse metabolic patterns (Schiaffino and Reggiani, 2011).Specifically, adult skeletal muscle comprehends slow-twitch oxidative fibers (red fibers) and three types of fast-twitch glycolytic fibers (white fibers). MyHC1β is a marker of slow-twitch fibers, which are very rich in mitochondria and myoglobin, given their high oxidative metabolic rate. On the other hand, MyHC2A and 2X in humans and 2B in rodents are expressed in fast-twitch fibers that mainly rely on glycolytic and anaerobic metabolism (Schiaffino and Reggiani, 2011). From a functional point of view, oxidative red fibers are

responsible for prolonged and mild physical activity, whereas white fibers are generally active during fast and intense physical effort. The percentage of different fibers in skeletal muscles is determined during embryonic development, as proof of skeletal muscle plasticity, and it can be modulated during adulthood by different cues, as physical exercise, cold exposition and by physiological conditions as blood flow and energy substrates availability (Egan et al., 2013).

1.4.1 Skeletal muscle development

Skeletal muscle stem cells (MuSC) are responsible for skeletal muscle development during embryonic life (Mokalled et al., 2012; Yin et al., 2013). In the somites, MuSC proliferate and express myogenic determination and differentiation factors that start the formation of early skeletal muscle of the trunk and the limbs. The most relevant transcription factors involved in the regulation of skeletal muscle development are Pax3, Pax7, Myf5, Mrf4, Myod1 and Myogenin (MyoG), whose different temporal and spatial expression is fundamental for proper development of the tissue (Buckingham et al., 2003; Buckingham and Rigby, 2014). Pax3 is expressed in presomitic mesoderm and throughout the epithelial somite, on both sides of the neural tube, before becoming restricted to the dermomyotome. It is necessary for the proliferation and survival of uncommitted myogenic progenitors. On the other hand, Pax7 is expressed in the central domain of dermomyotome where it controls both muscle progenitor proliferation through direct interaction with Pax3 and myogenic specification factors (Buckingham and Relaix, 2015; Seale et al., 2000). In the epaxial domain of somites, Pax3/Pax7 complex activates Myf5. Here, Myf5 upregulates Myod1 and Mrf4 expression, inducing the migration of myogenic progenitors from the dermomyotome to the underlying myotome and more distal limbs, starting the differentiation to trunk muscles and skeletal muscles. Subsequently, the central dermomyotome loses its epithelial structure and different populations of progenitor cells differentiate and proliferate, providing a cell reserve for muscle growth during development and maintenance during adulthood (Deries and Thorsteinsdottir, 2016).

Adult skeletal muscle is featured by high regenerative capacities. After injury or exercise, large numbers of newly formed muscle fibers are generated within few days as a result of expansion and differentiation of the self-renewing pool of satellite cells, which probably derive from a sub-population of embryonic progenitors (Charge and Rudnicki, 2004; Dumont et al., 2015; Peault et al., 2007). Normally, satellite cells are mitotically quiescent and reside in specific niches beneath the basal lamina of muscle fibers. Upon regeneration, satellite cells are activated, and give rise to daughter myogenic precursor cells. After several rounds of proliferation, precursor cells contribute to the formation of new muscle fibers. During cell division, a little population of myogenic precursor cells stays into quiescence as self-renewal process (Motohashi and

Asakura, 2014). Given the great importance of satellite cell pool for muscle regeneration and maintenance, muscle precursor cells are characterized by relevant heterogeneity. Recent findings defined at least three different myogenic progenitor types: (i) $Pax7^+$ cells that maintain progenitor pool, (ii) $Myod1^+$ myogenic cells that have entered the myogenic program, and (iii) $Myogenin^+$ myocytes partially differentiated and primed for fusion with existing or newly formed myotubes (Tierney and Sacco, 2016).

Recent findings indicate that RNA-binding proteins play key roles in regulating gene expression during skeletal muscle differentiation both *in vitro* and *in vivo*. Furthermore, several RBPs are even mutated or in some way altered in patients with specific forms of muscular dystrophy. The best-characterized RBPs in skeletal muscle biology are human antigen R (HuR), KH-type splicing regulatory protein (KSRP), CUG-binding protein 1 (CUGBP1), poly (A)-binding protein 1 (PABPN1), Lin-28, TTP and Muscleblind-like splicing regulator 1 (MBNL1) that all influence different stages of myogenesis (Thornton et al., 2006). HuR activity in skeletal muscle is primarily controlled through its compartmentalization that is mediated by the nuclear import receptor transportin 2 (TRN2). HuR is almost exclusively localized into the nucleus in myoblasts, but right after differentiation induction it accumulates in the cytoplasm (Figueroa et al., 2003). Upon differentiation, HuR is cleaved by caspases and generates a 24 kDa inhibitory polypeptide, which binds to TRN2 and blocks the import of HuR in the nucleus. This leads to the cytoplasmic accumulation of full-length HuR and subsequent stabilization of MyoD and myogenin mRNAs and increase of the relative proteins (Beauchamp et al., 2010). In addition, evidences suggest that HuR could lead to cell cycle withdrawal and subsequent induction of myogenesis (Guo et al., 1995). Analogously to HuR, CUGBP1 leads to mRNA stabilization of p21 and Cyclin D1 mRNAs leading to cell cycle exit and myogenic program start (Salisbury et al., 2008). On the other hand, KSRP counteracts HuR activity repressing myogenic mRNAs stability during myoblast proliferation, while its phosphorylation leads to the decrease of its binding affinity to mRNA and skeletal muscle differentiation (Briata et al., 2005). Finally, less is known about the myogenic role of TTP, even though data indicates that it is rapidly induced after muscle injury, suggesting a key role of this protein in the myogenic program (Sachidanandan et al., 2002).

1.4.2 MuSC and aging

Multiple rounds of asymmetric division have been demonstrated to cause the gradual loss of quiescent MuSC pool observed in aged subjects. During aging, satellite cell number decreases, resulting in attenuation of muscle regeneration capacity and loss muscle mass (also referred to as sarcopenia) (Fig. 1.7). Gradual loss of muscle function has a detrimental impact on individual

health and lifespan, showing a prevalence between 5-13% among 60-70 years old people and 11-50% after the age of 80 (Morley, 2008). In addition, it has been demonstrated that sarcopenia has huge costs for the healthcare system, reaching $18 billion in 2000 in US (Janssen et al., 2003).

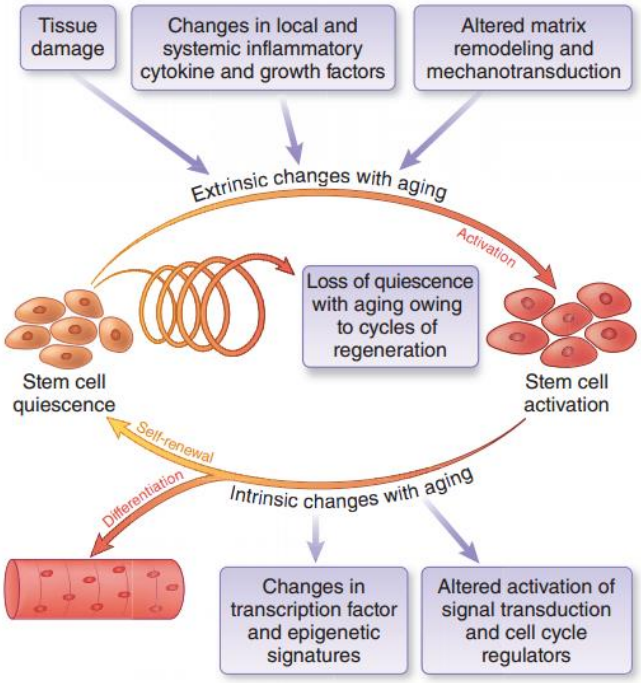

Fig. 1.7 Role of skeletal muscle stem cells or satellite cells (MuSC) in adult skeletal muscle. MuSC are quiescent cells activated by different extrinsic cues as physical exercise or injury. MuSC, as well as activated cells, present specific intrinsic factors that control their faith, as epigenetic marks and gene expression patterns. During aging, extrinsic and intrinsic changes bring to altered self-renewal capacity and senescence of these cells leading to skeletal muscle weight and strength loss (Blau et al., 2015).

Both intrinsic and extrinsic alterations have been associated to the alteration of skeletal muscle physiology during aging. After myofiber damage, extrinsic factors as cytokines and growth factors activate MuSC and favor skeletal muscle repair (Arnold et al., 2015; Kang et al., 2008). Simultaneously, MuSC undergo multiple rounds of self-renewing divisions that are essential to their function in regeneration (Bosnakovski et al., 2008; Cerletti et al., 2008; Kuang et al., 2007). In physiological conditions, feedback mechanisms ensure that asymmetric self-renewing divisions yield sufficient numbers of fusion-competent muscle progenitor cells that contribute to myofiber repair, and quiescent cells that serve as a bulk for subsequent skeletal muscle regeneration rounds (Chakkalakal et al., 2012; Gopinath et al., 2014). In aged muscles, self-renewal signals diminish and pro-inflammatory and fibrogenic pathways are upregulated and

persistent, causing aberrant MuSC activation and loss of quiescence. By elderly ages, a subpopulation of aged MuSC become senescent.

Less is known about the intrinsic factors that control MuSC self-renewal cycles and transition to senescence. New isolation methods are opening unknown perspectives on the molecular mechanism beneath quiescence loss that lead aged satellite cells to lose their ability to coordinate muscle regeneration (Cosgrove et al., 2014; Price et al., 2014). Recent findings suggest that intrinsic-dependent entrance in senescence depends on important signaling pathways that orchestrate cell cycle and differentiation, as aberrant and cell-autonomous activation of the stress-associated p38α/β mitogen-activated protein kinase (MAPK) signaling axis, the growth factor-stimulated FGFR–Sprouty1 signaling axis, the cytokine-stimulated Jak2–Stat3 signaling axis, and $p16^{Ink4a}$–Rb cell cycle inhibitors (Cosgrove et al., 2014; Price et al., 2014; Tierney et al., 2014). p38α/β MAPK and Jak2–Stat3 signaling axes can inhibit MuSC self-renewal by contrasting cell cycle progression and promoting myogenic differentiation increasing the expression of commitment genes such as Myod1, which is in fact activated in aged skeletal muscle (Sakuma et al., 2008; Tierney et al., 2014). Moreover, aberrant p38α/β activity suppresses Pax7 expression through repressive chromatin modifications, leading to impaired balance of MuSC asymmetric self-renewal and pool, forcing the commitment of both daughter cells (Palacios et al., 2010; Troy et al., 2012). Further experiments demonstrated that a significant fraction of MuSC from aged and geriatric mice show a premature cellular senescence phenotype, caused by the aging-associated upregulation of the cell cycle inhibitor $p16^{Ink4a}$. The resulting senescent cells are characterized by $p16^{Ink4a}$ and $p21^{Cip1}$ expression and cell cycle arrest (Sousa-Victor et al., 2014). Principal molecules of energy metabolism have been also demonstrated to be key regulators of MuSC commitment and stemness reprogramming. Recent data demonstrate that mitochondrial dysfunction is an early hallmark of MuSC, while animals fed with nicotinamide ribonucleotide (NR), a precursor of nicotinamide adenine dinucleotide (NAD^+) precursor, show increased lifespan and prolonged MuSC quiescence during aging. In addition, NR diet increased MuSC number and muscle function in aged mice, as well as in muscle dystrophic *mdx* mice (Zhang et al., 2016a). The great relevance of NAD^+ for MuSC reprogramming has been also demonstrated in selective skeletal muscle SIRT1 knockdown, a NAD^+ dependent enzyme (Ryall et al., 2015). SIRT1 ablation in skeletal muscle leads to histone H4 lysine 16 (H4K16) hyperacetylation and alteration of the myogenic program in SC. Furthermore, these mice display reduced myofiber size, impaired muscle regeneration, and derepression of muscle developmental genes (Ryall et al., 2015).These works belong to the mounting number of evidences that demonstrate how intrinsic factors tune MuSC response to

nutrients, and ultimately lifestyle, strongly influencing genome-proteome-metabolome functional interactions and determining disease via mitochondrial function and health.

2. Aim of the study

Skeletal muscle represents a large part of body weight in adult humans and its physiological roles span from movement generation to energy metabolism homeostasis. It is largely known that skeletal muscle is the primary site of glucose uptake and storage, but also one the most energetically active tissues with many mitochondria. Adult striated muscle maintenance and repair are sustained by the presence of skeletal muscle satellite cells (MuSC), or precursors, that in presence of specific extrinsic factors (i.e. cytokines, cold and physical exercise) quit quiescence and start asymmetric division prompting myocyte differentiation and skeletal muscle development (Tierney and Sacco, 2016).

As the main site of energy production, mitochondria play a crucial role in many cellular processes. Metabolic transition during cell differentiation is required for proper cell commitment and development. In the last years, a large amount of data indicated that mitochondria burst is a necessary step for cell phenotype transition. In this regard, stem cell reprogramming corresponds to a shift to a more glycolytic metabolism and rounded, cristae-poor mitochondria, while cell differentiation pushes hyper-fusion and cristae formation of mitochondria to afford the large energy demand (Wanet et al., 2015; Xu et al., 2013b; Zhang et al., 2016b). Research in the field has suggested the existence of a tight relationship between energy metabolism regulation, mitochondrial activity and cell differentiation (Almada and Wagers, 2016; Ryall et al., 2015; Shintaku et al., 2016). In addition, recent results demonstrated that diet supplementation of a NADH precursor improves MuSC asymmetric division and skeletal muscle physiology in aged mice, supporting the idea that control of metabolic landscape is a key player of skeletal muscle maintenance and development (Ryall, 2013; Ryall et al., 2015). Nevertheless, the regulatory circuitries of mitochondrial functional changes that underlie metabolic transition of myoblasts to myotubes still need to be fully understood. For this reason, the identification of new mitochondrial and skeletal muscle differentiation regulators represents a possible strategy to shed light on the molecular relationships between these organelles and skeletal muscle precursors. In light of this, the goal of this project is to characterize a new mitochondrial regulator and dissect the molecular mechanism by which this factor controls metabolic reprograming during the first phases of skeletal muscle commitment and differentiation.

3. Materials & Methods

3.1 Mice

C57BL6/J were purchased from Charles River (USA) and sacrificed fed at libitum after 2 weeks of maintenance. All experiments were conducted following the regulations of the European Community (Directive 86/609/EEC, Official Journal L 358, 18/ 12/1986 p. 0001-0028) and local regulations (e.g., Italian Legislative Decree n. 116 - 27/01/1992) for the care and use of laboratory animals. The Italian Ministry of Health approved the animal protocols of this study (ministerial decree n. 295/2012-A).

3.2 Cell cultures

C2C12 myoblasts (ATCC® CRL-1772™) were grown in complete media (DMEM supplemented of 10% fetal bovine serum, 2% glutamine, 2% pen/strep) at low confluency and normal growth condition (5% CO2 and 90% of humidity). The differentiation induction to myotubes in 24, 12 or 6-well plates was performed growing cells till complete confluence, then switching complete media to differentiation medium (2% horse serum, 2% glutamine, 2% pen/strep).

3.3 Cell transduction for gene over- and downregulation

Zc3h10 overexpression was obtained using an adenoviral vector (Human Adenovirus Type 5 dE1/dE3) carrying mouse Zc3h10 cDNA fused together with a Flag-tag to the N-terminal of the construct (Flag-Zc3) and under the control of a CMV promoter (Vector Biolabs, ADV-276549). As control, we used the same construct expressing the GFP under a CMV promoter (Vector Biolabs, 1768). For the experiments, Flag-Zc3h10 and GFP were overexpressed at a multiplicity of infection (MOI) of 5. On the other hand, Zc3h10 targeted silencing was performed by transducing cells with the adenoviral construct carrying a specific short hairpin RNA sequence under a U6 promoter (shADV-276549). As control, we used the same construct bearing a scrambled sequence (Vector Biolabs, 1122). Both construct were transduced at a MOI of 100. Cell transduction was performed following two different protocols (Fig 3.1). Briefly, in the pre-differentiation protocol (red), cells were transduced 2 days before the differentiation induction; on the other hand, in the post-differentiation protocol (blue) myocytes were infected 2 days after differentiation induction. Cells were then collected for the readouts at 24, 48, 72 hours and 4 days, respectively.

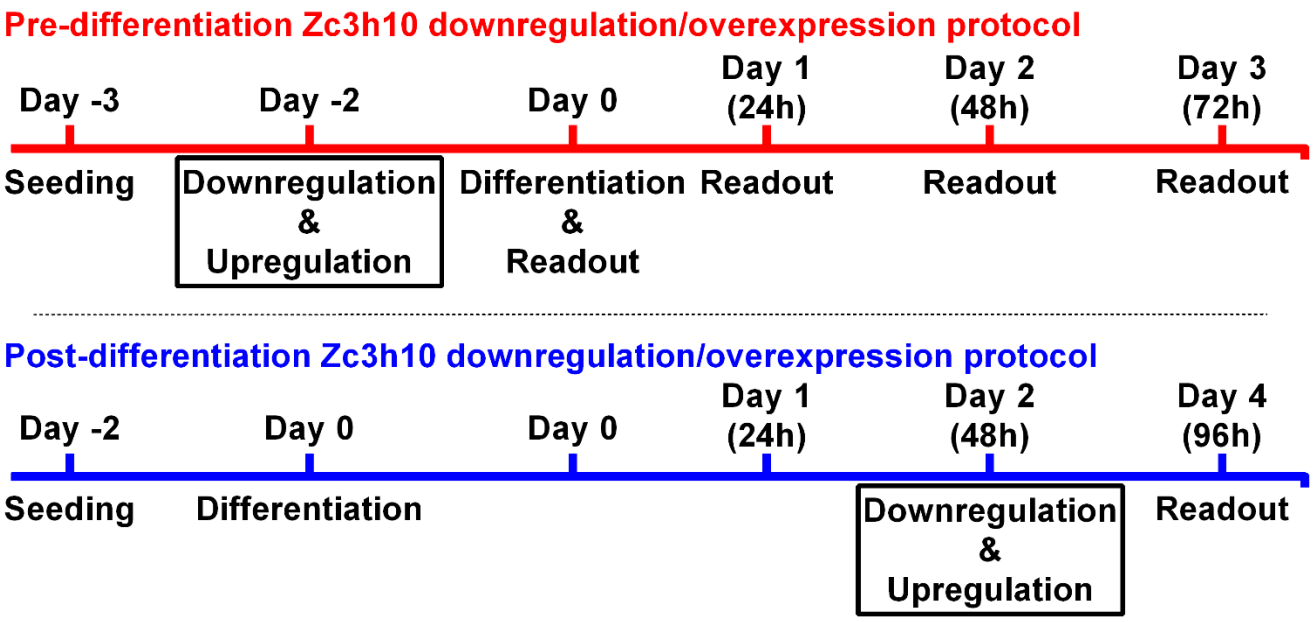

Fig 3.1. Experimental plan. The pre-differentiation protocol (red) was carried out transducing myoblasts 2 days before the differentiation induction, while in the post-differentiation protocol (blue) myocytes were infected 2 days after differentiation induction. The readouts were obtained at 24, 48, 72 and 4 days from the differentiation induction, respectively. We used a MOI of 5 for Zc3h10 overexpression and a MOI of 100 for shZc3h10 in both protocols. The same MOI was used for respective control sequences.

3.4 Gene expression analysis

Gene expression analyses were carried out through qPCR. Total RNA was obtained from C2C12 cells and different mouse tissues and organs using silica column approach (NucleoSpin® RNA extraction kit, Macherey-Nagel, 740955.250). Briefly, we removed media and washed cells with ice-cold PBS. We proceeded lysing cells with 350µl of RA1 buffer supplemented of 1% β-mercaptoethanol then adding 350µl of 70% ethanol. Cell lysates were then transferred to silica columns and spun 11000g for 30 seconds. After a wash step with MDB buffer, the extracts were treated with DNase for 15 min at RT. DNase was inactivated by adding 200µl RAW2 buffer and columns were spun 11000g for 1 minute. After two washes with RA3 buffer, total RNA was eluted from columns by adding 50µl of water. Total RNA amount was then quantified by UV spectrophotometry (NanoDrop 1000 Spectrophotometer, Thermo Scientific). Samples were then diluted to 5µg/µl and used for mRNA quantification.

Specific RNA sequences were amplified and quantitated by qPCR, using iScriptTM One Step for Probes and iTaq Universal SYBR Green One-Step Kit for qPCR (Bio-Rad, CA, USA), following the manufacturer's instructions. Experiments were performed in quintuplicate and repeated at least twice with different cell preparations. We calculated target mRNA levels comparing the target gene values with the houskeeping gene values. The qPCR protocol is composed of 40

cycles of amplifications, each consisting of a denaturation step at 95° C for 15 seconds and an annealing/extension step at 60° C for 60 seconds. The oligonucleotides used for qPCR were obtained from Eurofin MWG Operon (Ebersberg, Germany). qPCR primers sequences are reported below:

36B4	**fwd**	AGATGCAGCAGATCCGCAT
	rev	GTTCTTGCCCATCAGCACC
	probe	CGCTCCGAGGGAAGGCCG
Zc3h10	**fwd**	CCTACGAATGTAACTTGGCTCC
	rev	CTGCTCCAGAAGTACCTCATTG
	probe	AGTCTGCACTCAACCCCACGG
Tfam	**fwd**	CACCCAGATGCAAAACTTTCAG
	rev	CTGCTCTTTATACTTGCTCACAG
	probe	CCACAGGGCTGCAATTTTCCTAACC
Mef2c	**fwd**	GGATAAGGTGTTGCTCAAGTAC
	rev	GGGTGAGTGCATAAGAGGA
	probe	AACTCAGACATTGTGGAGGCATTGAAC
MyoD1	**fwd**	CGCTCCAACTGCTCTGATG
	rev	ACACAGCCGCACTCTTC
Myog	**fwd**	AATGCACTGGAGTTCGGTC
	rev	ATGGTTTCGTCTGGGAAGG
Slc25a37	**fwd**	CATCTCCTGGTCCGTTTATGAG
	rev	TGCGAGAACAAGAGGATGAAG

3.5 RNA immunoprecipitation for identification of target RNAs

Myoblasts were cultured and transduced with eGFP or Flag-Zc3h10 at 25 MOI 48 hours before performing the experiment in 180cm^2 flasks. At complete confluency, cells were resuspended in 1000ul of RIP lysis buffer (50mM trisHCl pH 7.4, 150mM NaCl, 1mM EDTA, 1% NP-40), kept in ice for 20min and vortex frequently. We centrifuged samples at 10000g for 10min at 4°C and removed DNA and membranes pellet. We save supernatant in 2ml tubes. We saved 1/10 from each sample for total RNA input. We brought RIP samples to 1ml final volume with RIP lysis buffer. Meanwhile, 40µl of agarose-Flag Ab beads (Sigma Aldrich, A2220) were washed in 380µl of TBS and spun down at 8000g for 1min at 4°C. We resuspended the beads to 40µl with RIP lysis buffer and transferred 20µl of the solution to each RIP sample. We proceeded incubating samples through constant rotation for 2 hours at 4°C. We later transferred samples to fresh 1.5ml tubes and centrifuged tubes at 8000g for 5 min at 4°C. Then, we extensively washed

beads with 1000µl of TBS-Tween 0.1% (5 min 10X). Before last wash, we saved 1/50 for IP western blot validation. Finally, we resuspended beads with 300µl of trizol for subsequent bound RNA isolation. Total RNA was subsequently quantified on 2100 Bioanalyzer (Agilent) and equal RNA amounts were used for the generation of polyA libraries and following RNA sequencing (Illumina HiSeq 2000).

3.6 RNA metabolism analyses

3.6.1 Total RNA sequencing

Total RNA levels were assessed as previously described(Rabani et al., 2011; Schwanhausser et al., 2011). Briefly, dishes were immediately transferred on ice and cells were rinsed with ice-cold PBS and harvested in 10 ml of ice-cold PBS. RNA samples were eluted in 50µl of ddH_2O, quantified by UV spectrophotometry and saved at -80°C. We then removed rRNA from total RNA samples by Ribo-Zero Magnetic Kit (Illumina, Mrzh116) following manufacturer's instructions. 100ng of all samples were finally used for cDNA libraries construction and next generation sequencing (Illumina HiSeq 2000). Assessment of differences between the two conditions was performed using DESeq2 software for total mRNA concentrations (RPKM).

3.6.2 Microarray assay

Microarray analysis for whole transcriptome analysis was performed using a MoGene 2.0 chip. Briefly, cells were differentiated for 2 days, then rinsed in 1 ml of ice-cold PBS. Total RNA was isolated as described above and 3µg of RNA were used for following analyses.

RNA quality control Test:

Total RNA concentration and purity was assessed by spectrophotometer (Nanodrop): 260/280 and 260/230 ratios were evaluated. Total RNA integrity was assessed by Agilent Bioanalyzer and the RNA Integrity Number (RIN) was calculated. The RIN ranges from 1 (totally degraded RNA) to 10 (completely intact RNA). The quality of each sample was assured by a RIN ≥ 6 and visual confirmation of clear, distinct 28S and 18S rRNA peaks.

Sample preparation:

An aliquot (100 ng) of RNA was used for the preparation of targets for Affymetrix® MoGene 2.0 ST arras, according to the Ambion WT Expression kit manual. Affymetrix® MoGene 2.0 ST arrays (which contain 41073 genes), were purchased from Affymetrix (Affymetrix, USA). The staining, washing and scanning of the arrays were conducted using the Fluidics 450 station,

Command Console Software and GeneChip® Scanner 3000 7G, generating .CEL files for each array (Affymetrix, USA).

Data collection and data analysis:
The images were scanned by Affymetrix GeneChip Command Console (AGCC) and analyzed with the Affymetrix GeneChip Expression Console. The quality control of the scanned data was first estimated by confirming the order of the signal intensities of the Poly-A and Hybridization controls using Expression Console Software (Affymetrix, USA). Raw expression values were imported as Affymetrix .CEL files into Partek Genomics Suite 6.6 (Partek Inc., MO, USA). Raw expression values from the Affymetrix MoGene 2.0 ST arrays were analyzed and normalized using Partek Genomics Suite 6.6, which includes the Preprocessing, Differentially Expressed Genes (DEGs) Finding and Clustering modules. A total of 9 .CEL files (4 .CEL files generated from CTRL samples and 5 .CEL files generated from Knock Down samples) were uploaded and normalized in PM (perfect match)-only conditions as a PM intensity adjustment. A Robust Multichip Analysis (RMA) quantification method was used as a probe set summarization algorithm for log transformation with base 2 (log2) and the Quantile normalization method was chosen to evaluate the preliminary data quality in the Preprocessing module, which functions as a data quality control through the Affymetrix Expression Console Software. The mean signal intensities of all genes were obtained using 2 array strips from each group.

Differentially expressed genes (DEGs) analysis:
DEGs clustering analysis was performed by using the Gene Set Enrichment Analysis (GSEA) software (Broad Institute, USA). To get an unbiased readout of the most represented clusters of genes, we interrogated all three gene ontology (GO) categories (molecular function, cell compartment and biological process) in the same analysis.

3.7 Western blot

Protein relative quantification analyses were carried out separating cell lysates on SDS-Page. Cells were first rinsed in ice-cold PBS and harvested from dishes. Later, they were transferred to 1.5 ml tube and spun at 5000g for 3 min at 4°C. The pellet was then resuspended in 200µl of RIPA buffer (15 mM NaCl, 0.1% NP-40, 0.05% Na-deoxycholate, 5 mM Tris-HCl pH 8.0, 0.1% SDS), moved to ice and sonicated twice at 10% of power for 10 seconds. Later, cell lysates were spun again at 10000g for 5 min at 4°C. Cell debris pellet was discarded, and protein concentration was measured using BCA method (Thermo Scientific/Pierce BCA protein assay kit, 23225). Proper protein amount was than loaded on 10% or 12.5% SDS-Page. After gel run,

proteins were transferred to a nitrocellulose membrane at 200mA for 2 hours at RT, then blocked in 5% bovine serum albumin (BSA) for 1.5 hours at RT. Membranes were then incubated O/N at 4°C with primary antibodies, previously resuspended in 0,1% TBS-Tween20 and 3% BSA. After extensive washes, membranes were incubated with HRP-conjugated secondary antibodies for 1 hour at RT. After washing, membranes were finally incubated with ECL substrate for bands detection. Primary and secondary antibodies were diluted as follows: Zc3h10 1:1000 (Aviva systems biology, ARP60671_P050), Tfam 1:1000 (Aviva systems biology, ARP31400_P050), Oxphos cocktail 1:1000 (Abcam, ab110413), Myosin Heavy Chain Fast (MyHCFast) 1:1000 (Monosan, Monx10807), Slc25a37 1:1000 (Aviva systems biology, ARP43968_P050), Hsp90 1:500 (Santa Cruz Biotech., sc-7947), β-actin 1:5000 (Sigma Aldrich, A5441), Histone H3 1:1000 (Upstate, 05-499), α-tubulin 1:1000 (Sigma Aldrich, T9026), Flag 1:5000 (Sigma Aldrich, F3165), α-mouse 1:5000 (Sigma Aldrich, A4416) and α-rabbit 1:2000 (Cell Signaling, 7074).

3.8 Immunofluorescence (IF) analyses

3.8.1 Evaluation of Zc3h10 protein expression levels

IF analysis were performed on C2C12 myoblasts. After removing the media, cells were washed with ice-cold PBS and fixed with 1% paraformaldehyde for 15 min at RT. After 3 washes with Triton X100 1% in PBS, we unmasked the antigen incubating cells with 1N HCl at 4°C for 10 min, then with 2N HCl for 10 min and finally with 2N HCl at 37°C for 10 min. Later, cells were treated with 0,1M sodium borate for 10 min at RT to low autofluorescence events. Cells were then blocked with 2% goat serum, 1% BSA, 0,1% tween20, 0,05% triton X100 in PBS for 2 hours at RT and finally incubated O/N at 4°C with Zc3h10 (1:250) primary antibody in PBS. After extensive washes, cells were then exposed to the goat anti-rabbit alexa fluor 488nm (Thermo Scientific, A-11008) secondary antibody (1:1000) for 1 hr at RT titrated. After extensive ice-cold PBS washes for 30 min, cells were finally incubated with DAPI (1:2000) in PBS for 10 min, washed with PBS for 5 min and mounted on glass slides with Permafluor (Thermo Scientific, TA-030-FM) for confocal imaging.

3.8.2 Fusion index analysis

IF analysis were performed on 72 hours differentiated myotubes as describe above. Myotubes were incubated O/N at 4°C with MyHCFast (1:250) primary antibody in PBS. After extensive washes, cells were then exposed to the goat anti-mouse alexa fluor 635nm (Thermo Scientific, A-31574) secondary antibody (1:1000) for 1 hr at RT titrated. After extensive ice-cold PBS washes for 30 min, cells were finally incubated with DAPI (1:2000) in PBS for 10 min, washed

with PBS for 5 min and mounted on glass slides with Permafluor (Thermo Scientific, TA-030-FM) for confocal imaging. Fusion index was calculated as the ratio between the number of nuclei in $MyHC^+$ fibers with 3 or more nuclei on total nuclei number in the field.

3.8.3 Evaluation of Zc3h10 protein expression levels in human quadriceps

6µm sections were obtained from adult human and 12 weeks, 6 months and 12 months old mice quadriceps. Slices were then fixed in 4% paraformaldehyde for 15 min at RT and extensively washed with PBS for 45 min. After blocking with 1% BSA and 0.1% triton X100, human and mouse slices were washed again with PBS for 15 min and labelled with Zc3h10 primary antibody (1:100) for 1.5 hours at RT. Human tissues were also co-labelled with fetal MyHC 1:100(Myosin heavy chain developmental, NCL-MHCd - clone: RNHY2-9D2, Leyca) and neonatal MyHC1:100(Myosin heavy chain neonatal, NCL-MHCn clone: WB-MHCn, Leyca). Samples were then washed again for 45 min with PBS, incubated with goat anti-rabbit alexa fluor 546nm secondary antibody for Zc3h10 and goat anti-rabbit alexa fluor 488nm secondary antibody for MyHCs, then washed again for 45 min with PBS and finally mounted on glass slides with Permafluor (Thermo Scientific, TA-030-FM) for confocal imaging.

3.9 Subcellular fractionation for Zc3h10 localization

C2C12 were grown in complete medium and then collected at different stages of differentiation for nuclei and cytosolic protein extraction. All centrifugations were performed at 4°C and samples were kept on ice throughout all the procedure. We rinsed and transferred cells from 10cm plates into 500µL fractionation buffer (250mM sucrose, 20mM HEPES pH 7.4, 10mM KCl, 2mM $MgCl_2$, 1mM EGTA, 1mM EDTA, protease inhibitor and 200mM DTT) by scraping. We passed cell suspensions through a 25-gauge needle 15 times using a 1 mL syringe and left them on ice for 20 min. We centrifuged sample at 720g for 5 min and saved pellet as crude nuclei fraction while supernatant was the cytosolic fraction. Nuclear pellets were later resuspended and washedwith 500µl of fractionation buffer before being passed through a 25-gauge needle other 15 times. Nuclear samples were centrifuge again at 720g for 10 min and pellet was saved nuclear fraction. The pellet was then resuspended in TBS with 0.1% SDS and sonicated20 sec at 10% to shear genomic DNA and homogenize the lysate. Finally, cytoplasmic fractions were spun at 10000g for 5 min and supernatant were saved as cytoplasmic fraction. Samples were subsequently diluted 1:2 with 2x SDS-Sample buffer (4% SDS, 10% 2-mercaptoehtanol, 20% glycerol, 0.004% bromophenol blue, 0.125M Tris HCl pH 6.8) and equally loaded on SDS-Page.

We interrogated cNLS Mapper software with a cutoff of 6.0 (Chatterjee et al., 2016) (http://nls-mapper.iab.keio.ac.jp/cgi-bin/NLS_Mapper_form.cgi) to verify the existence of a putative nuclear localization signal within the entire Zc3h10 sequence.

3.10 Steady state metabolic analyses by mass spectrometry (MS)

Cells were differentiated for 48 hours in 10cm dishes. After saving 1/10 of cells for DNA quantification, cells were scraped in 5 ml of ice-cold PBS and centrifuged at 1000g for 3 min at 4°C.Pellets were then resuspended in 250µl of D-Glucose-$^{13}C_6$ 1ng/µl (internal standard, Sigma Aldrich, 389374) andmethanol/acetonitrile 1:1 and spun at 10000g for 3 min at 4°C. Derivatization for aminoacids quantification was performed by adding 50µlof5% phenyl isothiocyanate (PITC) in 31.5% EtOH and 31.5% pyridine. Briefly, samples were incubated with PITC solution for 20 min at RT, dried under nitrogen flow and resuspended in 2.5mM ammonium acetate in MeOH/H_2O 1:1.

For the quantification of different metabolic families, the MS analysis was performed with a flow injection analysis-tandem mass spectrometry (FIA-MS/MS) method. The identity of all metabolites was confirmed using pure standards. Methanolic samples were analyzed by a 5 min run in both positive (aminoacids) and negative (Acyl-carnitines and metabolites) ion mode with a 268 multiple reaction monitoring (MRM) transition in positive mode and 88 MRM transition in negative mode, respectively. An ESI source connected with an API 4000 triple quadrupole instrument (ABSciex, USA) was used. The mobile phase was 0.1% formic acid in MeOH for FIA positive analysis and 5 mM ammonium acetate pH 7.00 in MeOH for FIA negative. MultiQuant™ software version 3.0.2 was used for data analysis and peak review of chromatograms. Semiquantitative evaluation of all metabolites was performed based on external standards and normalized data were analyzed by using MetaboAnalyst software (Xia et al., 2015; Xia and Wishart, 2011).

3.11 Total and mitochondrial DNA quantification

Total genomic and mtDNA were isolated using genomic DNA from tissues kit (Macherey-Nagel, 740952.250). Briefly, samples were scraped from dishes or collected from metabolomic analyses as described above and spun at 1000g for 3 min at 4°C. Cells were then lysed in 200µl of buffer B3 at 70°C for 10 min. We subsequently added 210µl of 100% EtOH and transferred samples on silica columns. After spinning at 11000g for 1 min, samples were washed twice with BW and B5 buffers and spun at 11000 for 2 min. Finally, samples were eluted in 70µl of RNase free water

and quantified by UV spectrophotometry. Total DNA was used to normalize metabolomics data, while qPCR analyses were performed to assess mtDNA levels.

3.12 Oxygen consumption assessment

Oxygen consumption analyses were performed by using a Clark type oxygen electrode (Hansatech, DW1 electrode chamber). Confluent, 2 days or 4 days differentiated C2C12 were rinsed in pre-warmed PBS (37°C) and resuspended in coupled respiration buffer (2% FFA-BSA, 1mM Na-pyruvate, 25 mM D-glucose, 40 µg/ml digitonin) or electron flow buffer (2% FFA-BSA, 10 mM Na-pyruvate, 2mM malate, 4µM carbonyl cyanide m-chlorophenyl hydrazine (CCCP), digitonin 40µg/ml). Samples were then transferred to the electrode chamber for the oxygen consumption rate measurement. After measuring basal respiration, uncoupled and maximal respiration were evaluated by adding 2.5mM oligomycin and 1mM CCCP, respectively. Complex I, II and IV activity was evaluated through the electron flow protocol. Once transferred into the chamber, CI activity was evaluated. After 10µM rotenone and 5mM succinate addition, we assessed complex II activity. We then added 100µM antimycin A and 20 mM/0.8 mM Ascorbate/N,N,N',N'-tetramethyl-p-phenylenediamine (TMPD) to measure complex IV activity. All samples values were normalized on total protein content.

3.13 C2C12 myoblasts transfection and co-transfection

We transfected C2C12 myoblasts with a retro-transfection approach. First, we incubated 1.25µg of cDNA (pcDNA3 empty vector, Pgc-1α and Zc3h10) with Fugene6 (Promega, E2691) at 1:5 µg/µl ratio in 50µl of DMEM media without antibiotics and serum. After 30 min, we added 100000 cells resuspended in 50µl of DMEM media to each mix and incubated the solution for 40 min at RT. We finally added 900µlof complete media and seeded 100µl of transfection solution per well in black 96-well plates. Co-transfection of pcDNA3 empty vector, Pgc-1α and Zc3h10 with pTK-luc or pTK-Tfam promoter-luc plasmids was performed as described above. We transfected 2µg of total DNA (2 parts of cDNA and 1 part of reporter plasmid) with lipofectamine 2000 (Thermo Scientific, 11668027) at 1:2.5 ratio µg/µl.

3.14 ATP content measurement

The ATP production was analyzed 60 hours after transfection of C2C12 myoblasts using a specific kit (Perkin Elmer, 6016941). Before assessing ATP levels, we set up the following solutions:

1. Oligomycin 5 µM in serum free DMEM media

2. DMSO 5 µM in serum free DMEM media
3. Standard curve solutions: ATP 50, 5, 0.5, 0.05, 0.005, 0.0005 µM in PBS
4. ATP buffer solution

We treated samples with solutions 1 or 2 at 37° C for 24 hours (100µl/well).We the aliquoted 50µl of solution 4 in each well together with standard curve solutions. After 2 min of incubation at RT on orbital shaker, we measured luminescence (EnVision, PerkinElmer) to calculate cytosolic and total ATP production. Mitochondrial ATP was inferred from previous measurements. Data were normalized on total protein content.

3.15 Tfam-promoter activity assay

The Tfam promoter activity or the pTK-LUC was analyzed 24 hours after co-transfection of C2C12 myoblasts in 96 multi-well plates. We removed media and washed cells once with PBS. We then added 50ul of fresh Britelite solution prepared according the manufacturer's instructions and incubated2 min before measuring luminescence intensity (Perkin Elmer, EnVision). Data were normalized on total protein content.

3.16 Cell proliferation assay

Cells were seeded at a density of 2 x 10^5 per well and incubated in complete media. Twenty-four hours later, cells were scraped and resuspended in 10ml of PBS or transfected with scramble or ShZc3h10 sequence. 500 µl of resuspended cells were used for cell count by Z2 beck man coulter and considered as blank. 30 hours and 60 hours later scramble and ShZc3h10 transduced cells proliferation was analyzed as well.

3.17 Iron quantification

Intracellular ferric (Fe^{3+}) and total iron content were evaluated through cytochemistry and spectrophotometry analyses.

3.17.1 Ferric iron content assay

Cells were first washed once with PBS and then fixed in 10% formalin for 15 min at RT. After fixation, samples were incubated with 20% hydrochloric acid and 5% potassium ferrocyanide (Prussian blue staining) for 30 min. Cells were then extensively washed under ddH_2O. After microscopic analysis, ferric iron was quantified by using imageJ software ver. 1.6.0.

3.17.2 Total iron content measurement

Ferric iron and total iron levels were also measured as previously demonstrated (Riemer et al., 2004). Samples were washed with PBS and lysed in 250µl 50mM NaOH. We proceeded by sonication at 20% for 10 sec and spinning at 5000g for 5 min. 100µl of each samples were equally loaded in 2 96-well plate wells. 50µl of 10mM HCl together with 12.5µl ferrous iron buffer (6.5 mM ferrozine (Sigma Aldrich, 160601) and 2.5 M ammonium acetate) or 12.5µl of total iron buffer (6.5 mM ferrozine, 2.5 M ammonium acetate, and 1 M ascorbic acid). Samples were incubated for 30 min and absorbance measured at 570nm. Iron concentration was obtained comparing absorbance values to a standard curve built with $FeCl_3$ as follows:

Standard #	Volume of 1mM iron standard (µl, $FeCl_3$)	H20 (µl)	Final volume in well (µl)	Final iron concentration (nmol/well)
1	0	300	100	0
2	6	294	100	2
3	12	288	100	4
4	18	282	100	6
5	24	276	100	8
6	30	270	100	10

3.18 Statistical analysis

Statistical analyses were performed with Student's t test or one-way ANOVA followed by Dunnett's Post Test when necessary using GraphPadPrism version 6.0.

4. Preliminary results

The mitochondrial regulators described so far act by modulating the expression levels of Tfam, either in a direct or indirect fashion. For this reason, the activation of Tfam promoter by a high-throughput screening represents a good tool to identify new mitochondrial regulatory factors and/or pathways. To dissect new features of the genome, the Genomics Institute of the Novartis Research Foundation (GNF) developed technology to evaluate the role of genes in a high-throughput manner in cell-based assays. Specifically, GNF assembled genome-wide cDNA and siRNA collections, arrayed them in 384-well format, also developing robotics/automation and procedures to manipulate and evaluate gene activity in transfected cells in a high-throughput screening (HTS) manner.

In collaboration with the GNF, we used this technology to identify genes that modulate mitochondrial number and function. To this end, two cDNA libraries accounting for 70% of known genes (MGCv2, mouse and human; Origene, mouse and human) were overexpressed by transient transfection in HEK 293 cells. Single cDNAs were co-transfected with the reporter system described in Fig. 4.1, in order to evaluate their ability to control Tfam promoter activity.

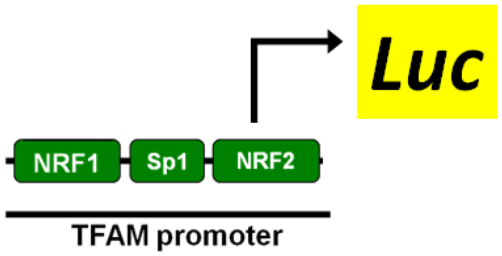

Fig. 4.1 Schematic representation of Tfam promoter reporter system. Luciferase cDNA was cloned downstream of Tfam promoter and used as readout in the primary HTS.

As positive controls, we selected PGC-1α and SIRT1 cDNAs and Mybbp1a cDNA as negative control. Libraries were screened in duplicate and data were evaluated to select hits. A hit is considered if it regulated Tfam expression more than empty vector. The genomic HTS yielded 441 clones able to induce and 300 clones able to reduce Tfam promoter activity (Fig. 4.2A). We then focused our attention on positive hits. Hence, we confirmed all 441 positive hits by analyzing mitochondrial function and density after their transient overexpression and flow cytometry analysis in a secondary screening.120 positive candidates were confirmed to modulate mitochondrial density and activity in HEK293 cells (Fig. 4.2B).

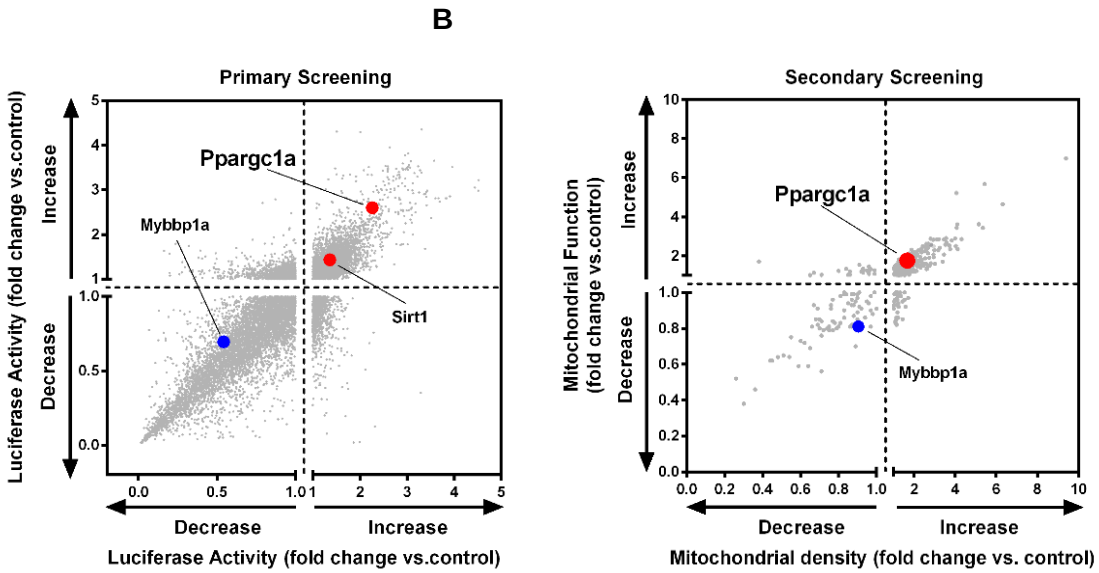

Fig. 4.2 Scatter plot of HTS in HEK293. A) HEK293 were co-transfected with cDNA libraries and Tfam-promoter reporter system. From primary HTS, 441 positive hits and 300 negative hits were obtained. B) In the secondary screening, positive hits were confirmed in HEK293 cells by flow cytometry analyses after staining with Mitotracker Green and Mitotracker CM-H2X-ROS, two indicators of mitochondrial density and function, respectively.

To narrow down the number of possible candidates, we selected those hits significantly expressed in skeletal muscle and C2C12 myotubes (Fig. 4.3A). This analysis was conducted interrogating the BioGPS database (The Scripps Research Institute, Ver. 2FDC271) and data previously obtained in our lab, respectively. In addition, we chose only those hits still not associated with mitochondrial physiology and belonging to different protein classes (Fig. 4.3B). From this analysis, we selected 20 candidates for further investigations in C2C12 myoblasts.

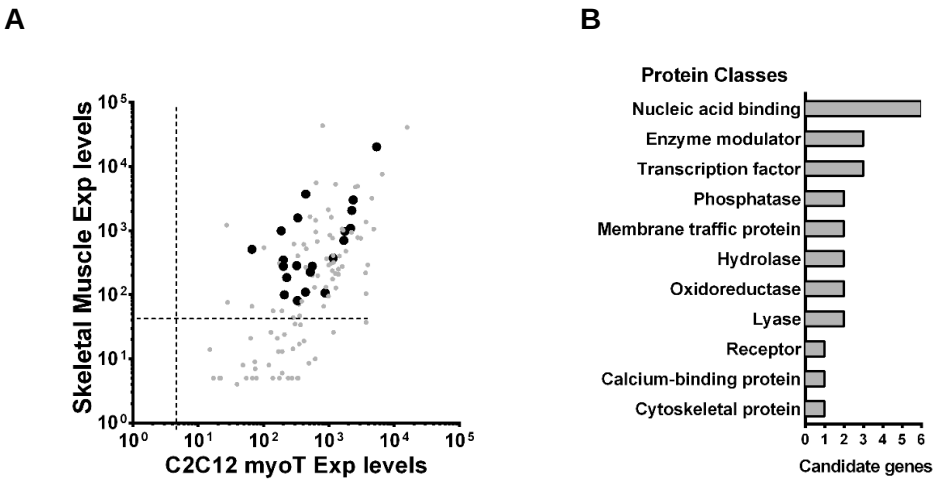

Fig. 4.3 Scatter plot of 21 selected hits. Hits were selected based on their expression levels in C2C12 cells and skeletal muscle, on their protein class and lack of association to mitochondrial physiology.

The 20 candidates were transiently overexpressed in proliferating myoblasts. After 48 hours from transfection, cells we assessed oxygen consumption rate, as marker of mitochondrial activity, and mtDNA levels, as marker of mitochondrial density, to identify the most promising hit. The scatter plot in fig. 4.4 indicates that all 21 candidates increase both mitochondrial function and mitochondrial density compared to control and that the best hit is Zinc finger CCCH-type containing 10. Notably, Zc3h10 upregulates mitochondrial density more than 2.5 fold and mitochondrial function almost of 2 fold. For these reasons, we decided to better characterize the biological role of Zc3h10 and its impact on mitochondrial biology.

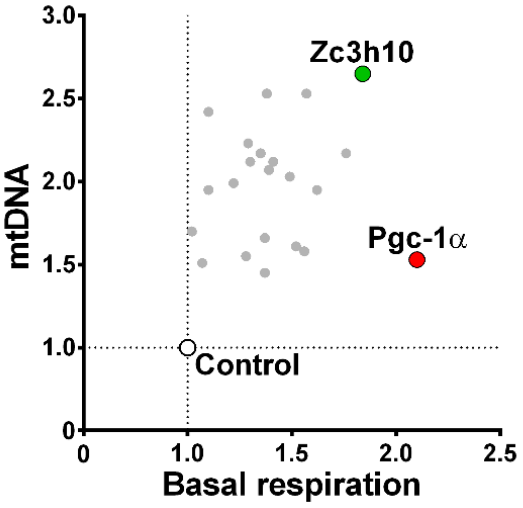

Fig. 4.4 Scatter plot of the transiently transfected 21 most valuable hits in C2C12 myoblasts. MtDNA and basal respiration were used as parameters of mitochondrial density and function, respectively. All experiments were performed on three biological replicates.

5. Results

5.1 Zc3h10 gene and protein sequences are highly conserved among different species

We first analyzed human ZC3H10 gene by UCSC Genome Browser webtool (Human genome hg38). As shown in fig. 5.1, ZC3H10 is localized in chromosome 12 and consists of 3 exons and 2 introns. The coding sequence (CDS) is present uniquely in exon 3 and in only one of the four alternative splicing isoforms. Alignment of vertebrates' genomes demonstrates that human (h)ZC3H10 CDS sequence is highly conserved between different species.

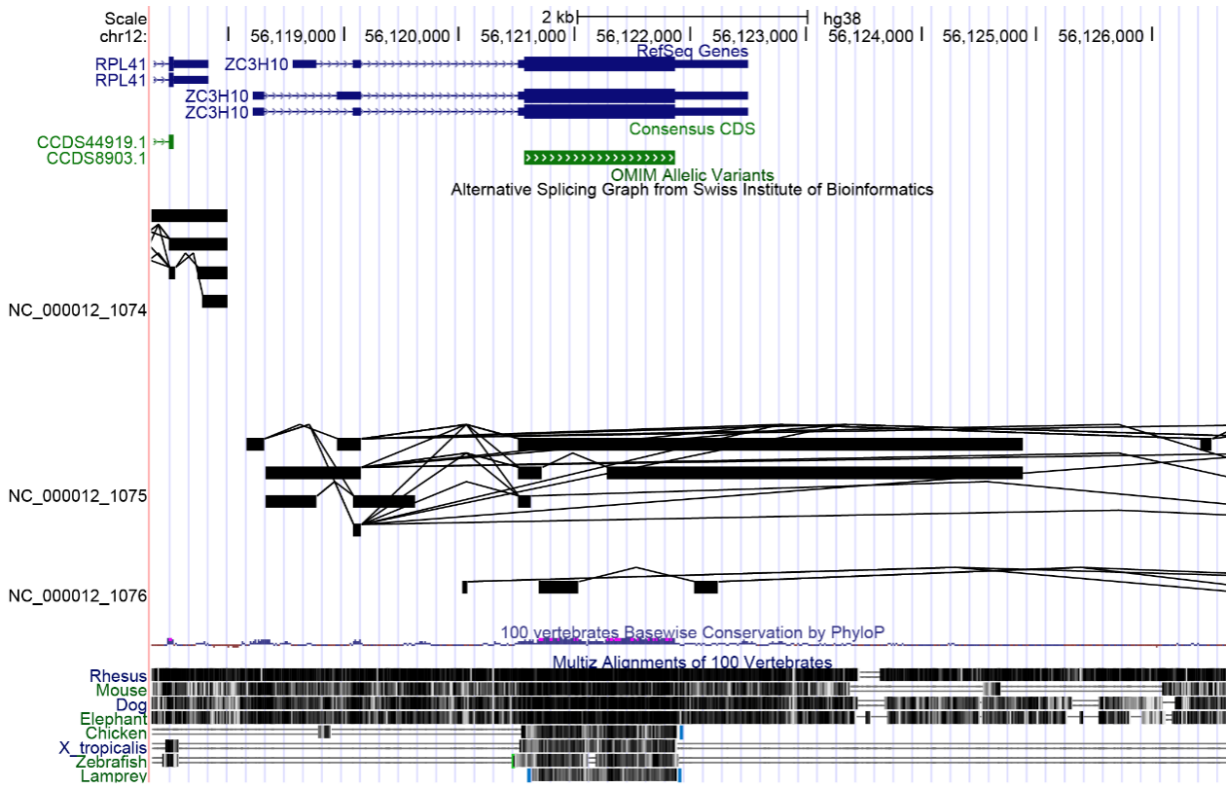

Fig. 5.1 UCSD Genome browser hZC3H10representation. From top to bottom, we analyzed gene structure, CDS sequence (CCDS8903.1), alternative splicing isoforms (NC_000012_1075) and sequence conservation among 8 vertebrate species.

We later characterized the gene expression levels of Zc3h10 in different mouse tissues (Fig. 5.2). Our data indicate that our candidate is widely expressed in mouse tissues with lower levels in visceral white adipose tissue (viWAT) and higher levels in the brain, specifically in the cortex, cerebellum and hypothalamus. Most importantly, Zc3h10 is expressed also in several skeletal muscles (i.e. vastus lateralis, gastrocnemius and soleus) of 12 weeks old mice (Fig. 5.2).

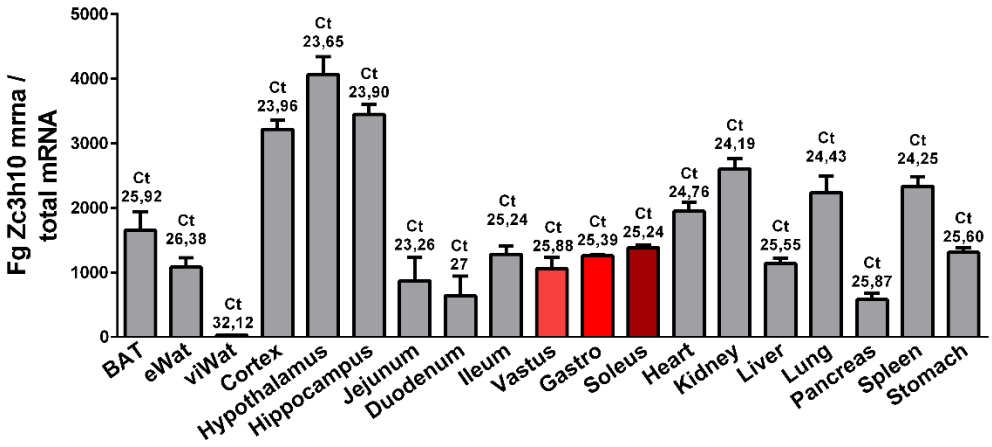

Fig. 5.2 Zc3h10 gene expression in mouse tissues. Zc3h10 expression levels were compared to a standard curve built with known content of Zc3h10 cDNA. Data are expressed as femtograms of Zc3h10 on total RNA content of qPCR samples. n=4.

Since we used mouse (m)Zc3h10 cDNA in the HTS and that human and mouse are the most represented *in vivo* systems used in research, we also compared hZC3H10 and mZc3h10 protein sequences by UniProt database (Fig. 5.3. As shown, data indicates that human and mouse Zc3h10 homologues share 97.011% of protein sequence, corroborating the high homology of exon 3 and suggesting that Zc3h10 mechanism of action might be highly conserved among different species.

```
Q96K80 ZC3HA_HUMAN      1    MPDRDSYANGTGSSGGGPGGGGSEEASGAGVGSGGASSDAICRDFLRNVCKRGKRCRYRH   60
Q8R205 ZC3HA_MOUSE      1    MPDRDSYANGTGSSGGGPGGGGSEEASGAGTGSGGATSDAICRDFLRNVCKRGKRCRYRH   60
                             ******************************.*****:**********************

Q96K80 ZC3HA_HUMAN     61    PDMSEVSNLGVSKNEFIFCHDFQNKECSRPNCRFIHGSKEDEDGYKKTGELPPRLRQKVA  120
Q8R205 ZC3HA_MOUSE     61    PDMSEVSNLGVSKNEFIFCHDFQNKECSRPNCRFIHGSKEDEDGYKKTGELPPRLRQKVA  120
                             ************************************************************

Q96K80 ZC3HA_HUMAN    121    AGLGLSPADLPNGKEEVPICRDFLKGDCQRGAKCKFRHLQRDFEFDARGGGGTGG-GSTG  179
Q8R205 ZC3HA_MOUSE    121    AGLGLSPADLPNGKEEVPICRDFLKGDCQRGAKCKFRHLQRDFEFDARGGGGTGGGGSTG  180
                             ************************************************** ****

Q96K80 ZC3HA_HUMAN    180    SVLPGRRHDLYDIYDLPDRGFEDHEPGPKRRRGGCCPPDGPHFESYEYSLAPPRGVECRL  239
Q8R205 ZC3HA_MOUSE    181    SAPPGRRHDLYDIYDLPERGFEDHEPGPKRRRGGCCPPDGPHFESYECNLAPLRGVECRL  240
                             *. **************:****************************** .*** *******

Q96K80 ZC3HA_HUMAN    240    LEEENAMLRKRVEELKKQVSNLLATNEVLLEQNAQFRNQAKVITLSSTAPATEQTLAPTV  299
Q8R205 ZC3HA_MOUSE    241    LEEENALLRKRVEELKKQVSNLLATNEVLLEQNAQFRNQAKVMTLSSTAPATEQTLAPTV  300
                             ******:**********************************:*****************

Q96K80 ZC3HA_HUMAN    300    GTVATFNHGIAQTHTTLSSQALQPRPVSQQELVAPAGAPAAPPTNAAPPAAPPPPPPHLT  359
Q8R205 ZC3HA_MOUSE    301    GTVATFNHGIAQTHTTLSSQALQPRPVSQQELVAPTGAPAAPPTNAAPPAAPPPPPPHLN  360
                             **********************************:**********************.

Q96K80 ZC3HA_HUMAN    360    PEITPLSAALAQTIAQGMAPPPVSMAPVAVSVAPVAPVAVSMAQPLAGITMSHTTTPMVT  419
Q8R205 ZC3HA_MOUSE    361    PEITPLSAALAQTIAQGMAPPPVSMAPVAVSVAPVAPVAVSMAQPLAGITMSHTTTPMVT  420
                             ************************************************************

Q96K80 ZC3HA_HUMAN    420    YPIASQSMRITAMPH                                              434
Q8R205 ZC3HA_MOUSE    421    YPIASQSMRITAMPH                                              435
                             ***************
```

Fig. 5.3 UniProt alignment of hZC3H10 (ID Q96K80) and mZc3h10 (ID Q8R205). Dots indicate similar aminoacids while asterisks indicate identical aminoacids. Protein localization of each aminoacid is indicated by numbers beside sequence.

Further analyses carried out by ExPASy database indicate the presence of a glycine-rich domain and three zinc fingers in the N-terminal portion, a coiled-coil domain in the center and a poly-glycine and a proline-rich domain at the C-terminal of both human and mouse Zc3h10 (Table 5.1). This analysis corroborates previous results (Liang et al., 2008; Peng et al., 2012) and our hypothesis that both Zc3h10 gene and protein are conserved through different vertebrate species.

hZc3h10 (434 AA)		mZc3h10 (435 AA)	
Domain	**AA**	**Domain**	**AA**
Gly-rich	10-35	Gly-rich	10-35
Zinc finger 1	36-63	Zinc finger 1	36-63
Zinc finger 2	73-99	Zinc finger 2	73-99
Zinc finger 3	134-161	Zinc finger 3	134-161
Coiled coil	234-280	Coiled coil	235-281
Poly-gly	169-176	Poly-gly	169-177
Pro-rich	323-396	Pro-rich	324-397

Table 5.1 hZc3h10 and mZc3h10 protein sequences are conserved. ExPASy analysis was performed by comparing hZc3h10 and mZc3h10 primary sequences.

5.2 Myoblast Tfam expression and mitochondrial activity are positively regulated by Zc3h10

We proceeded by validating HTS results analyzing Tfam promoter activity and Tfam expression after Zc3h10 transient overexpression in murine myoblasts. From fig. 5.4A, it appears that Zc3h10 upregulation increases Tfam promoter activity (Fig. 5.4B) and promotes Tfam expression (Fig. 5.4C & D) 48 hours after transfection, confirming HEK293 data.

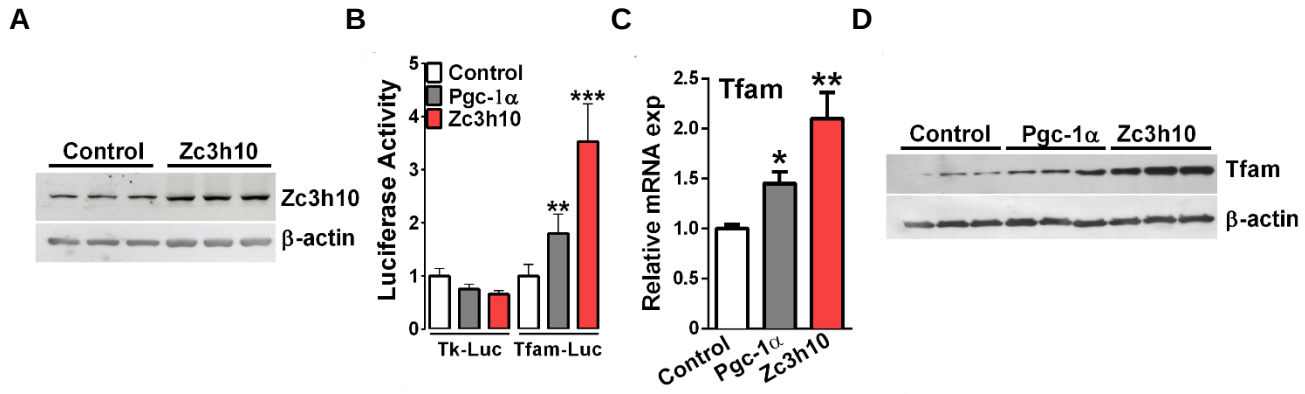

Fig. 5.4 HTS validation in C2C12 cells. Myoblasts co-transfected with Zc3h10 and Pgc-1α were used to assess Tfam promoter activity (B), Tfam gene expression (C) at 24 hours from transfection and protein expression (D) 48 hours from transfection. One way ANOVA followed by Dunnett's multiple comparison test, *p<0.05, **p<0.01, ***p<0.001 vs control (cells transfected with the empty vector pcDNA3). n=8.

We later dissected the effect of Zc3h10 overexpression on mitochondrial function. As we have already shown (Fig. 4.4), Zc3h10 overexpression increases mitochondrial activity in HEK293 cells assessed by basal cellular respiration (Fig. 4.4A). Our results indicate that Zc3h10 overexpression increases mitochondrial function, evaluated by basal, uncoupled and maximal uncoupled respiration (Fig. 5.5A). As expected, the upregulation of mitochondrial function leads to increased levels of total ATP content, whose main contribution is given by mitochondrial ATP (Fig. 5.5B). In addition, western blot analysis of some subunits of the electron transport chain indicates that the upregulation of mitochondrial function is due to higher levels of ETC complexes expression (Fig. 5.5C).

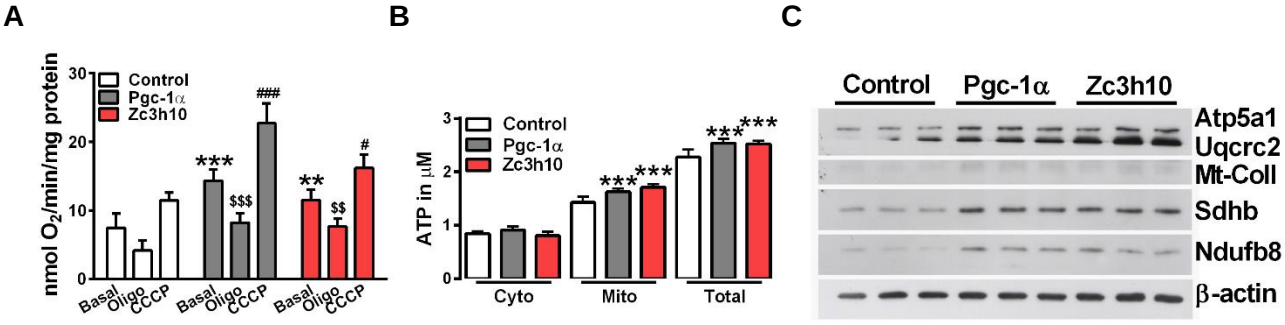

Fig. 5.5 Zc3h10 is a positive regulator of mitochondrial function in myoblasts. Basal, uncoupled and maximal uncoupled respiration (A) were evaluated 48 hours from transfection to assess mitochondrial function. Proteins were used for data normalization and western blot analysis (C) of Atp5a1, Uqcrc2, mt-CoII, Sdhb and Ndufb8 relative content. Cytosolic ATP and mitochondrial ATP concentration were evaluated 48 hours from transfection in 5 μM oligomycin treated cells and untreated cells, respectively. Panel A: One way ANOVA followed by Dunnett's multiple

comparison test, **p<0.01, ***p<0.001 vs control. $^{$$}$p<0.01, $^{$$$}$p<0.001 vs control oligomycin; $^{\#}$p<0.05, $^{\#\#\#}$p<0.001 vs control CCCP. n=6. Panel B: One way ANOVA followed by Dunnett's multiple comparison test, ***p<0.001 vs control of each experimental group. n=6.

5.3 Zc3h10 is upregulated at the beginning of C2C12 myoblasts differentiation

We later assessed Zc3h10 expression levels and its localization during C2C12 differentiation to myotubes. As shown in fig. 5.6A and B, Zc3h10 is upregulated in the first phases of myotubes differentiation, raising the hypothesis that Zc3h10 be in some way associated with the beginning of myofiber development.

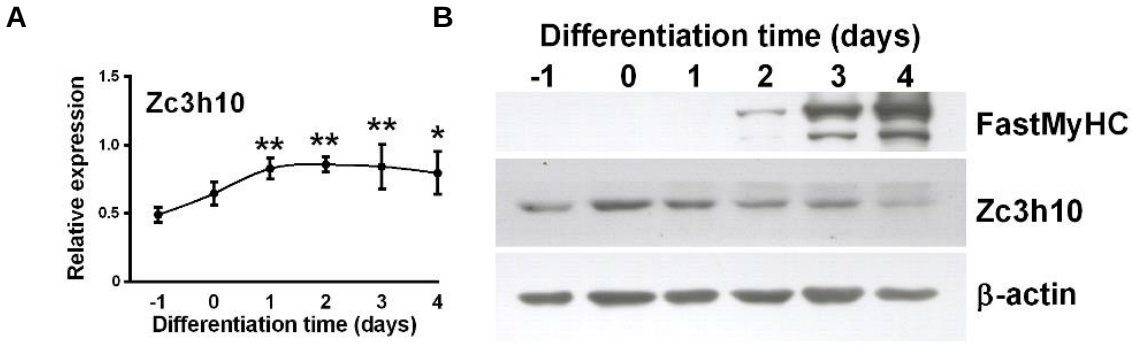

Fig. 5.6 Zc3h10 is upregulated with differentiation induction. Both gene (A) and protein (B) expression were performed at different time points, specifically from 1 day before to 4 days after differentiation induction. One way ANOVA followed by Dunnett's multiple comparison test, *p<0.05, **p<0.01 vs day -1. n=3.

We then analyzed Zc3h10 protein levels in adult human quadriceps, 12 weeks, 6 months and 12 months old mice by immunofluorescence. As shown in fig. 5.7A, our results suggest that Zc3h10 is present only in neonatal MHC^{+} and fetal MHC^{+} myocytes. Additionally, IF analyses on mice quadriceps suggests that Zc3h10 expression decreases during aging (Fig. 5.7B).

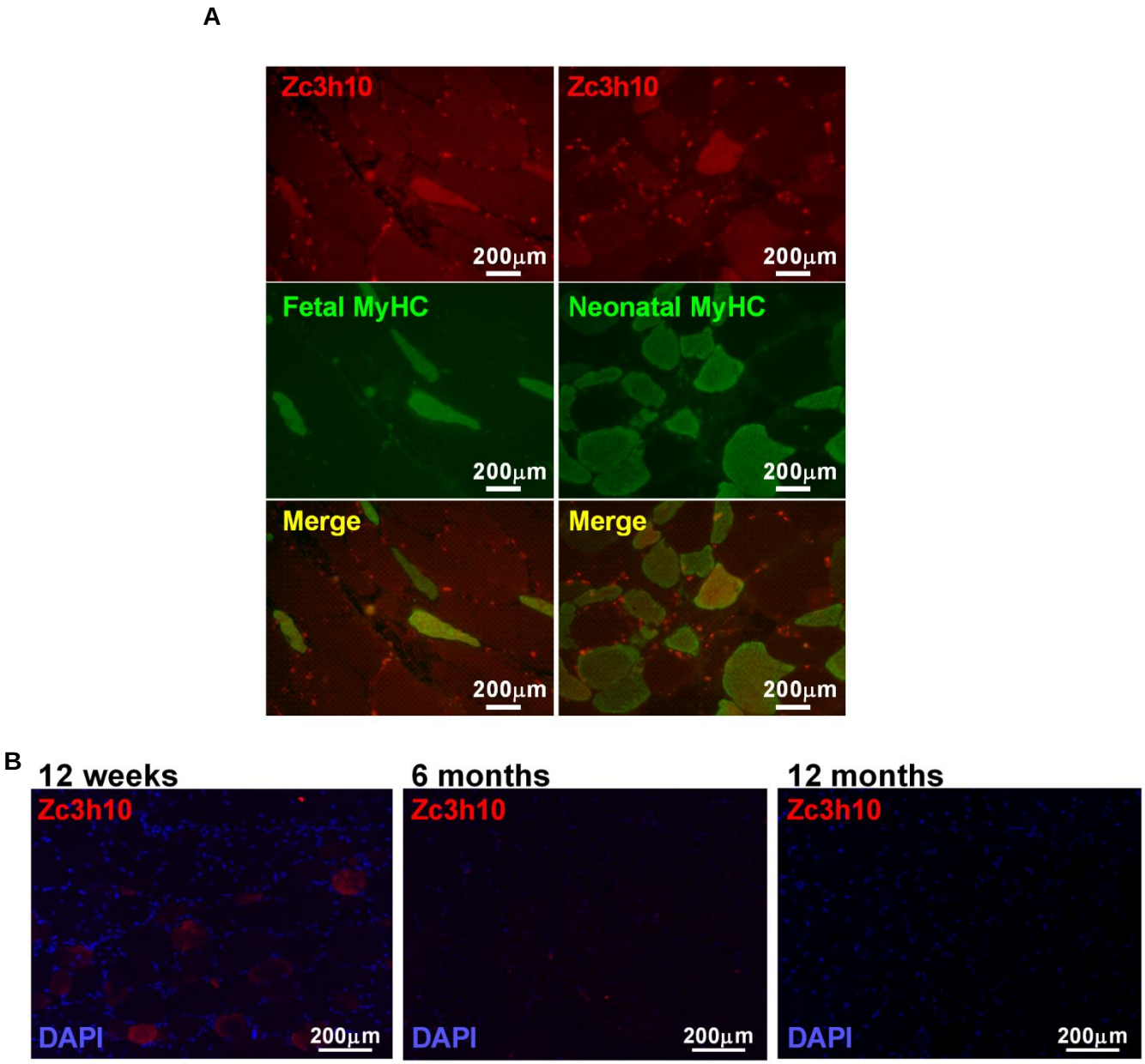

Fig. 5.7 Zc3h10 expression levels in human and mice quadriceps. IF images performed on an adult male subject, 12 weeks, 6 months and 1 year old mice.

5.4 Zc3h10 is a nuclear protein

We proceeded by verifying the subcellular localization of Zc3h10. cNLS mapper software (Fig. 5.8A) suggests the presence of two monopartite signals (recognized by α-importin (Van Dusen et al., 2010)) within the middle region with a score of 15/15. We then isolated C2C12 nuclei from cytoplasm to validate cNLS prediction. Western blot analysis (Fig. 5.8B) clearly indicates that Zc3h10 is a nuclear protein through all myotube formation process, while IF analysis (Fig. 5.8C) suggests that a fraction of Zc3h10 is localized in the perinuclear zone. This data are coherent with a role of Zc3h10 in nuclear RNA metabolism and transport to cytoplasm.

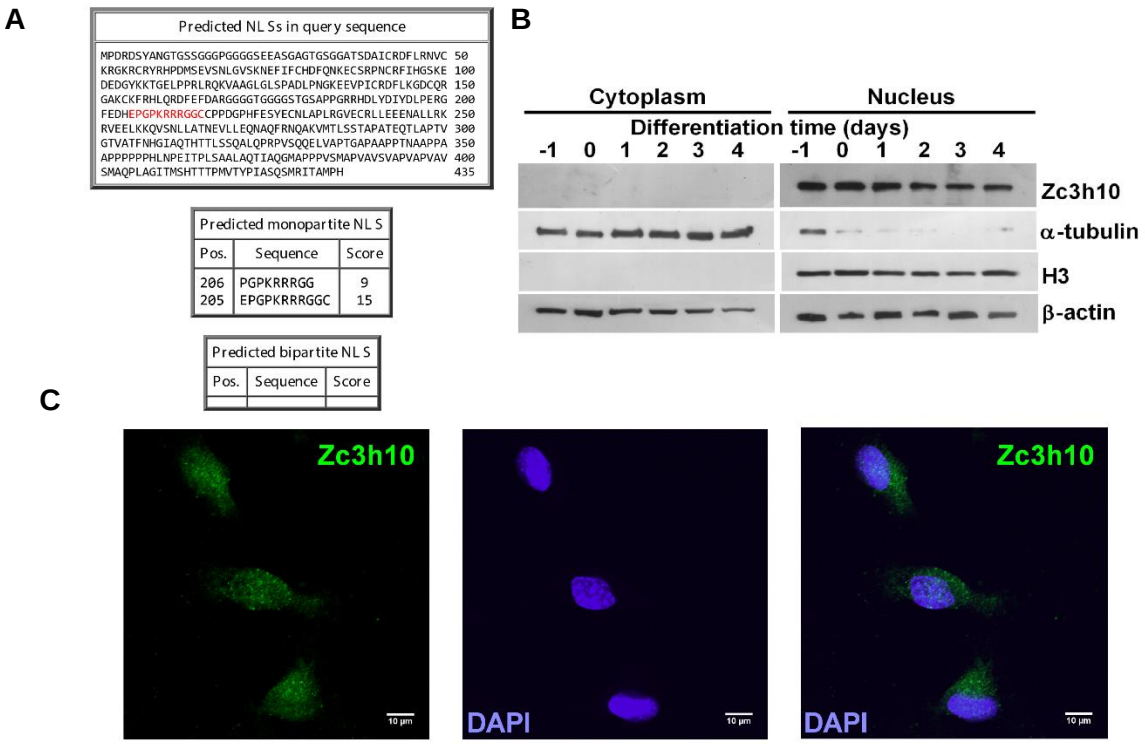

Fig 5.8 Zc3h10 is a nuclear protein. cNLS database was set up with 6.0 of cutoff (A) and the middle region NLS was highlighted in red. Nuclear and cytoplasm extracts of myoblast and myotubes were loaded on SDS-Page to validate cNLS prediction (B), while IF images were obtained in proliferating myoblasts (C).

5.5 Downregulation of Zc3h10 affects mitochondrial function in myoblasts

To better understand the role of Zc3h10 on mitochondrial function, we downregulated it through short hairpin RNA interference in C2C12 myoblasts (pre-differentiation protocol, Fig. 3.1). qPCR, western blot and IF results indicate that we repressed Zc3h10 by 50% compared to control cells (cells infected with scrambled shZc3h10) (Fig. 5.9A - C).

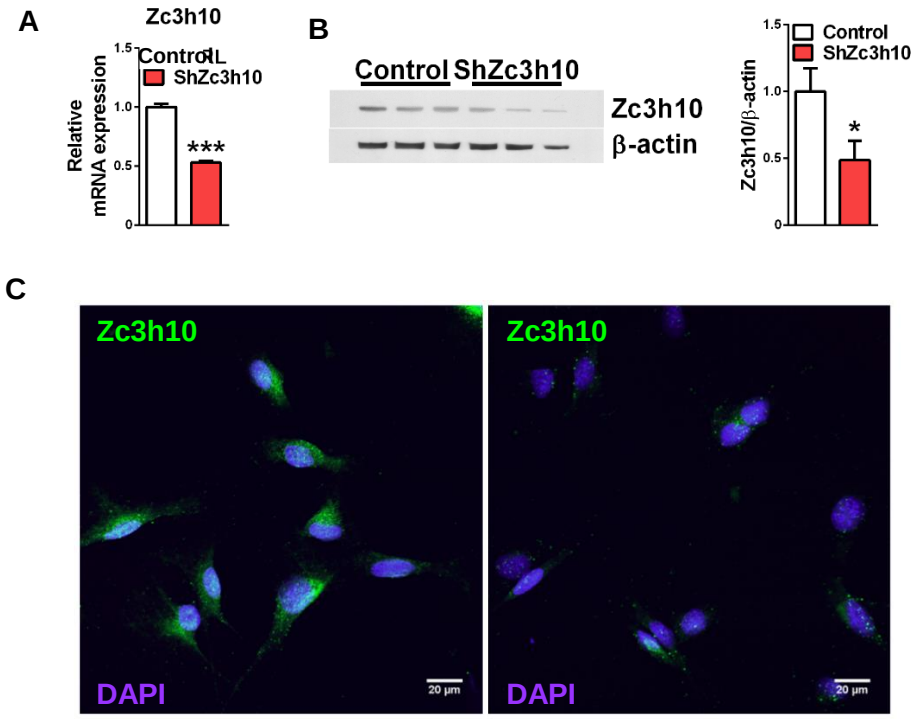

Fig 5.9 Validation of Zc3h10 downregulation. qPCR analysis of Zc3h10 (A), Zc3h10 western blot normalized on β-actin (B) and IF against Zc3h10 (green) and chemical staining of nuclei (blue) (C). Panel A: Student's t-test, *p<0.05, ***p<0.001 vs control, n=6. Panel B: Student's t-test, *p<0.05, ***p<0.001 vs control. n=3.

We then focused our attention on mitochondrial activity in ShZc3h10 cells. Unexpectedly, the downregulation of our hit did not lead to lower levels of mtDNA, indicating no differences in mitochondrial density (Fig. 5.10A). On the other hand, Zc3h10 partial silencing significantly decreases mitochondrial function as indicated by lower levels of basal, uncoupled and maximal uncoupled respiration (Fig. 5.10B). The reduced expression of mitochondrial activity is likely due to the lower expression of OXPHOS subunits, specifically Ndufb8 (Complex I), Sdhb (Complex II), and Mt-CoII (Complex IV) (Fig. 5.10C). Mass spectrometry analysis of ATP, ADP, and AMP intracellular levels showed that our candidate is a positive regulator of ATP production, corroborating the results described in figure 5.4B. Indeed, Zc3h10 downregulation led to lower levels of ATP together with higher levels of both ADP and AMP, leading to a lower adenylate energy charge (Fig. 5.910 and E).Taken together, these data demonstrate that the downregulation of Zc3h10 is sufficient to decrease energy supply in these cells by suppressing ETC activity.

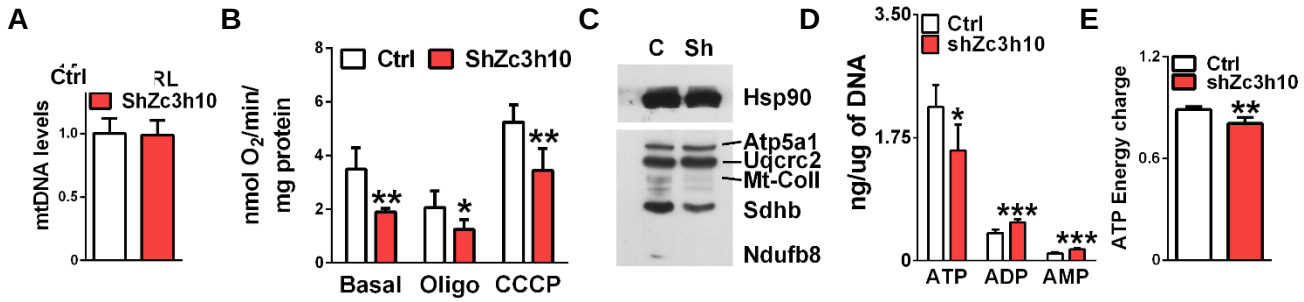

Fig. 5.10 Zc3h10 reduced expression impairs mitochondrial function in myoblasts. MtDNA levels were analyzed to assess mitochondrial density (A). Mitochondrial function was evaluated by cell respiration (B), expression levels of OXPHOS subunits (C), intracellular levels of ATP, ADP, AMP (D) and the energy charge index (E). Student's t-test, *p<0.05, *p<0.01, ***p<0.001 vs control. n=6.

5.6 Zc3h10 controls energy metabolism transcriptomic profile in myoblasts

According to literature (Castello et al., 2012; Ray et al., 2013) we know that Zc3h10 is an mRNA binding protein active in the first phases of cell differentiation. Hence, we decided to perform a comprehensive transcriptomic and metabolomic analysis in confluent myoblast to dissect the role which pathways are mainly regulated by Zc3h10. To this end, we integrated results from microarray analysis, new synthesis and total RNA-seq analyses, and mass spectrometry metabolomics.

We first analyzed the total RNA profile in control and ShZc3h10 myoblasts. Our results suggest that Zc3h10 repression leads to the misregulation of total RNA levels of 1526 (12% of total expressed genes) genes. Of 1526, 1195 are downregulated and the 331 are upregulated (Fig. 5.10). In addition, bioinformatic analyses based on KEGG database indicate that calcium signaling is the most enriched pathway among upregulated genes. On the other hand, TCA cycle, purine metabolism, one carbon pool by folate and nicotinate and nicotinamide metabolism are the most affected pathways in Zc3h10 reduced cells (Fig. 5.11).

Taken together, these data suggest that partial loss of Zc3h10 leads to a significant change of transcriptomic profile in myoblasts, predominantly through the regulation of mRNA processing and splicing.

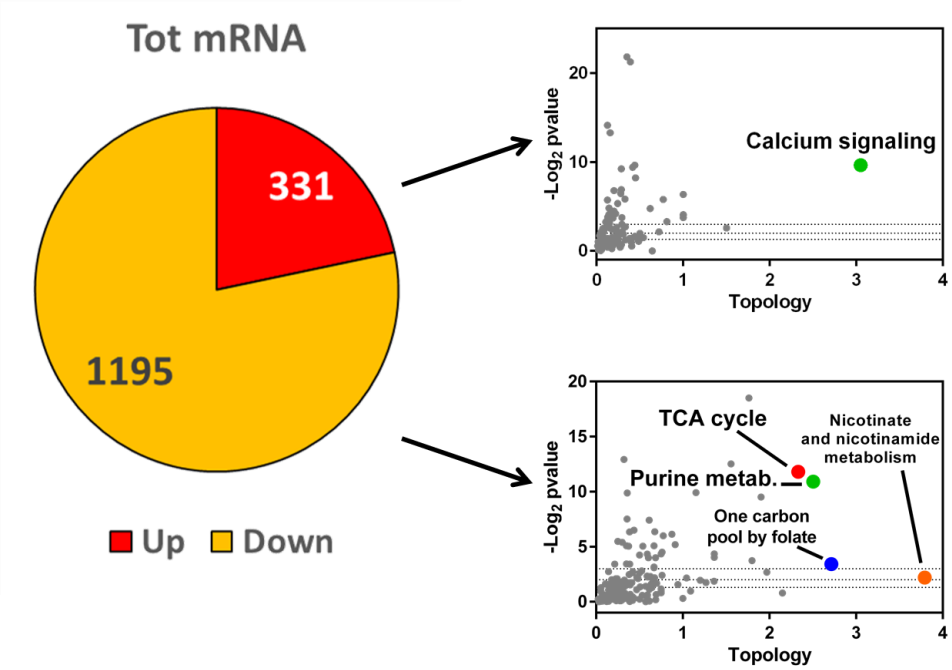

Fig. 5.11 Zc3h10 regulates RNA metabolism. Total RNA levels (Reads Per Kilobase per Million, RPKM) were interrogated by MetaboAnalyst software to analyse the most enriched pathways. Horizontal dot lines correspond, from top to bottom, to the Log2 of p-value of 0.001, 0.01 and 0.05, respectively. n=3.

5.7 Zc3h10 silencing impacts myoblasts metabolic profile

Since mitochondrial regulators modulate the metabolic profile (Li et al., 2012; Montanez et al., 2013; Vernochet et al., 2012), we also evaluated the intracellular levels of products belonging to the main metabolic pathways (i.e. glycolysis, TCA cycle, pentose phosphate pathway (PPP) and β-oxidation). Principal component analysis (PCA) and hierarchical clustering revealed that ShZc3h10 cells possess different metabolic profiles (Fig.5.12A and B).

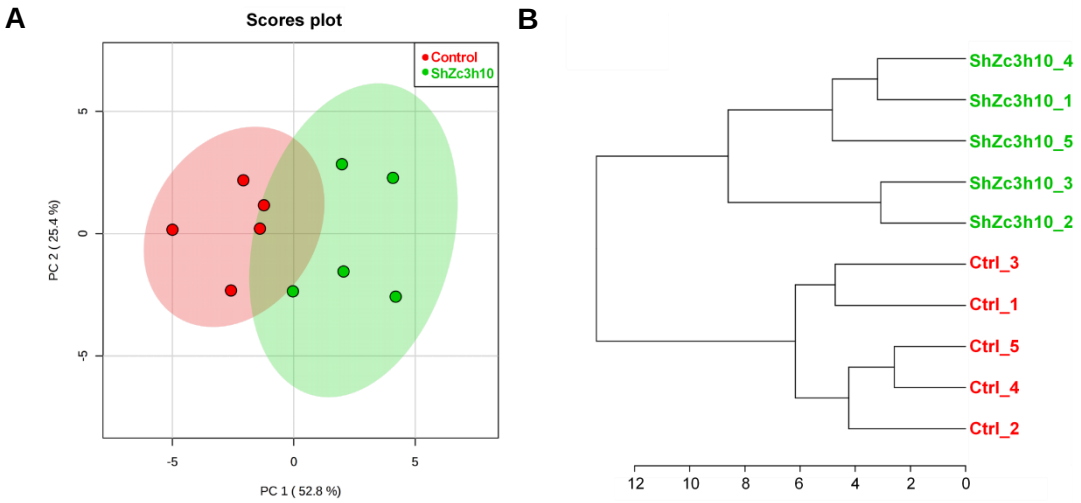

Fig 5.12 Zc3h10 silencing impacts metabolic landscape of myoblasts. MetaboAnalyst webtool was used to calculate principal component analysis (PCA) (A) and hierarchical clustering (B) of metabolomic analysis in control (Red) and ShZc3h10 (Green) samples.

Specific evaluation of metabolomics data indicates that Zc3h10 downregulation mainly affects glycolysis and TCA cycle metabolites levels. In fact, ShZc3h10 cells show lower levels of glyceraldehyde-3P and pyruvate, but also α-ketoglutarate, fumarate, malate and oxaloacetate. On the contrary, AMP, ADP and succinate levels are significantly increased (Fig. 5.13).

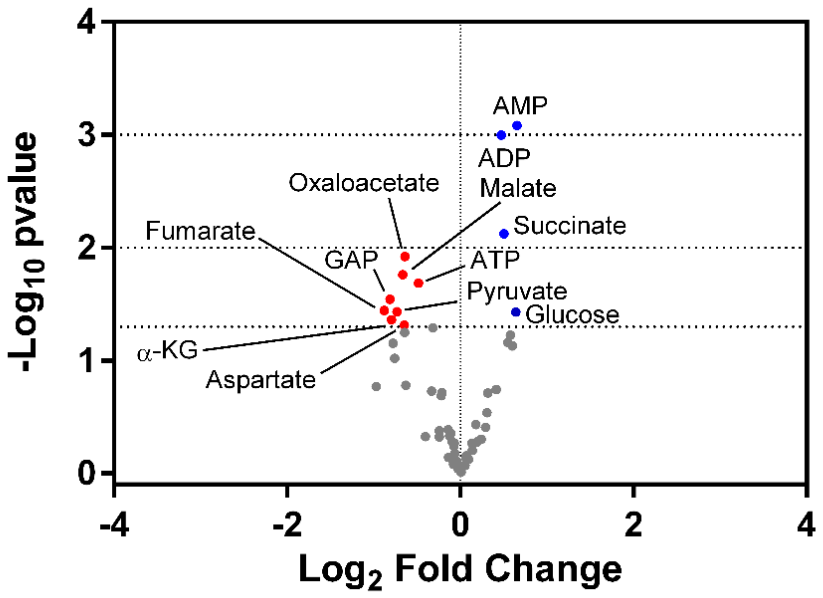

Fig 5.13 Zc3h10 silencing leads to an overall decrease of important metabolites belonging to the main energetic pathways. The graph correlates the p-Value (Log10 scale, Y Axis) and the fold change (Log2 scale, X axis). Red dots indicate significantly downregulated metabolites and blue dots indicate upregulated metabolites, respectively. Horizontal dot lines correspond, from top to bottom, to the Log10 of p-value of 0.001, 0.01 and 0.05, respectively.

To better understand which metabolic pathways are mainly affected by Zc3h10 silencing, we integrated metabolomic and transcriptomic data with total RNA and new synthesis RNA levels. Integration of different "-omics" data is now rising as a fundamental tool to better understand the role of specific factors in wide biological structures and dynamics. Data shown in figure 5.14 demonstrate that Zc3h10 significantly impairs TCA cycle pathway.

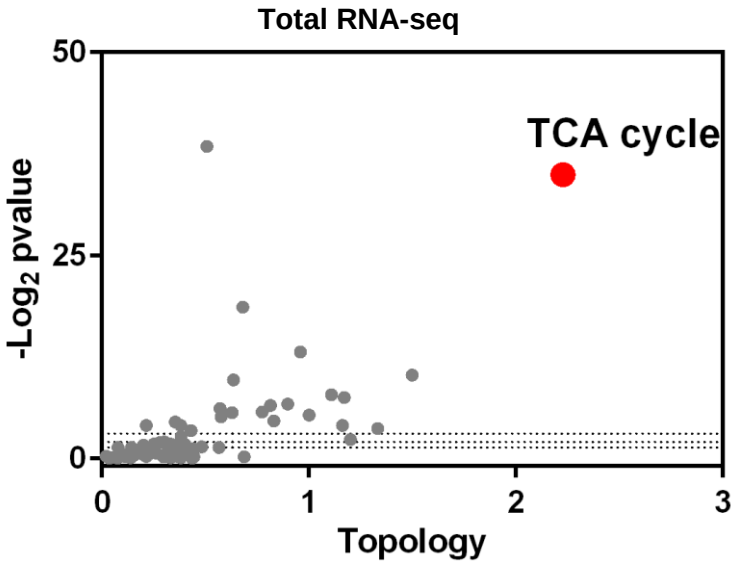

Fig. 5.14 Zc3h10 mainly controls TCA cycle. Scatter plot of enriched pathways results obtained crossing microarray data with targeted metabolomic results through MetaboAnalyst webtool. Log2p-value and topology were used to calculate the most affected metabolic pathways. Horizontal dot lines correspond, from top to bottom, to the Log2 of p-value of 0.001, 0.01 and 0.05, respectively.

5.9 Zc3h10 controls myotubes mitochondrial function and cell differentiation

We later evaluated if Zc3h10 downregulation in myoblasts might lead to impaired mitochondrial function also in myotubes. By using the same infection protocol, we obtained similar downregulation levels also in developing myofibers (Fig. 5.15A). Western blot shows that we got about 50% of Zc3h10 silencing at different time-points of differentiation as 24, 48, and 72 hours, which correspond to lower levels of Tfam (Fig. 5.15B) and OXPHOS subunits. In fact, western blot analysis in figure 5.15C indicates that additionally to Ndufb8, Sdhb and Mt-CoII, also Atp5a1 and Uqcrc2 expression is affected by partial loss of Zc3h10. Once again, lower mitochondrial component expression is associated with impaired mitochondrial function (Fig. 5.15D) but unaffected mitochondrial density (Fig. 5.15E). To confirm these data, we analyzed in detail the mitochondrial function at 48 hours from differentiation induction. At this time-point basal,

uncoupled and maximal uncoupled respiration are significantly lower in shZc3h10 cells (Fig. 5.15F), as well as the activity of complex I, II and IV of the ETC (Fig. 5.15G).

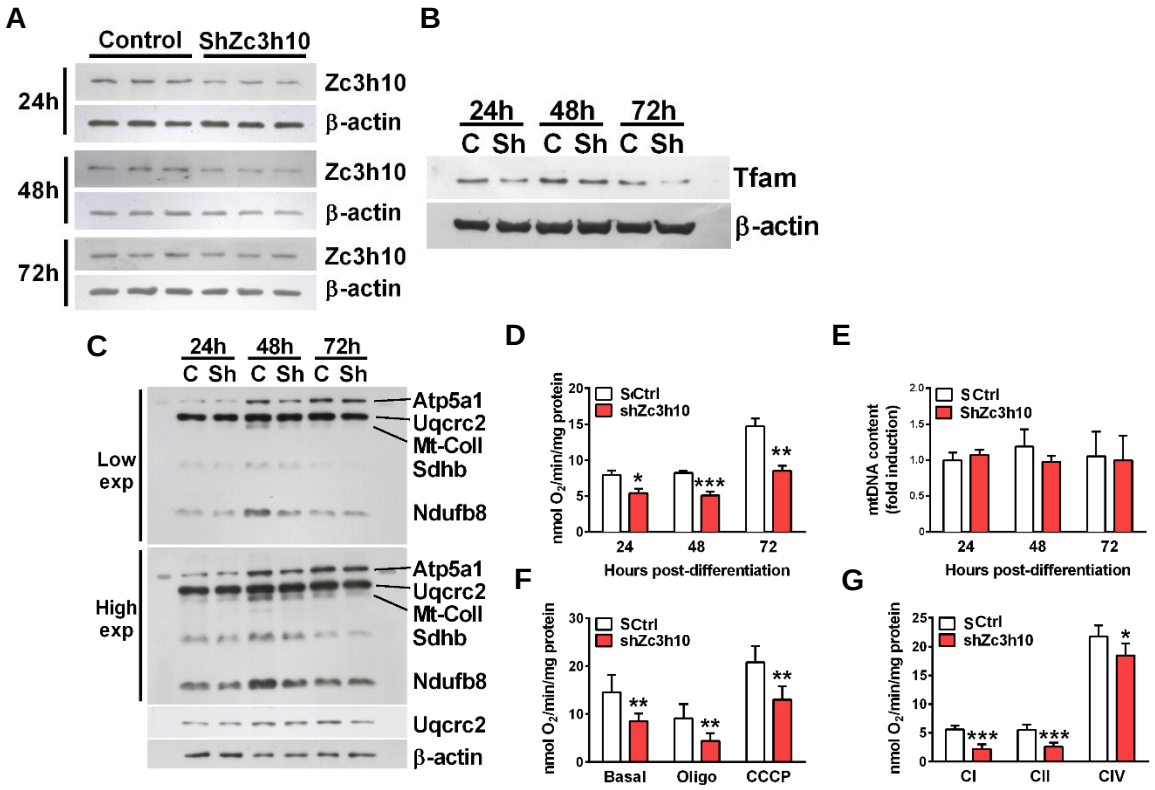

Fig. 5.15 Mitochondrial function in differentiating myotubes is regulated by Zc3h10. Western blot assays were performed at 24, 48 and 72 hours from differentiation induction (A, B and C) as well as basal respiration analysis and mtDNA levels evaluation (D and E). Coupled respiration and electron transport chain activity assays were performed at only 48 hours from differentiation start (F and G). Student's t-test, *p<0.05, *p<0.01, ***p<0.001 vs control. n=6.

As previously discussed, the upregulation of mitochondrial function drives metabolic shift during myoblasts differentiation. For this reason, we investigated if Zc3h10 could affect C2C12 development at different time-points from differentiation start. The analysis of myotubes morphology at 72 hours from differentiation induction shows that Zc3h10 silencing impaired myotubes formation. Indeed, ShZc3h10 MyHC^{+} cells appear thinner and shorter compared to control myotubes (Fig. 5.16A) and show a 50% reduction of fusion index levels (Fig. 5.16B). Additionally, protein and gene expression analysis of myogenesis markers Fast myosin heavy chain (Fig. 5.16C) and the myogenesis regulators MyoD, Mef2c, and Myogenin (Fig. 5.16D) show a strong decrease of their expression levels at both 24 and 48 hours from differentiation start, supporting the regulatory activity of myogenesis by Zc3h10.

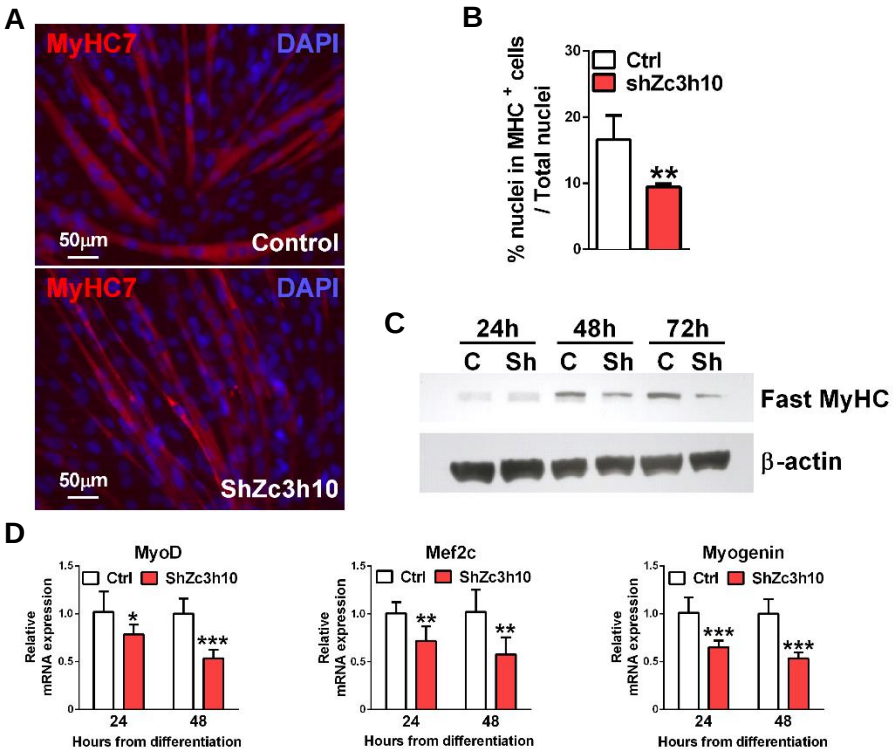

Fig. 5.16 Zc3h10 partial loss represses myotubes formation. IF was performed against MyHC Fast (red) and nuclei were revealed with DAPI (blue) (A). Quantification of fusion index was performed by calculating nuclei number in MyHC$^+$ cells with 3 or more nuclei and normalized on total number of nuclei in the field. Cells were fixed at 72 hours from differentiation induction (B). Western blot was performed with the same antibody used in the IF analysis at three different time points from differentiation (C), while gene expression evaluation of MyoD, Mef2c and Myogenin were performed at only 24 and 48 hours from differentiation start (D). Student's t-test, *p<0.05, *p<0.01, ***p<0.001 vs control. n=5.

To sustain our previous observations, we performed a transcriptomic analysis in 48 hours differentiated myofibers and run a gene set enrichment analysis (GSEA) to evaluate in an unbiased fashion which processes are mainly regulated by Zc3h10. As expected, Zc3h10 is positively associated with the expression of genes belonging to muscle structural components, mitochondrial part, and adherent junctions (Fig 5.17). On the other hand, Zc3h10 seems to be negatively associated with cell cycle progress, specifically with genes belonging to the M phase of mitotic cell cycle, chromosome segregation and cell cycle check point. In addition, KEGG pathway analysis demonstrates that cell cycle and focal adhesion are the most enriched pathways among upregulated genes. On the other hand, TCA cycle, glycolysis, fatty acid metabolism, pentose phosphate pathway and cardiac muscle contraction component are the most represented pathways among downregulated genes in ShZc3h10 myotubes. Altogether, these data sustain the positive role of Zc3h10 on mitochondrial function and C2C12 differentiation.

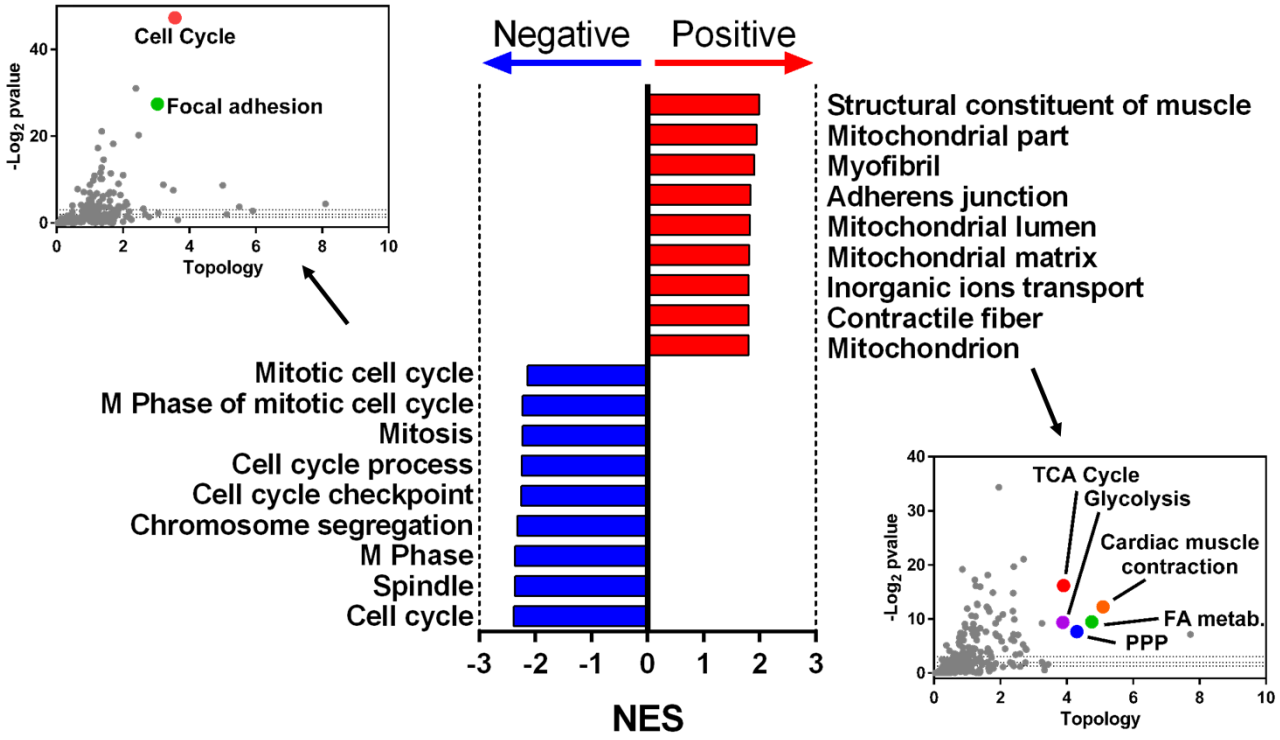

Fig. 5.17 Transcriptomic analysis in Zc3h10 silenced C2C12 myotubes. Normalized enrichment score (NES) of the 20 highest positively (red) and negatively (blue) Zc3h10 associated gene ontology (GO) categories was used to express data. GSEA analysis was performed considering simultaneously all GO categories (Molecular function, cell compartment, and biological process). NES were also interrogated by KEGG pathway analysis through MetaboAnalyst software to assess the most enriched pathways among up- and downregulated genes. The experiment was performed on five biological replicates for each experimental condition. Horizontal dot lines correspond, from top to bottom, to the Log2 of p-value of 0.001, 0.01 and 0.05, respectively.

To demonstrate that Zc3h10 specifically control differentiation program without affecting proliferation, we also evaluated cell growth after Zc3h10 silencing. As shown in figure 5.18, we did not observe any difference between the two conditions.

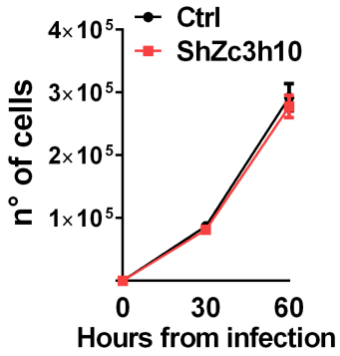

5.18 Zc3h10 does not control cell proliferation. Seeded cells were counted at infection time and considered as blank. Control and ShZc3h10 cell number was analyzed 30 and 60 hours post-infection. n=5.

5.10 Myotubes metabolic profile is affected by Zc3h10 downregulation

To demonstrate that Zc3h10 controls metabolic profile also in myotubes, we performed metabolomics analysis in 48 hours differentiated myotubes. We first verified the presence of outliers by principal component analysis (PCA) and hierarchical analyses. As shown in fig. 5.19A and B we have two distinct metabolic populations and no presence of outliers. In addition, these data suggest that Zc3h10 silencing at myoblast stage has detrimental consequences on the metabolic output upon differentiation to myotubes.

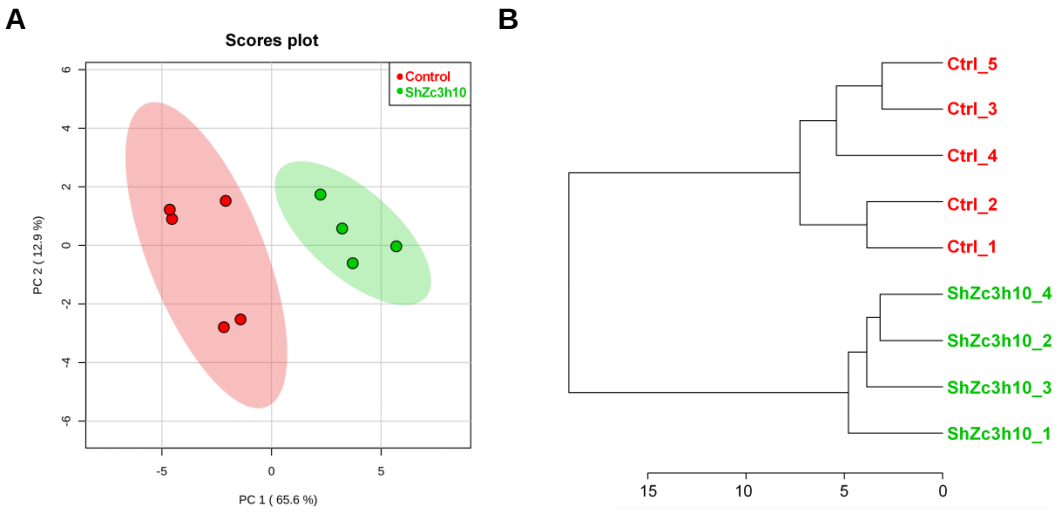

Fig 5.19 Zc3h10 silencing impacts metabolic landscape of myotubes. MetaboAnalyst webtool was used to calculate principal component analysis (PCA) (A) and hierarchical clustering (B) of metabolomic analysis in control (Red) and ShZc3h10 (Green) samples.

To better understand which pathways are mainly affected by Zc3h10 deficiency we verified differentially abundant metabolites (Fig. 5.20). Specifically, we observe lower glucose uptake and conversion to glucose-6-phosphate in ShZc3h10 cells. Additionally, we observed decreased levels of either xilulose-5-phosphate and erythrose-4-phosphate, and lower intracellular levels of nucleotide cofactors as NAD^+, NADH, and NADPH and nucleotides ATP, ADP and AMP. These data are in line with lower expression of solute carrier family 2 member 4 (Slc2a4, facilitated glucose transporter Glut4) in ShZc3h10 myotubes (Fold change = 0.63, p-value = 0.0029), according to microarray analysis. On the other hand, glutamate levels are significantly upregulated in ShZc3h10 cells (Fold change = 2.034, p-value = 0.005. Our analyses also demonstrate that several TCA cycle by-products levels are significantly downregulated in ShZc3h10 cells, like citrate (fold change = 0.6, p-value = 0.004), *cis*-aconitate (fold change = 0.5, p-value = 0,0004), α-ketoglutarate (fold change = 0.5, p-value = 0.01), malate (fold change = 0.15, p-value = 0.001).

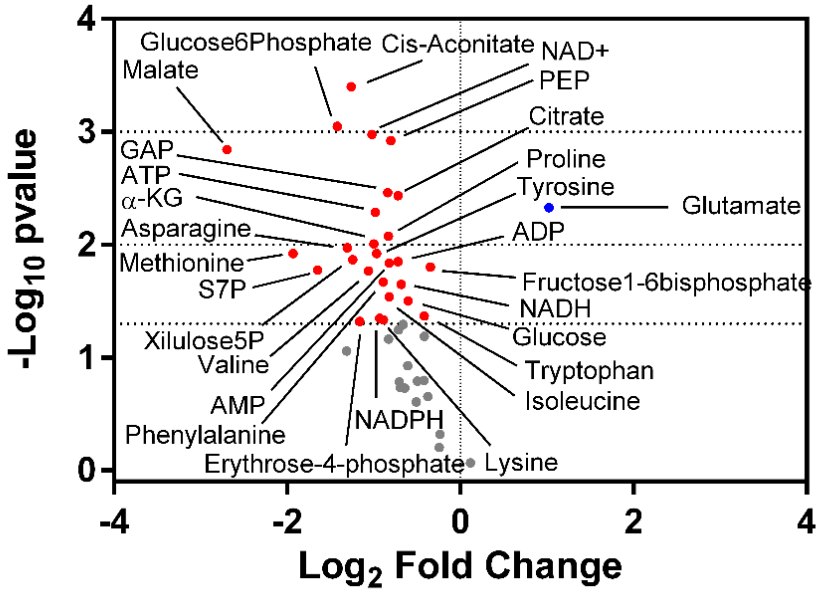

Fig 5.20 Zc3h10 deficiency leads to an overall decrease of important metabolites belonging to the main energetic pathways. The graph correlates the p-Value (Log10 scale, Y Axis) and the fold change (Log2 scale, X axis). Red dots indicate significantly downregulated metabolites and blue dots indicate upregulated metabolites. Horizontal dot lines correspond, from top to bottom, to the Log10 of p-value of 0.001, 0.01 and 0.05, respectively.

Like C2C12 myoblasts, we crossed metabolomics and transcriptomics analyses to identify the most affected metabolic pathway. Statistical and topological analyses confirm fig. 5.17 observation, indicating TCA cycle and pentose phosphate pathway (PPP) as the most affected metabolic processes by Zc3h10 silencing (Fig. 5.21).

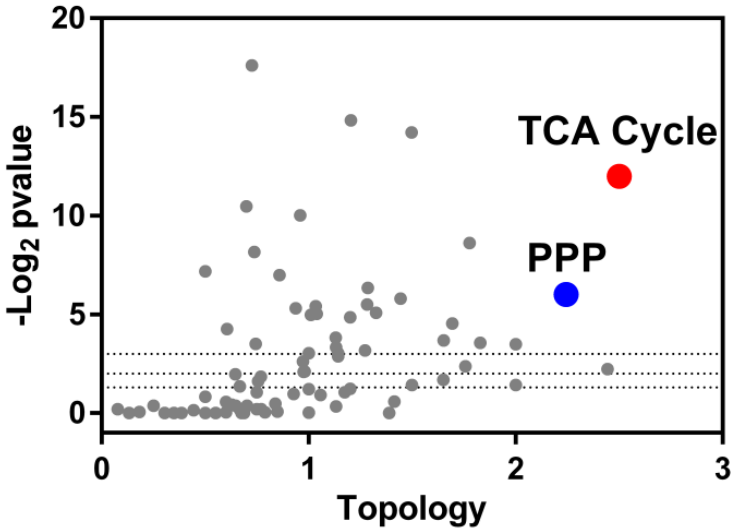

Fig. 5.21 ShZc3h10 impacts nucleotide metabolism and TCA cycle in myotubes. Scatter plot of enriched pathways results obtained crossing microarray data with targeted metabolomic results through MetaboAnalyst webtool. Log2p-value and topology were used to calculate the most affected metabolic pathways. Horizontal dot lines correspond to from top to bottom to the Log2 of the p-value of 0.001, 0.01 and 0.05, respectively.

5.11 Post-differentiation downregulation of Zc3h10 does not affect mitochondrial activity

To verify if Zc3h10 controls mitochondrial function in differentiated myotubes, we decided to downregulate our candidate 2 days after differentiation induction and assess mitochondrial density and function at day 4 (post-differentiation protocol, Fig. 3.1).Our data indicate that despite of Zc3h10 50% downregulation (Fig. 5.22A and B), neither Tfam gene expression (Fig. 5.22C), mtDNA levels (Fig. 5.22D) and basal cellular respiration (Fig. 5.22E) were significantly different compared to control, suggesting that Zc3h10 presence is necessary in the first but not in the late stages of C2C12 differentiation.

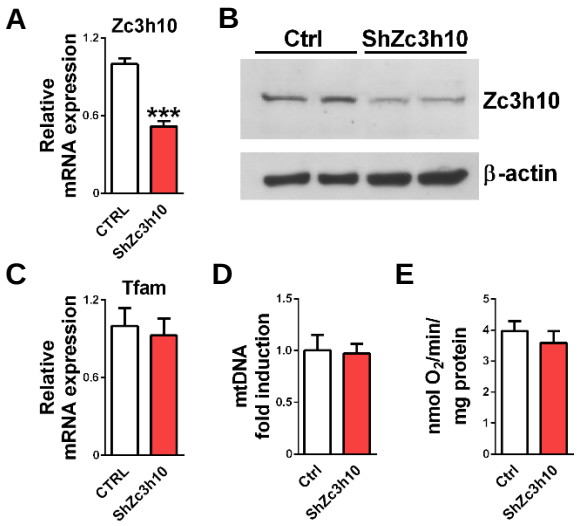

Fig. 5.22 Zc3h10 loss does not affect mitochondrial activity if downregulation after differentiation induction. Gene expression and western blot analyses were used to validate Zc3h10 repression (A and B). Tfam gene expression (C), mitochondrial density and function (D and E) were used to evaluate mitchondrial effects of Zc3h10 downregulation. Student's t-test, ***p<0.001 vs control. n=5.

5.12 Zc3h10 controls Mitoferrin1 mRNA metabolism

Once demonstrated that Zc3h10 is a specific mitochondrial and RNA metabolism regulator in both myoblasts and myotubes, we shifted our attention on the molecular mechanism underlying the phenotype. To assess which processes are directly affected by Zc3h10, we performed a RNA immunoprecipitation (RIP) assay coupled to NGS to identify and characterize the target messengers of our candidate. To get a high-efficient Zc3h10 immunoprecipitation, we decided to overexpress the flag-tag fused Zc3h10in proliferating myoblasts. First, we validated if flag-Zc3h10 overexpression recapitulated our previous results (Chapter 5.2). After physiological overexpression of Zc3h10 (MOI of 5, Fig. 5.23A), we demonstrated that flag-Zc3h10 overexpression (Fig. 5.23B) can upregulate both mitochondrial density at 48 and 72 hours from differentiation induction (Fig. 5.23C) and activity (Fig. 5.23D) at all time points by ≈50% compared to control. Further, flag-Zc3h10 increases ETC complexes activity (Fig. 5.23E) as well as uncoupled and maximal uncoupled respiration (Fig. 5.23F). Additionally, flag-Zc3h10 overexpression upregulated myotubes formation by almost 2-fold (Fig. 5.23G) confirming the strong regulatory effect of Zc3h10 upon myotubes differentiation.

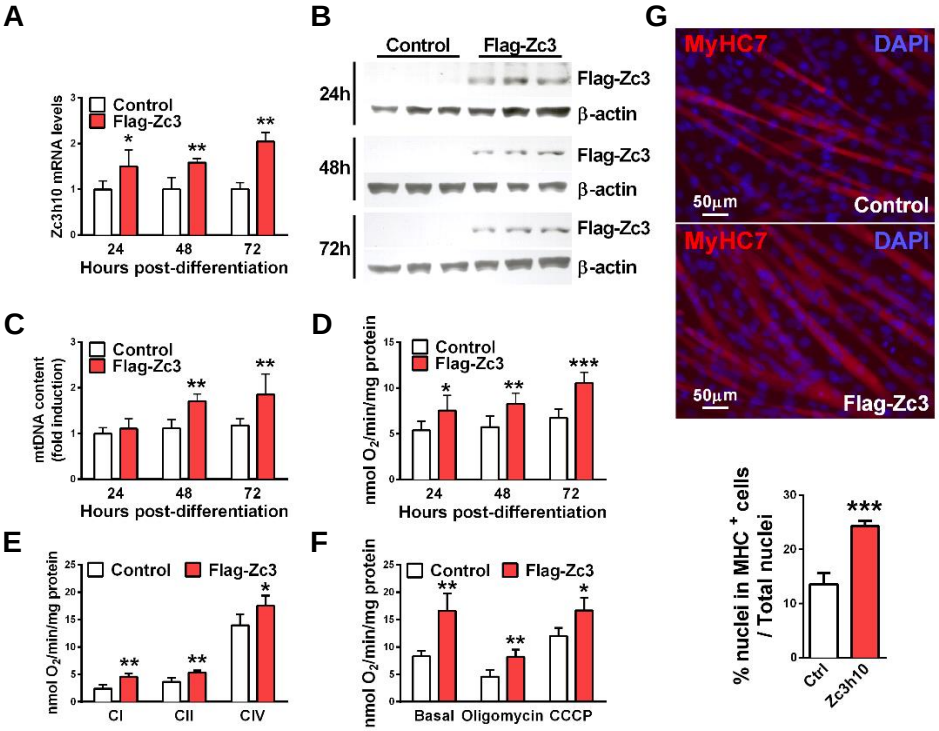

Fig. 5.23 Flag-Zc3h10 overexpression induces mitochondrial function and C2C12 differentiation. Zc3h10 overexpression was evaluated by gene and protein expression (A and B). Mitochondrial density and function were assessed by mtDNA levels evaluation (C) cellular respiration (D and E) and ETC complexes activity (F). Finally, myotubes morphology and formation were assessed by IF analyses and fusion index quantification, respectively (G). Student's t-test, *p<0.05, **p<0.01 and ***p<0.001 vs control of each experimental condition. n=5.

We then validated the immunoprecipitation of Zc3h10. As shown in fig 5.24, we efficiently overexpressed and immunoprecipitated Flag-Zc3h10, prompting us to proceed with following sequencing of Zc3h10 bound transcripts.

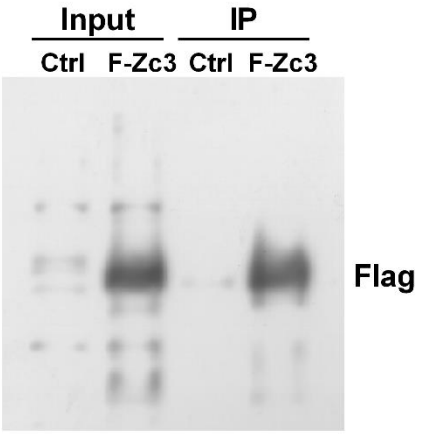

Fig. 5.24 Zc3h10 immunoprecipitation. Western blot on SDS-Page was used to validate Flag-Zc3h10 immunoprecipitation. 10% of whole cell lysate (input) was used as overexpression validation.

Subsequent sequencing of immunoprecipitated RNA demonstrated that Zc3h10 significantly binds to 410 transcripts. Biological process GO analysis of Zc3h10 targets indicated that a large part of these genes is associated with the regulation of skeletal muscle development (Fig. 5.25).

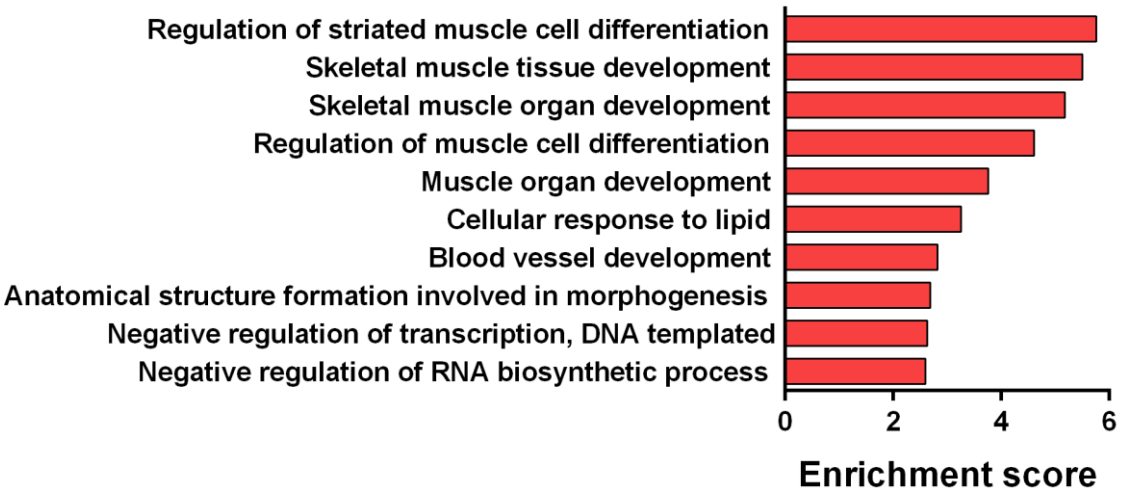

Fig. 5.25 Clustering of Zc3h10 bound RNAs by biological processes. GO analysis was performed by Panther webtool (Release 11.1).

In addition, by analyzing total RNA-seq results of Zc3h10 silenced myoblasts with DEXSeq software (Huber et al., 2012), we found that 233 (56.82%) out of 410 targets undergo to at least one alternative splicing, indicating that Zc3h10 might be directly involved in their splicing regulation (FDR < 0.25). Gene ontology analysis demonstrated that these 233 transcripts are mainly involved in intracellular cation and metal anion binding (Fig. 5.26).

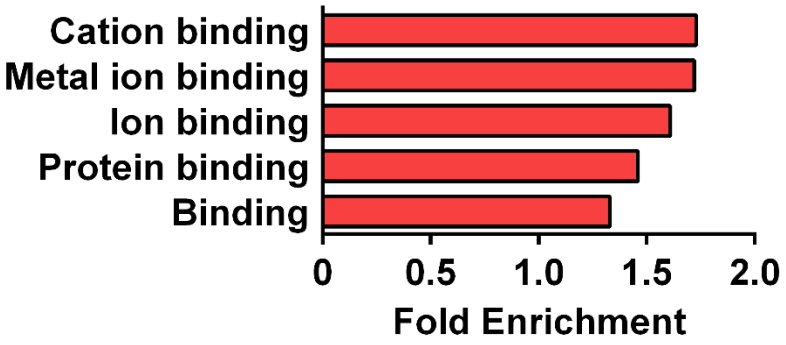

Fig. 5.26 Clustering of differentially spliced transcripts bound by Zc3h10 by molecular function (FDR < 0.25). GO analysis was performed by Panther webtool (Release 11.1).

Interestingly, the most enriched mRNA is Slc25a37 (Mitoferrin1), enriched by 14.96-fold compared to control. As discussed in the introduction chapter, mitoferrin1 is a fundamental iron importer of mitochondria which favors the formation of ISC and heme prosthetic groups. In addition, Slc25a37$^{-/-}$ mice dye during embryonic life. Surprisingly, from DEXSeq analysis we found that Slc25a37 intron 1 (Log10 padj = -0.81) and 2 (Log10 padj = -0.68) are significantly retained in ShZc3h10 myoblasts (Fig. 5.27).

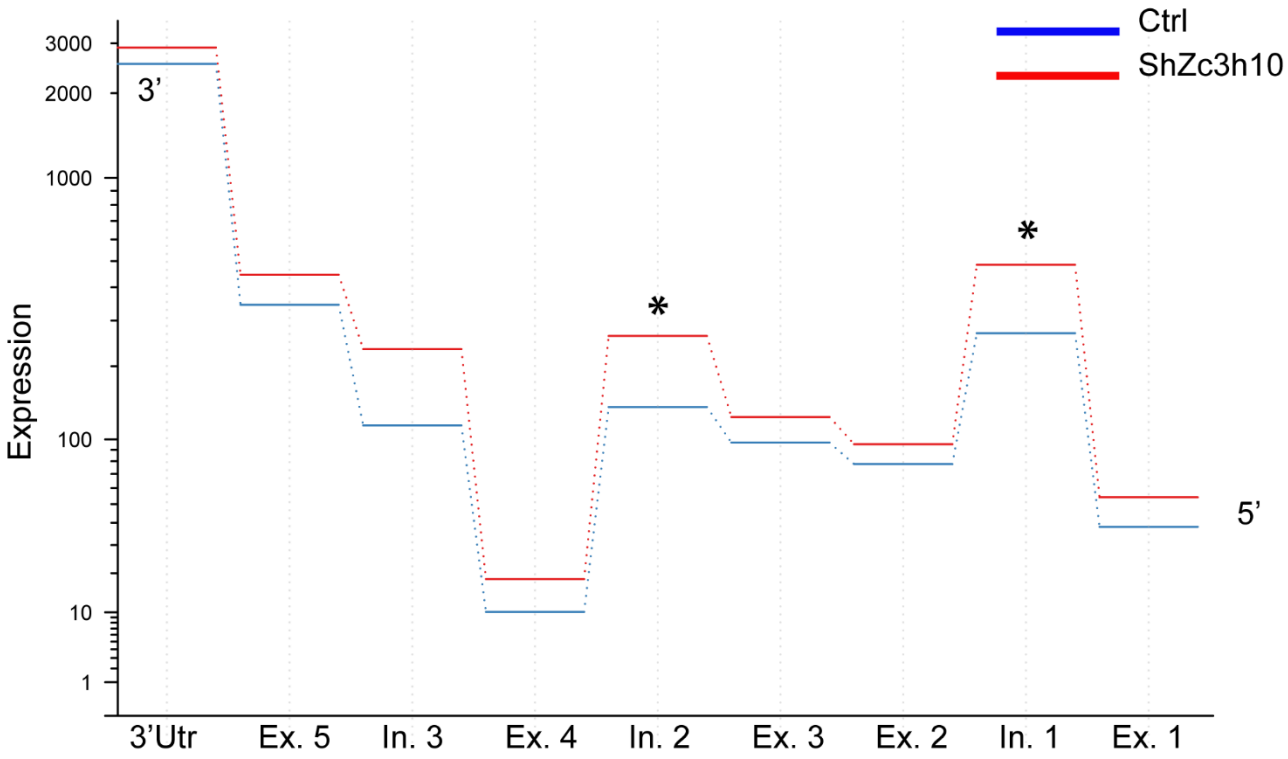

Fig. 5.27 Zc3h10 regulates Slc25a37 alternative splicing. DEXSeq software was used to identify alternative splicing (AS) events. Slc25a37 expression levels were obtained from total RNA-seq analysis of ShZc3h10 (red line) and control myoblasts (blue line). FDR < 0.25. n=3.

Given that alternative splicing events are linked also to impaired mRNA nuclear export, we explored the possibility that the mRNA binding protein Zc3h10 be involved in the processing of Slc25a37 transcript. Evaluation of mRNA export, assessed by measuring the mRNA levels in the nuclear and cytoplasmic compartments, shows that Slc25a37 nuclear export is downregulated after Zc3h10 silencing only 48 hours from differentiation (Fig. 5.28A). Surprisingly, Slc25a37 gene expression studies indicate that Zc3h10 is not involved in neither its export and transcriptional control (Fig. 5.28B).

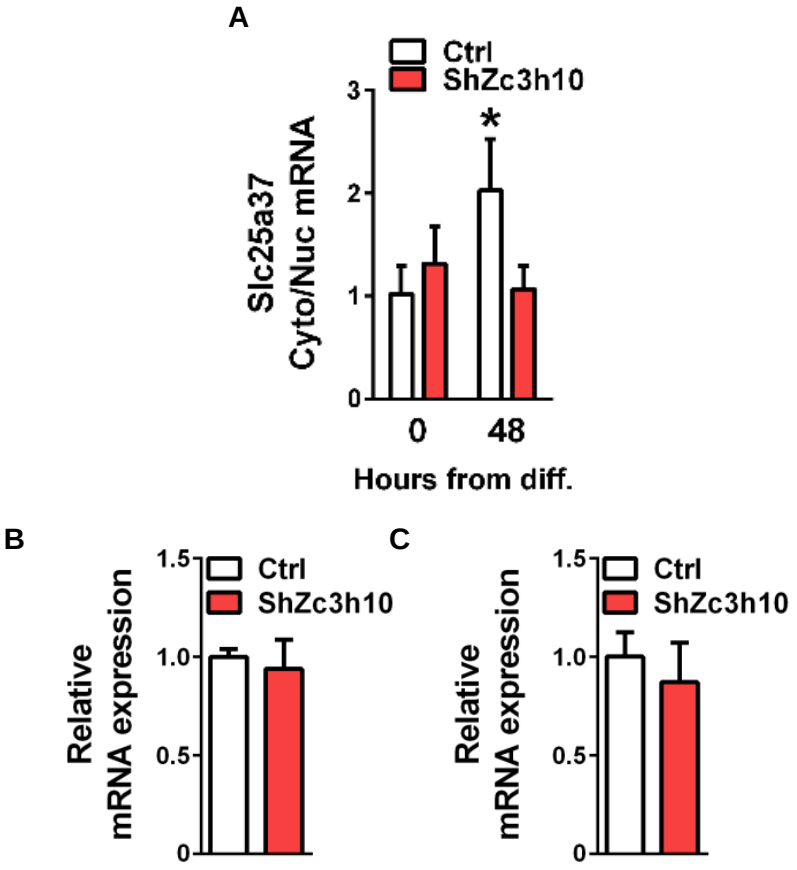

Fig. 5.28 Slc25a37 nuclear export and transcript levels are not directly regulated by Zc3h10. Nuclei and cytoplasm were separated and transcript analyses on both fractions were conducted by qPCR (A). Gene expression analyses were performed on total RNA extracts in confluent myoblasts (B) and 48 hours differentiated myotubes (C). Panel A:One way ANOVA followed by Dunnett's multiple comparison test, *p<0.05 vs control. n=3. Panel B: Student's t-test, **p<0.01vs control. n=5.

Previous data show that intron 2 retention of Slc25a37 transcript may be associated with a truncated isoform of mitoferrin1 (Visconte et al., 2014). We verified if Slc25a37 protein was affected by Zc3h10 silencing using an antibody recognizing only the wild-type and not the

truncated mitoferrin1 isoform. Indeed, Zc3h10 downregulation decreases mitoferrin1 protein levels in both myoblasts (Fig. 5.29A) and during myotubes differentiation (Fig.5.29B).

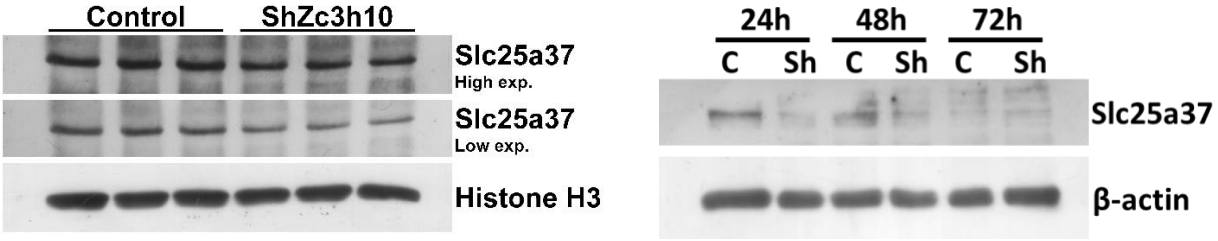

Fig. 5.29 Zc3h10 downregulation affects mitoferrin1 protein levels. Slc25a37 protein expression was evaluated on whole cell extracts in myoblasts and in myotubes at 24, 48 and 72 hours from differentiation induction.

5.13 Zc3h10 downregulation affects iron homeostasis in both myoblasts and myotubes

To assess if Slc25a37 downregulation in ShZc3h10 myoblasts and myotubes may have some functional consequences, we performed cytochemistry and spectrophotometry assays to evaluate both ferric (Fe^{3+}) and total iron content in C2C12 myoblasts. Both analyses indicate that downregulation of Zc3h10 leads to iron overload, increasing both ferric and total iron levels (Fig. 5.30A and B).

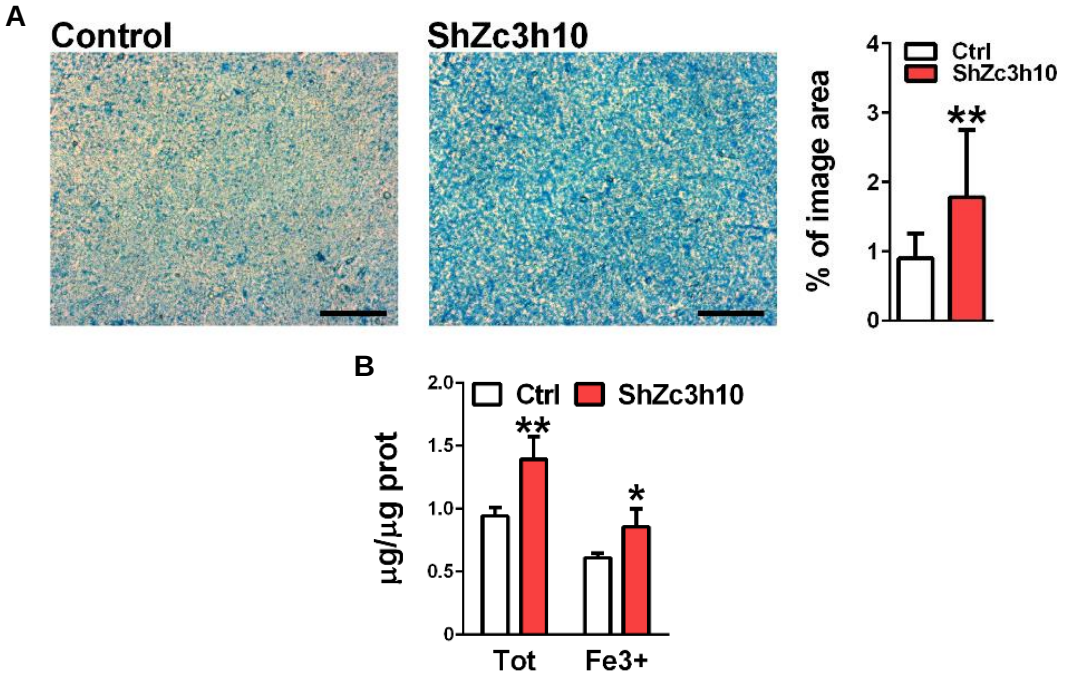

Fig. 5.30 Zc3h10 leads to iron overload in myoblasts. C2C12 cells were stained with Prussian blue to evaluate ferric iron content (A). Spectrophotometry analysis was performed by using ferrozine indicator to assess both total and ferric

iron levels (B).Panel A: Student's t-test, **p<0.01vs control, n=16.Panel B: Student's t-test, *p<0.05, **p<0.01vs control. n=4.

To support the functional role of Zc3h10 on intracellular iron levels, we decided to rescue Zc3h10 expression in ShZc3h10 myoblasts. As shown in figure 5.31A we could recover Zc3h10 to control levels, leading to the complete rescue of intracellular iron levels in these cells (Fig. 5.31B).

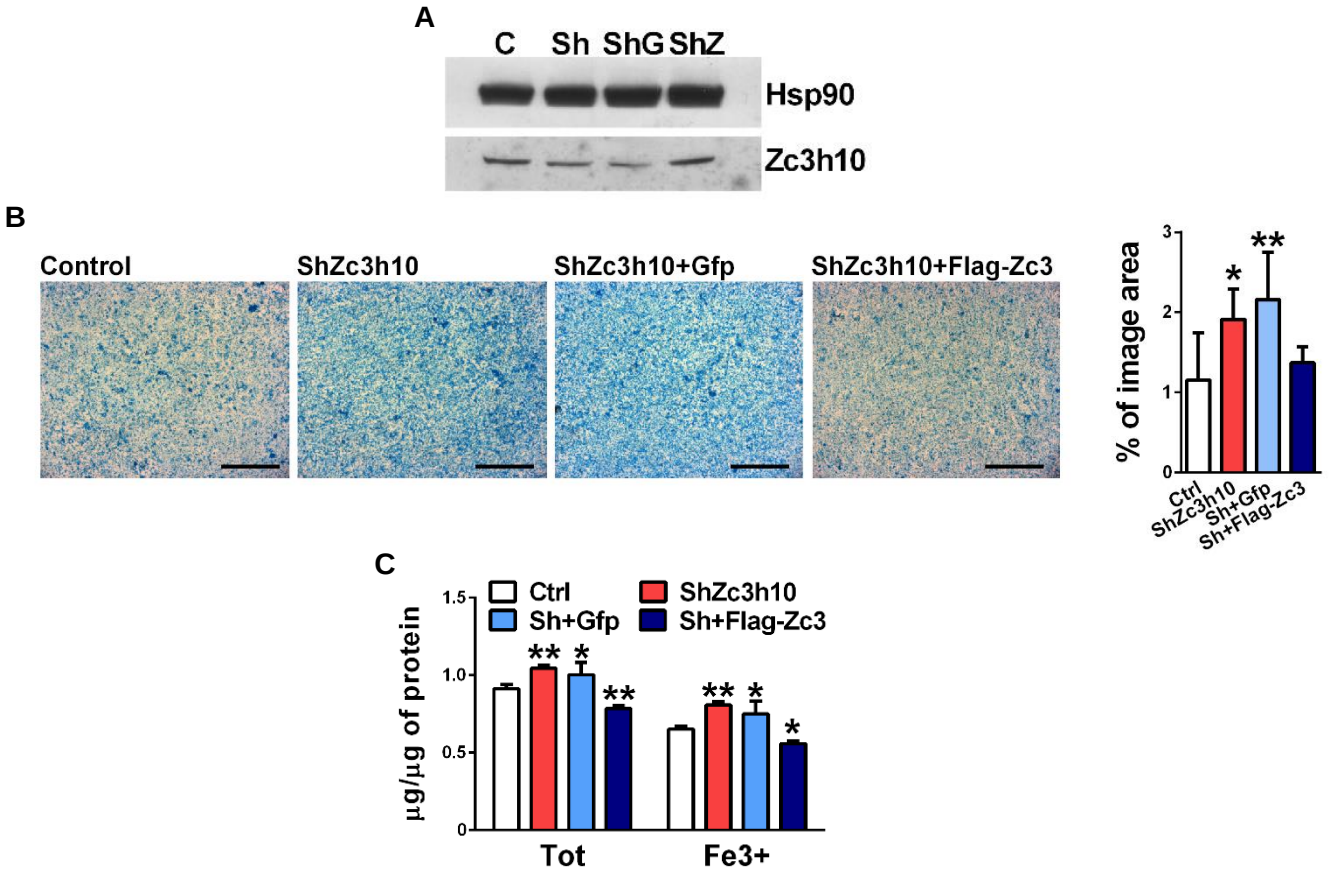

Fig. 5.31 Zc3h10 overexpression rescues iron homeostasis. C2C12 cells were first silenced and then transduced with flag-Zc3h10. Silencing and re-overexpression were validated through western blot analysis (A). C2C12 were stained with Prussian blue to evaluate ferric iron content (B), while spectrophotometry analysis was performed by using ferrozine indicator to assess both total and ferric iron levels (A). Panel A: One-way ANOVA followed by Dunnett's Post Test, *p<0.05, **p<0.01 vs control, n=7. Panel B: One-way ANOVA followed by Dunnett's Post Test, *p<0.05, **p<0.01 vs control. n=4.

To further demonstrate the role of Zc3h10 in iron homeostasis and mitochondrial iron import, we analyzed intracellular levels of lipoate, the protein-conjugated cofactor of pyruvate dehydrogenase and α-KG dehydrogenase. Lipoate synthesis in mitochondria has been demonstrated to be iron-dependent since lipoic acid synthase requires a 4-iron-4-sulfur cluster for its function. As shown in figure 5.12, 5.21 and 5.32, lipoic acid levels are dramatically decreased in ShZc3h10 myoblasts and myotubes supporting the positive association between Zc3h10 and iron import in mitochondria.

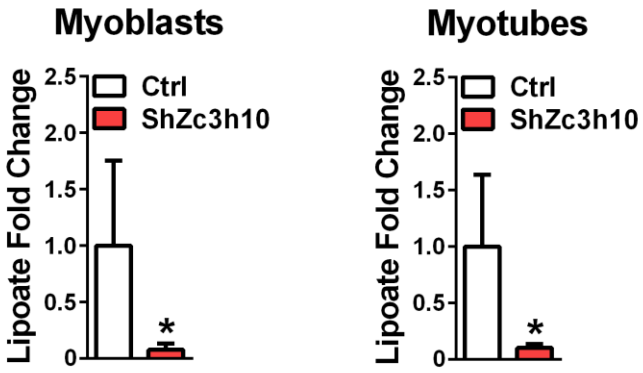

Fig. 5.32 Lipoate levels are decreased by Zc3h10 silencing. Lipoate levels were measured in C2C12 myoblasts and 48 hours differentiated myotubes total cell lysates. *p<0.05 vs control. n=5.

6. Discussion

Mitochondria are widely known for their role in energy metabolism. Considered the cell powerhouses, they are the crossway of the main metabolic processes like glycolysis, Krebs's cycle, β-oxidation, fatty acid synthesis and the oxidative phosphorylation. Beyond their role to ATP production, mitochondria also participate to many other processes, as apoptosis, calcium homeostasis, iron sulfur cluster and heme biosynthesis, and heat production. By these means, they directly affect fundamental steps of cell life, like stemness, cell division, commitment and differentiation. Mitochondria are the only organelles to possess their own genome, a double-stranded circular DNA sequence. Compared to nuclear genome, mtDNA is extremely small, consisting of only ~16kb and encoding for just 13 proteins, 2 rRNAs and 22 tRNAs. mtDNA replication and transcription are mainly controlled by a nuclear encoded transcription factor called mitochondria transcription factor A, whose transcription is in turn regulated by many other transcription factors and cofactors (i.e. Pgc-1α, Pgc-1β, Pparγ, Pparα, Errα, YY1) (Scarpulla et al., 2012). The tight nucleus-mitochondria relationship is further demonstrated by that Tfam is only one of the ~1500 mitochondrial genes expressed in the nucleus, and that many mitochondrial metabolites are required for a large number of nuclear functions (i.e. DNA replication, RNA transcription, splicing and nuclear export). Nevertheless, many aspects of mitochondrial biology still need to be fully understood, as i) mtDNA transcription and replication mechanisms, ii) mitochondrial morphology regulation and iii) mitochondrial ATP production control in different cellular context. Given the great impact of mitochondria on whole body metabolism and physiology, mitochondrial dysfunctions are associated with an extended spectrum of diseases (Chinnery, 2014). Mitochondrial genetic dysfunctions are usually divided in three major categories: the first two groups include pathologies linked to ETC genes mutations, which can be either mtDNA (maternally) or nDNA inherited (mendelian). In the third group, we find mitochondrial diseases associated with no-ETC mitochondrial gene mutations (IDH1/2, Parkin and Frataxin). Further, mitochondrial dysfunctions are tightly associated to many diseases, as type 2 diabetes, obesity, neurodegenerative disorders, cancer, myopathies and aging.

Currently, the rising of new research approaches and technologies (high-throughput screening, next generation sequencing, mass spectrometry proteomic and metabolomic analyses) offers the possibility to extensively dissect new roles of mitochondria in cell physiology and pathophysiology. For example, Wolf et al. set up the MitoString screen to identify new factors involved in mitochondria RNA metabolism, while Chen et al. recently developed a new experimental approach by which they specifically immunoprecipitated mitochondria from whole cell lysates and measured metabolic compartmentalization due to different external cues by mass spectrometry (Chen et al., 2016; Wolf and Mootha, 2014). Further, the necessity to better

characterize the phenotypical traits of mtDNA-mutation diseases and the impossibility to directly transfect mtDNA haplotypes in cell lines prompted the generation of reliable mouse models. To this end, a recent approach based on coupling breeding, histological and next generation sequencing analyses led to the isolation of the C5024T mutation of mitochondrial $tRNA^{ALA}$ that, in turn, leads to decreased mitochondrial translation efficiency, cardiomyopathy and loss of body weight in male mice (Kauppila et al., 2016).

Skeletal muscle holds essential roles in whole body physiology, from movement generation to energy metabolism homeostasis. Skeletal muscle is also a high energy-demanding tissue and very rich in mitochondria. Adult striated muscle maintenance and repair are sustained by the presence of skeletal muscle satellite cells (MuSC), or precursors, that under specific conditions (i.e. presence of cytokines, injury and physical exercise) switch from quiescence to asymmetric division prompting myocyte differentiation and skeletal muscle development. Recent results indicate the existence of a direct association between energy metabolism regulation, mitochondrial activity and committed cell differentiation (Almada and Wagers, 2016; Ryall et al., 2015; Shintaku et al., 2016). Yet, the intrinsic regulatory circuitries of mitochondrial functional changes that underlies metabolic transition of myoblasts to fully differentiated myotubes still need to be fully understood. Nowadays, a great challenge is the identification and characterization of new players involved in the regulation of mitochondrial function, whose link with mitochondrial physiology is not reported yet. Specifically, the classification of new regulators of energy metabolism during cell commitment and differentiation is an important goal to better understand the molecular mechanism underlying the association between mitochondrial function and skeletal muscle development.

Genome-wide high throughput screening (HTS), biochemical and bioinformatic experiments previously performed in our laboratory indicated zinc finger CCCH-type containing 10 (Zc3h10) as a new mitochondrial regulator in HEK293 cells. Zc3h10 is an mRNA binding protein whose biological function is still unknown (Castello et al., 2013; Ray et al., 2013). Our characterization of its biological role suggests that this protein is a positive mitochondrial regulator in C2C12 myoblasts, confirming the reliability of our HTS. Zc3h10 overexpression in undifferentiated cells leads to the upregulation of several mitochondrial parameters as Tfam expression, cellular oxygen consumption rate and ATP production. In addition, targeted silencing experiments strongly corroborate that our candidate controls mitochondrial function in both myoblasts and myotubes, as specifically described by transcriptomics and targeted metabolomics analyses. We demonstrated that Zc3h10 regulates the TCA cycle activity, which might partially explain why only ~50% of Zc3h10 downregulation in myoblasts leads to a strong mitochondrial phenotype. Furthermore, our results indicate that Zc3h10 can control skeletal muscle development. C2C12

analyses show that Zc3h10 is localized in the nucleus and expressed just in the first phases of cell differentiation. In addition, transcriptomic and biochemical analyses of Zc3h10 silenced myotubes demonstrate that, besides mitochondrial function, Zc3h10 positively controls skeletal muscle cell differentiation. Immunofluorescence analysis performed in human skeletal muscle demonstrate that Zc3h10 is expressed in the first phases of human skeletal muscle differentiation as well, as indicated by its coexpression with fetal and neonatal myosin heavy chains. Immunofluorescence experiments in young and adult mice also show that our candidate is more expressed in 12 weeks old than in 6 and 12 months old mice quadriceps, where the number of developing fibers is significantly downregulated (Perrimon et al., 2013). Interestingly, cell growth analysis indicates that Zc3h10 is not directly involved in the regulation of cell cycle, even though cell cycle transcripts expression is upregulated in ShZc3h10 myotubes. Our hypothesis is that Zc3h10 silenced cells are unable to properly differentiate and try to cope this defect by regulating cell cycle-related gene expression.

Full dissection of causative relationship between mitochondrial activity and skeletal muscle development is a very difficult and interesting topic. From literature, it is clear that these two aspects are tightly correlated. For example, the master regulator of myogenesis MyoD has been recently demonstrated to control skeletal muscle metabolism directly interacting with Pgc-1β, while a large number of metabolic regulators controls skeletal muscle morphology (Blattler et al., 2012; Mootha et al., 2004; Shintaku et al., 2016). For this reason, we decided to understand if Zc3h10 primarily controls mitochondrial function or cell differentiation, by identifying its target mRNAs through RNA immunoprecipitation coupled to next generation sequencing (RIP-seq). Our data demonstrate that the most enriched transcript is the iron transporter Slc25a37/Mitoferrin1, enriched by ~15 fold compared to control condition, directly linking Zc3h10 to mitochondrial physiology. Furthermore, Zc3h10 binds more than 400 transcripts mainly involved in the skeletal muscle tissue development, indicating once again that mitochondrial function and skeletal muscle differentiation are tightly associated. Out of 410, 235 target transcripts display incorrect splicing events in Zc3h10 silenced cells. Following bioinformatic analyses showed that Zc3h10 silencing in myoblasts leads to significant Slc25a37 intron 2 retention in Slc25a37 mature transcript, which associates with significant ferric iron overload and Mitoferrin1 protein downregulation in ShZc3h10 myoblasts and myotubes. These results are in line with other data already reported in literature, where it has been demonstrated that patients carrying a mutation on the splicing factor (SF) 3B1 have increased gene expression of mitoferrin1 coupled to Slc25a37 intron 2 retention and higher levels of intracellular ferric iron (Fe^{3+}) compared to healthy subjects (Visconte et al., 2014). The authors also show the presence of a premature terminating codon (PTC) in the retained intron 2, which might lead to the

formation of a truncated isoform of Mitoferrin1 and impaired mitochondrial iron flux. As proof of concept, mass spectrometry evaluation of intracellular lipoic acid levels, whose mitochondrial synthesis has been demonstrated to be iron (Hiltunen et al., 2009), suggest that Zc3h10 downregulation affects mitochondrial iron import and utilization. Nevertheless, the understanding of which cell compartment mainly accumulates ferric iron in Zc3h10 downregulated cells will be matter of future experiments, as well as comprehending if Slc25a37 intron 2 retention is a physiological event in skeletal muscle development and how Zc3h10 controls this phenomenon.

The role of RNA binding proteins in skeletal muscle development is now widely reported in literature (Apponi et al., 2011). On the other hand, the role of mRNA binding proteins in the post transcriptional regulation of energy metabolism related genes, and more specifically of mitochondria related genes, needs more characterization. Within this project, we identified and characterized for the first time a new mitochondrial regulator that links mRNA splicing to energy metabolism and cell differentiation. Furthermore, our data represent an important hint on the causative relationship between mitochondrial function upregulation and cell differentiation. High conservation of Zc3h10 protein sequence among different species and the ubiquitous expression of Zc3h10 transcript in different mouse tissues might suggest that the molecular mechanisms regulated by this protein are conserved among mammals and different tissues. It will be extremely useful to verify if Zc3h10 is involved in the mitochondrial activity of other differentiating cell lines. The generation of conditional knockout models will help us to better analyze the role of this protein in different phases of specific tissues development as well. Moreover, a mouse model of mitochondrial and/or cell differentiation defects (i.e. muscular atrophy) will be a useful resource to better understand the biological role of Zc3h10 in a more pathological context.

In conclusion, our results partially annotated for the first time the cell localization, the biological role, and the molecular function of the previously unknown protein Zc3h10. Specifically, the integration of cutting-edge technologies and different experimental approaches helped us to propose Zc3h10 as a new mitochondrial and cell differentiation regulator in C2C12 myoblasts acting like a splicing factor of Slc25a37.

7. Bibliography

Akimoto, T., Pohnert, S.C., Li, P., Zhang, M., Gumbs, C., Rosenberg, P.B., Williams, R.S., and Yan, Z. (2005). Exercise stimulates Pgc-1alpha transcription in skeletal muscle through activation of the p38 MAPK pathway. J Biol Chem *280*, 19587-19593.

Almada, A.E., and Wagers, A.J. (2016). Molecular circuitry of stem cell fate in skeletal muscle regeneration, ageing and disease. Nat Rev Mol Cell Biol *17*, 267-279.

Amati-Bonneau, P., Valentino, M.L., Reynier, P., Gallardo, M.E., Bornstein, B., Boissiere, A., Campos, Y., Rivera, H., de la Aleja, J.G., Carroccia, R.*, et al.* (2007). OPA1 mutations induce mitochondrial DNA instability and optic atrophy 'plus' phenotypes. Brain *131*, 338-351.

Anandatheerthavarada, H.K., Biswas, G., Robin, M.A., and Avadhani, N.G. (2003). Mitochondrial targeting and a novel transmembrane arrest of Alzheimer's amyloid precursor protein impairs mitochondrial function in neuronal cells. J Cell Biol *161*, 41-54.

Apponi, L.H., Corbett, A.H., and Pavlath, G.K. (2011). RNA-binding proteins and gene regulation in myogenesis. Trends in pharmacological sciences *32*, 652-658.

Arnold, L., Perrin, H., de Chanville, C.B., Saclier, M., Hermand, P., Poupel, L., Guyon, E., Licata, F., Carpentier, W., Vilar, J.*, et al.* (2015). CX3CR1 deficiency promotes muscle repair and regeneration by enhancing macrophage ApoE production. Nat Commun *6*, 8972.

Audano, M., Ferrari, A., Fiorino, E., Kuenzl, M., Caruso, D., Mitro, N., Crestani, M., and De Fabiani, E. (2014). Energizing Genetics and Epi-genetics: Role in the Regulation of Mitochondrial Function. In Current genomics (Netherlands), pp. 436-456.

Bachi, A., Braun, I.C., Rodrigues, J.P., Pante, N., Ribbeck, K., von Kobbe, C., Kutay, U., Wilm, M., Gorlich, D., Carmo-Fonseca, M.*, et al.* (2000). The C-terminal domain of TAP interacts with the nuclear pore complex and promotes export of specific CTE-bearing RNA substrates. RNA (New York, NY) *6*, 136-158.

Barupala, D.P., Dzul, S.P., Riggs-Gelasco, P.J., and Stemmler, T.L. (2016). Synthesis, delivery and regulation of eukaryotic heme and Fe-S cluster cofactors. Arch Biochem Biophys *592*, 60-75.

Bayeva, M., Chang, H.C., Wu, R., and Ardehali, H. (2013). When less is more: novel mechanisms of iron conservation. Trends Endocrinol Metab *24*, 569-577.

Bayeva, M., Khechaduri, A., Puig, S., Chang, H.C., Patial, S., Blackshear, P.J., and Ardehali, H. (2012). mTOR regulates cellular iron homeostasis through tristetraprolin. Cell Metab *16*, 645-657.

Beauchamp, P., Nassif, C., Hillock, S., van der Giessen, K., von Roretz, C., Jasmin, B.J., and Gallouzi, I.E. (2010). The cleavage of HuR interferes with its transportin-2-mediated nuclear import and promotes muscle fiber formation. Cell death and differentiation *17*, 1588-1599.

Blättler, S., Verdeguer, F., Liesa, M., Cunningham, J., Vogel, R., Chim, H., Liu, H., Romanino, K., Shirihai, O., Vazquez, F.*, et al.* (2012). Defective mitochondrial morphology and bioenergetic function in mice lacking the transcription factor Yin Yang 1 in skeletal muscle. Molecular and cellular biology *32*, 3333-3346.

Blattler, S.M., Verdeguer, F., Liesa, M., Cunningham, J.T., Vogel, R.O., Chim, H., Liu, H., Romanino, K., Shirihai, O.S., Vazquez, F.*, et al.* (2012). Defective mitochondrial morphology and bioenergetic function in mice lacking the transcription factor Yin Yang 1 in skeletal muscle. Molecular and cellular biology *32*, 3333-3346.

Blau, H.M., Cosgrove, B.D., and Ho, A.T. (2015). The central role of muscle stem cells in regenerative failure with aging. Nat Med *21*, 854-862.

Bogenhagen, D.F. (2012). Mitochondrial DNA nucleoid structure. Biochim Biophys Acta *1819*, 914-920.

Bonawitz, N.D., Clayton, D.A., and Shadel, G.S. (2006). Initiation and beyond: multiple functions of the human mitochondrial transcription machinery. Mol Cell *24*, 813-825.

Bosnakovski, D., Xu, Z., Li, W., Thet, S., Cleaver, O., Perlingeiro, R.C., and Kyba, M. (2008). Prospective isolation of skeletal muscle stem cells with a Pax7 reporter. Stem cells (Dayton, Ohio) *26*, 3194-3204.

Briata, P., Forcales, S.V., Ponassi, M., Corte, G., Chen, C.Y., Karin, M., Puri, P.L., and Gherzi, R. (2005). p38-dependent phosphorylation of the mRNA decay-promoting factor KSRP controls the stability of select myogenic transcripts. Mol Cell *20*, 891-903.

Bruijn, L.I., Miller, T.M., and Cleveland, D.W. (2004). Unraveling the mechanisms involved in motor neuron degeneration in ALS. Annual review of neuroscience *27*, 723-749.

Buckingham, M., Bajard, L., Chang, T., Daubas, P., Hadchouel, J., Meilhac, S., Montarras, D., Rocancourt, D., and Relaix, F. (2003). The formation of skeletal muscle: from somite to limb. Journal of anatomy *202*, 59-68.

Buckingham, M., and Relaix, F. (2015). PAX3 and PAX7 as upstream regulators of myogenesis. Seminars in cell & developmental biology *44*, 115-125.

Buckingham, M., and Rigby, P.W. (2014). Gene regulatory networks and transcriptional mechanisms that control myogenesis. Developmental cell *28*, 225-238.

Busiello, R.A., Savarese, S., and Lombardi, A. (2015). Mitochondrial uncoupling proteins and energy metabolism. Frontiers in physiology *6*.

Cameron, J.M., Janer, A., Levandovskiy, V., Mackay, N., Rouault, T.A., Tong, W.H., Ogilvie, I., Shoubridge, E.A., and Robinson, B.H. (2011). Mutations in iron-sulfur cluster scaffold genes NFU1 and BOLA3 cause a fatal deficiency of multiple respiratory chain and 2-oxoacid dehydrogenase enzymes. Am J Hum Genet *89*, 486-495.

Cardinali, B., Cappella, M., Provenzano, C., Garcia-Manteiga, J.M., Lazarevic, D., Cittaro, D., Martelli, F., and Falcone, G. (2016). MicroRNA-222 regulates muscle alternative splicing through Rbm24 during differentiation of skeletal muscle cells. Cell death & disease *7*, e2086.

Caspersen, C., Wang, N., Yao, J., Sosunov, A., Chen, X., Lustbader, J.W., Xu, H.W., Stern, D., McKhann, G., and Yan, S.D. (2005). Mitochondrial Abeta: a potential focal point for neuronal metabolic dysfunction in Alzheimer's disease. FASEB journal : official publication of the Federation of American Societies for Experimental Biology *19*, 2040-2041.

Castello, A., Fischer, B., Eichelbaum, K., Horos, R., Beckmann, B.M., Strein, C., Davey, N.E., Humphreys, D.T., Preiss, T., Steinmetz, L.M*., et al.* (2012). Insights into RNA biology from an atlas of mammalian mRNA-binding proteins. In Cell (United States: 2012 Elsevier Inc), pp. 1393-1406.

Castello, A., Horos, R., Strein, C., Fischer, B., Eichelbaum, K., Steinmetz, L.M., Krijgsveld, J., and Hentze, M.W. (2013). System-wide identification of RNA-binding proteins by interactome capture. Nature protocols *8*, 491-500.

Cerletti, M., Jurga, S., Witczak, C.A., Hirshman, M.F., Shadrach, J.L., Goodyear, L.J., and Wagers, A.J. (2008). Highly efficient, functional engraftment of skeletal muscle stem cells in dystrophic muscles. Cell *134*, 37-47.

Chakkalakal, J.V., Jones, K.M., Basson, M.A., and Brack, A.S. (2012). The aged niche disrupts muscle stem cell quiescence. Nature *490*, 355-360.

Chan, D.C. (2012). Fusion and fission: interlinked processes critical for mitochondrial health. Annual review of genetics *46*, 265-287.

Chanvorachote, P., and Luanpitpong, S. (2016). Iron induces cancer stem cells and aggressive phenotypes in human lung cancer cells. Am J Physiol Cell Physiol *310*, C728-739.

Charge, S.B., and Rudnicki, M.A. (2004). Cellular and molecular regulation of muscle regeneration. Physiological reviews *84*, 209-238.

Chatterjee, A., Seyfferth, J., Lucci, J., Gilsbach, R., Preissl, S., Bottinger, L., Martensson, C.U., Panhale, A., Stehle, T., Kretz, O*., et al.* (2016). MOF Acetyl Transferase Regulates Transcription and Respiration in Mitochondria. Cell *167*, 722-738.e723.

Chen, C.T., Shih, Y.R., Kuo, T.K., Lee, O.K., and Wei, Y.H. (2008). Coordinated changes of mitochondrial biogenesis and antioxidant enzymes during osteogenic differentiation of human mesenchymal stem cells. Stem cells (Dayton, Ohio) *26*, 960-968.

Chen, H., Chomyn, A., and Chan, D. (2005). Disruption of fusion results in mitochondrial heterogeneity and dysfunction. The Journal of biological chemistry *280*, 26185-26192.
Chen, H., Detmer, S.A., Ewald, A.J., Griffin, E.E., Fraser, S.E., and Chan, D.C. (2003). Mitofusins Mfn1 and Mfn2 coordinately regulate mitochondrial fusion and are essential for embryonic development. J Cell Biol *160*, 189-200.
Chen, H., Vermulst, M., Wang, Y.E., Chomyn, A., Prolla, T.A., McCaffery, J.M., and Chan, D.C. (2010). Mitochondrial fusion is required for mtDNA stability in skeletal muscle and tolerance of mtDNA mutations. Cell *141*, 280-289.
Chen, W., Paradkar, P.N., Li, L., Pierce, E.L., Langer, N.B., Takahashi-Makise, N., Hyde, B.B., Shirihai, O.S., Ward, D.M., Kaplan, J.*, et al.* (2009). Abcb10 physically interacts with mitoferrin-1 (Slc25a37) to enhance its stability and function in the erythroid mitochondria. Proc Natl Acad Sci U S A *106*, 16263-16268.
Chen, W.W., Freinkman, E., Wang, T., Birsoy, K., and Sabatini, D.M. (2016). Absolute Quantification of Matrix Metabolites Reveals the Dynamics of Mitochondrial Metabolism. Cell *166*, 1324-1337.e1311.
Chinnery, P.F. (2014). Mitochondrial Disorders Overview.
Chong, P.S., Vucic, S., Hedley-Whyte, E.T., Dreyer, M., and Cros, D. (2003). Multiple Symmetric Lipomatosis (Madelung's Disease) Caused by the MERRF (A8344G) Mutation: A Report of Two Cases and Review of the Literature. Journal of clinical neuromuscular disease *5*, 1-7.
Cogliati, S., Frezza, C., Soriano, M.E., Varanita, T., Quintana-Cabrera, R., Corrado, M., Cipolat, S., Costa, V., Casarin, A., Gomes, L.C.*, et al.* (2013). Mitochondrial cristae shape determines respiratory chain supercomplexes assembly and respiratory efficiency. Cell *155*, 160-171.
Cosgrove, B.D., Gilbert, P.M., Porpiglia, E., Mourkioti, F., Lee, S.P., Corbel, S.Y., Llewellyn, M.E., Delp, S.L., and Blau, H.M. (2014). Rejuvenation of the muscle stem cell population restores strength to injured aged muscles. Nat Med *20*, 255-264.
Cunningham, J., Rodgers, J., Arlow, D., Vazquez, F., Mootha, V., and Puigserver, P. (2007). mTOR controls mitochondrial oxidative function through a YY1-PGC-1alpha transcriptional complex. Nature *450*, 736-740.
D.C., W. (2010). Energetics, epigenetics, mitochondrial genetics. *10*, 12–31.
Davis, G.C., Williams, A.C., Markey, S.P., Ebert, M.H., Caine, E.D., Reichert, C.M., and Kopin, I.J. (1979). Chronic Parkinsonism secondary to intravenous injection of meperidine analogues. Psychiatry research *1*, 249-254.
Decker, C.J., and Parker, R. (2012). P-bodies and stress granules: possible roles in the control of translation and mRNA degradation. Cold Spring Harbor perspectives in biology *4*, a012286.
DeFronzo, R.A., Jacot, E., Jequier, E., Maeder, E., Wahren, J., and Felber, J.P. (1981). The effect of insulin on the disposal of intravenous glucose. Results from indirect calorimetry and hepatic and femoral venous catheterization. Diabetes *30*, 1000-1007.
Deries, M., and Thorsteinsdottir, S. (2016). Axial and limb muscle development: dialogue with the neighbourhood. Cellular and molecular life sciences : CMLS.
Devi, L., Prabhu, B.M., Galati, D.F., Avadhani, N.G., and Anandatheerthavarada, H.K. (2006). Accumulation of amyloid precursor protein in the mitochondrial import channels of human Alzheimer's disease brain is associated with mitochondrial dysfunction. The Journal of neuroscience : the official journal of the Society for Neuroscience *26*, 9057-9068.
Dickinson, A., Yeung, K.Y., Donoghue, J., Baker, M.J., Kelly, R.D., McKenzie, M., Johns, T.G., and St John, J.C. (2013). The regulation of mitochondrial DNA copy number in glioblastoma cells. Cell death and differentiation *20*, 1644-1653.
DiMauro, S., Hirano, M., and Schon, E.A. (2006). Approaches to the treatment of mitochondrial diseases. Muscle & nerve *34*, 265-283.
Dufour, E., and Larsson, N.G. (2004). Understanding aging: revealing order out of chaos. Biochim Biophys Acta *1658*, 122-132.

Dumont, N.A., Bentzinger, C.F., Sincennes, M.C., and Rudnicki, M.A. (2015). Satellite Cells and Skeletal Muscle Regeneration. Comprehensive Physiology *5*, 1027-1059.
Duno, M., Wibrand, F., Baggesen, K., Rosenberg, T., Kjaer, N., and Frederiksen, A.L. (2012). A novel mitochondrial mutation m.8989G>C associated with neuropathy, ataxia, retinitis pigmentosa - the NARP syndrome. Gene *515*, 372-375.
Edward J. Novotny, Jr., Gurparkash, S., Douglas, C.W., Leslie, J.D., Anne, L., Richard, L.S., and Lawrence, S. (1986). Leber's disease and dystonia.
Egan, B., O'Connor, P.L., Zierath, J.R., and O'Gorman, D.J. (2013). Time course analysis reveals gene-specific transcript and protein kinetics of adaptation to short-term aerobic exercise training in human skeletal muscle. PLoS One *8*, e74098.
Faes, L., and Callewaert, G. (2011). Mitochondrial dysfunction in familial amyotrophic lateral sclerosis. J Bioenerg Biomembr *43*, 587-592.
Farge, G., Mehmedovic, M., Baclayon, M., van den Wildenberg, S.M., Roos, W.H., Gustafsson, C.M., Wuite, G.J., and Falkenberg, M. (2014). In vitro-reconstituted nucleoids can block mitochondrial DNA replication and transcription. Cell Rep *8*, 66-74.
Faustino, N.A., and Cooper, T.A. (2003). Pre-mRNA splicing and human disease. Genes Dev *17*, 419-437.
Figueroa, A., Cuadrado, A., Fan, J., Atasoy, U., Muscat, G.E., Munoz-Canoves, P., Gorospe, M., and Munoz, A. (2003). Role of HuR in Skeletal Myogenesis through Coordinate Regulation of Muscle Differentiation Genes. Molecular and Cellular Biology *23*, 4991-5004.
Friedman, J.R., Lackner, L.L., West, M., DiBenedetto, J.R., Nunnari, J., and Voeltz, G.K. (2011). ER tubules mark sites of mitochondrial division. Science *334*, 358-362.
Friedman, J.R., and Nunnari, J. (2014). Mitochondrial form and function. Nature *505*, 335-343.
Ganz, T. (2013). Systemic iron homeostasis. Physiological reviews *93*, 1721-1741.
Gautier, C.A., Kitada, T., and Shen, J. (2008). Loss of PINK1 causes mitochondrial functional defects and increased sensitivity to oxidative stress. Proc Natl Acad Sci U S A *105*, 11364-11369.
Gegg, M.E., Cooper, J.M., Schapira, A.H., and Taanman, J.W. (2009). Silencing of PINK1 expression affects mitochondrial DNA and oxidative phosphorylation in dopaminergic cells. PLoS One *4*, e4756.
Genova, M.L., and Lenaz, G. (2013). Functional role of mitochondrial respiratory supercomplexes. Biochim Biophys Acta *1837*, 427-443.
Gils, Marko, K.R., Cora, M.B., Peter, J.v.S., Anique, J., Coen van, S., Jim, S., Hetty, C.d.B., Erna, A.P., Roel, B*., et al.* (2013). Quaking, an RNA-Binding Protein, Is a Critical Regulator of Vascular Smooth Muscle Cell PhenotypeNovelty and Significance.
Gong, C., and Maquat, L.E. (2011). lncRNAs transactivate STAU1-mediated mRNA decay by duplexing with 3' UTRs via Alu elements. Nature *470*, 284-288.
Gopinath, S.D., Webb, A.E., Brunet, A., and Rando, T.A. (2014). FOXO3 promotes quiescence in adult muscle stem cells during the process of self-renewal. Stem cell reports *2*, 414-426.
Guegan, C., Vila, M., Rosoklija, G., Hays, A.P., and Przedborski, S. (2001). Recruitment of the mitochondrial-dependent apoptotic pathway in amyotrophic lateral sclerosis. The Journal of neuroscience : the official journal of the Society for Neuroscience *21*, 6569-6576.
Guo, K., Wang, J., Andres, V., Smith, R.C., and Walsh, K. (1995). MyoD-induced expression of p21 inhibits cyclin-dependent kinase activity upon myocyte terminal differentiation. Molecular and cellular biology *15*, 3823-3829.
Hafner, M., Landthaler, M., Burger, L., Khorshid, M., Hausser, J., Berninger, P., Rothballer, A., Ascano, M., Jr., Jungkamp, A.C., Munschauer, M*., et al.* (2010a). Transcriptome-wide identification of RNA-binding protein and microRNA target sites by PAR-CLIP. Cell *141*, 129-141.
Hafner, M., Landthaler, M., Burger, L., Khorshid, M., Hausser, J., Berninger, P., Rothballer, A., Ascano, M., Jungkamp, A.C., Munschauer, M*., et al.* (2010b). PAR-CliP--a method to identify transcriptome-wide the binding sites of RNA binding proteins. Journal of visualized experiments : JoVE.

Handschin, C., Chin, S., Li, P., Liu, F., Maratos-Flier, E., Lebrasseur, N.K., Yan, Z., and Spiegelman, B.M. (2007). Skeletal muscle fiber-type switching, exercise intolerance, and myopathy in PGC-1alpha muscle-specific knock-out animals. J Biol Chem *282*, 30014-30021.

Harbauer, A.B., Zahedi, R.P., Sickmann, A., Pfanner, N., and Meisinger, C. (2014). The protein import machinery of mitochondria-a regulatory hub in metabolism, stress, and disease. Cell Metab *19*, 357-372.

Hartig, M.B., Iuso, A., Haack, T., Kmiec, T., Jurkiewicz, E., Heim, K., Roeber, S., Tarabin, V., Dusi, S., Krajewska-Walasek, M.*, et al.* (2011). Absence of an orphan mitochondrial protein, c19orf12, causes a distinct clinical subtype of neurodegeneration with brain iron accumulation. Am J Hum Genet *89*, 543-550.

Hasegawa, H., Matsuoka, T., Goto, Y., and Nonaka, I. (1993). Cytochrome c oxidase activity is deficient in blood vessels of patients with myoclonus epilepsy with ragged-red fibers. Acta neuropathologica *85*, 280-284.

Hiltunen, J.K., Schonauer, M.S., Autio, K.J., Mittelmeier, T.M., Kastaniotis, A.J., and Dieckmann, C.L. (2009). Mitochondrial Fatty Acid Synthesis Type II: More than Just Fatty Acids*. In J Biol Chem, pp. 9011-9015.

Hodge, C.A., Tran, E.J., Noble, K.N., Alcazar-Roman, A.R., Ben-Yishay, R., Scarcelli, J.J., Folkmann, A.W., Shav-Tal, Y., Wente, S.R., and Cole, C.N. (2011). The Dbp5 cycle at the nuclear pore complex during mRNA export I: dbp5 mutants with defects in RNA binding and ATP hydrolysis define key steps for Nup159 and Gle1. Genes Dev *25*, 1052-1064.

Hofmann, A.D., Beyer, M., Krause-Buchholz, U., Wobus, M., Bornhauser, M., and Rodel, G. (2012). OXPHOS supercomplexes as a hallmark of the mitochondrial phenotype of adipogenic differentiated human MSCs. PLoS One *7*, e35160.

Holt, I.J., Harding, A.E., Petty, R.K., and Morgan-Hughes, J.A. (1990). A new mitochondrial disease associated with mitochondrial DNA heteroplasmy. Am J Hum Genet *46*, 428-433.

Horvath, R., Kemp, J.P., Tuppen, H.A., Hudson, G., Oldfors, A., Marie, S.K., Moslemi, A.R., Servidei, S., Holme, E., Shanske, S.*, et al.* (2009). Molecular basis of infantile reversible cytochrome c oxidase deficiency myopathy. Brain *132*, 3165-3174.

Huber, S.A., Alejandro, R., and Wolfgang (2012). Detecting differential usage of exons from RNA-seq data.

Jager, S., Handschin, C., St-Pierre, J., and Spiegelman, B.M. (2007). AMP-activated protein kinase (AMPK) action in skeletal muscle via direct phosphorylation of PGC-1alpha. Proc Natl Acad Sci U S A *104*, 12017-12022.

Janssen, I., Shepard, D.S., Katzmarzyk, P.T., and Roubenoff, R. (2003). The healthcare costs of sarcopenia in the United States. Journal of the American Geriatrics Society *52*, 80-85.

Jourdain, A., and Martinou, J.C. (2010). Mitochondrial dynamics: quantifying mitochondrial fusion in vitro. BMC biology *8*, 99.

Kaguni, L.S. (2004). DNA polymerase gamma, the mitochondrial replicase. Annual review of biochemistry *73*, 293-320.

Kang, D., Kim, S.H., and Hamasaki, N. (2007). Mitochondrial transcription factor A (TFAM): roles in maintenance of mtDNA and cellular functions. Mitochondrion *7*, 39-44.

Kang, J., Albadawi, H., Patel, V.I., Abbruzzese, T.A., Yoo, J.H., Austen, W.G., Jr., and Watkins, M.T. (2008). Apolipoprotein E-/- mice have delayed skeletal muscle healing after hind limb ischemia-reperfusion. J Vasc Surg *48*, 701-708.

Kanki, T., Ohgaki, K., Gaspari, M., Gustafsson, C., Fukuoh, A., Sasaki, N., Hamasaki, N., and Kang, D. (2004). Architectural role of mitochondrial transcription factor A in maintenance of human mitochondrial DNA. Molecular and cellular biology *24*, 9823-9834.

Kapranov, P., Cheng, J., Dike, S., Nix, D.A., Duttagupta, R., Willingham, A.T., Stadler, P.F., Hertel, J., Hackermuller, J., Hofacker, I.L.*, et al.* (2007). RNA maps reveal new RNA classes and a possible function for pervasive transcription. Science *316*, 1484-1488.

Katajisto, P., Dohla, J., Chaffer, C.L., Pentinmikko, N., Marjanovic, N., Iqbal, S., Zoncu, R., Chen, W., Weinberg, R.A., and Sabatini, D.M. (2015). Stem cells. Asymmetric apportioning of aged mitochondria between daughter cells is required for stemness. Science *348*, 340-343.
Kaufmann, P., Engelstad, K., Wei, Y., Kulikova, R., Oskoui, M., Sproule, D.M., Battista, V., Koenigsberger, D.Y., Pascual, J.M., Shanske, S.*, et al.* (2011). Natural history of MELAS associated with mitochondrial DNA m.3243A>G genotype. Neurology *77*, 1965-1971.
Kauppila, J.H., Baines, H.L., Bratic, A., Simard, M.L., Freyer, C., Mourier, A., Stamp, C., Filograna, R., Larsson, N.G., Greaves, L.C.*, et al.* (2016). A Phenotype-Driven Approach to Generate Mouse Models with Pathogenic mtDNA Mutations Causing Mitochondrial Disease. Cell Rep *16*, 2980-2990.
Kelley, D.E., He, J., Menshikova, E.V., and Ritov, V.B. (2002). Dysfunction of mitochondria in human skeletal muscle in type 2 diabetes. Diabetes *51*, 2944-2950.
Kelly, D.P., and Scarpulla, R.C. (2004). Transcriptional regulatory circuits controlling mitochondrial biogenesis and function. Genes Dev *18*, 357-368.
Khoshnevis, S., Gross, T., Rotte, C., Baierlein, C., Ficner, R., and Krebber, H. (2010). The iron-sulphur protein RNase L inhibitor functions in translation termination. EMBO Rep *11*, 214-219.
Knowles, M.K., Guenza, M.G., Capaldi, R.A., and Marcus, A.H. (2002). Cytoskeletal-assisted dynamics of the mitochondrial reticulum in living cells. Proc Natl Acad Sci U S A *99*, 14772-14777.
Konig, J., Zarnack, K., Luscombe, N.M., and Ule, J. (2012). Protein-RNA interactions: new genomic technologies and perspectives. Nature reviews Genetics *13*, 77-83.
Kuang, S., Kuroda, K., Le Grand, F., and Rudnicki, M.A. (2007). Asymmetric self-renewal and commitment of satellite stem cells in muscle. Cell *129*, 999-1010.
Kukat, C., and Larsson, N.G. (2013). mtDNA makes a U-turn for the mitochondrial nucleoid. Trends in cell biology *23*, 457-463.
Kuznetsov, A.V., Javadov, S., Guzun, R., Grimm, M., and Saks, V. (2013). Cytoskeleton and regulation of mitochondrial function: the role of beta-tubulin II. Frontiers in physiology *4*, 82.
Lagouge, M., Argmann, C., Gerhart-Hines, Z., Meziane, H., Lerin, C., Daussin, F., Messadeq, N., Milne, J., Lambert, P., Elliott, P.*, et al.* (2006). Resveratrol improves mitochondrial function and protects against metabolic disease by activating SIRT1 and PGC-1alpha. Cell *127*, 1109-1122.
Lake, N.J., Compton, A.G., Rahman, S., and Thorburn, D.R. (2015). Leigh syndrome: One disorder, more than 75 monogenic causes. Annals of neurology *79*, 190-203.
Langston, J.W., Forno, L.S., Tetrud, J., Reeves, A.G., Kaplan, J.A., and Karluk, D. (1999). Evidence of active nerve cell degeneration in the substantia nigra of humans years after 1-methyl-4-phenyl-1,2,3,6-tetrahydropyridine exposure. Annals of neurology *46*, 598-605.
Lapuente-Brun, E., Moreno-Loshuertos, R., Acin-Perez, R., Latorre-Pellicer, A., Colas, C., Balsa, E., Perales-Clemente, E., Quiros, P.M., Calvo, E., Rodriguez-Hernandez, M.A.*, et al.* (2013). Supercomplex assembly determines electron flux in the mitochondrial electron transport chain. Science *340*, 1567-1570.
Li, F., Patterson, A.D., Krausz, K.W., Tanaka, N., and Gonzalez, F.J. (2012). Metabolomics reveals an essential role for peroxisome proliferator-activated receptor alpha in bile acid homeostasis. Journal of lipid research *53*, 1625-1635.
Li, M., Ona, V.O., Guegan, C., Chen, M., Jackson-Lewis, V., Andrews, L.J., Olszewski, A.J., Stieg, P.E., Lee, J.P., Przedborski, S.*, et al.* (2000). Functional role of caspase-1 and caspase-3 in an ALS transgenic mouse model. Science *288*, 335-339.
Liang, J., Song, W., Tromp, G., Kolattukudy, P.E., and Fu, M. (2008). Genome-wide survey and expression profiling of CCCH-zinc finger family reveals a functional module in macrophage activation. PLoS One *3*, e2880.
Liu, H., He, L., and Tang, L. (2012). Alternative splicing regulation and cell lineage differentiation. Current stem cell research & therapy *7*, 400-406.
Lowell, B.B., and Shulman, G.I. (2005). Mitochondrial dysfunction and type 2 diabetes. Science *307*, 384-387.

Lu, B., Lee, J., Nie, X., Li, M., Morozov, Y.I., Venkatesh, S., Bogenhagen, D.F., Temiakov, D., and Suzuki, C.K. (2013). Phosphorylation of human TFAM in mitochondria impairs DNA binding and promotes degradation by the AAA+ Lon protease. Mol Cell *49*, 121-132.
Maassen, J.A., LM, T.H., Van Essen, E., Heine, R.J., Nijpels, G., Jahangir Tafrechi, R.S., Raap, A.K., Janssen, G.M., and Lemkes, H.H. (2004). Mitochondrial diabetes: molecular mechanisms and clinical presentation. Diabetes *53 Suppl 1*, S103-109.
Maechler, P., and Wollheim, C.B. (2001). Mitochondrial function in normal and diabetic beta-cells. Nature *414*, 807-812.
Manczak, M., Anekonda, T.S., Henson, E., Park, B.S., Quinn, J., and Reddy, P.H. (2006). Mitochondria are a direct site of A beta accumulation in Alzheimer's disease neurons: implications for free radical generation and oxidative damage in disease progression. Hum Mol Genet *15*, 1437-1449.
Manfredi, G., and Xu, Z. (2005). Mitochondrial dysfunction and its role in motor neuron degeneration in ALS. Mitochondrion *5*, 77-87.
Mann, M. (2006). Functional and quantitative proteomics using SILAC. Nat Rev Mol Cell Biol *7*, 952-958.
Mao, K., and Klionsky, D.J. (2013). Participation of mitochondrial fission during mitophagy. In Cell cycle, pp. 3131-3132.
Martin, L.J. (2012). Biology of Mitochondria in Neurodegenerative Diseases. Progress in molecular biology and translational science *107*, 355-415.
Matlin, A.J., Clark, F., and Smith, C.W. (2005). Understanding alternative splicing: towards a cellular code. Nat Rev Mol Cell Biol *6*, 386-398.
Matsushima, Y., and Kaguni, L.S. (2012). Matrix proteases in mitochondrial DNA function. Biochim Biophys Acta *1819*, 1080-1087.
Milenkovic, D., Matic, S., Kuhl, I., Ruzzenente, B., Freyer, C., Jemt, E., Park, C.B., Falkenberg, M., and Larsson, N.G. (2013). TWINKLE is an essential mitochondrial helicase required for synthesis of nascent D-loop strands and complete mtDNA replication. Hum Mol Genet *22*, 1983-1993.
Min, F., Wang, S., and Zhang, L. (2015). Survey of Programs Used to Detect Alternative Splicing Isoforms from Deep Sequencing Data In Silico. BioMed research international *2015*, 831352.
Mitra, K. (2013). Mitochondrial fission-fusion as an emerging key regulator of cell proliferation and differentiation. BioEssays : news and reviews in molecular, cellular and developmental biology *35*, 955-964.
Mochel, F., Knight, M.A., Tong, W.H., Hernandez, D., Ayyad, K., Taivassalo, T., Andersen, P.M., Singleton, A., Rouault, T.A., Fischbeck, K.H.*, et al.* (2008). Splice mutation in the iron-sulfur cluster scaffold protein ISCU causes myopathy with exercise intolerance. Am J Hum Genet *82*, 652-660.
Mohyeldin, A., Garzon-Muvdi, T., and Quinones-Hinojosa, A. (2010). Oxygen in stem cell biology: a critical component of the stem cell niche. Cell Stem Cell *7*, 150-161.
Mokalled, M.H., Johnson, A.N., Creemers, E.E., and Olson, E.N. (2012). MASTR directs MyoD-dependent satellite cell differentiation during skeletal muscle regeneration. Genes Dev *26*, 190-202.
Montanez, J.E., Peters, J.M., Correll, J.B., Gonzalez, F.J., and Patterson, A.D. (2013). Metabolomics: An Essential Tool to Understand the Function of Peroxisome Proliferator–Activated Receptor Alpha. Toxicol Pathol *41*, 410-418.
Mootha, V., Bunkenborg, J., Olsen, J., Hjerrild, M., Wisniewski, J., Stahl, E., Bolouri, M., Ray, H., Sihag, S., Kamal, M.*, et al.* (2003a). Integrated analysis of protein composition, tissue diversity, and gene regulation in mouse mitochondria. Cell *115*, 629-640.
Mootha, V.K., Handschin, C., Arlow, D., Xie, X., Pierre, J.S., Sihag, S., Yang, W., Altshuler, D., Puigserver, P., Patterson, N.*, et al.* (2004). Errα and Gabpa/b specify PGC-1α-dependent oxidative phosphorylation gene expression that is altered in diabetic muscle.
Mootha, V.K., Lindgren, C.M., Eriksson, K.F., Subramanian, A., Sihag, S., Lehar, J., Puigserver, P., Carlsson, E., Ridderstrale, M., Laurila, E.*, et al.* (2003b). PGC-1alpha-responsive genes involved in oxidative phosphorylation are coordinately downregulated in human diabetes. Nat Genet *34*, 267-273.

Moraes, C.T., DiMauro, S., Zeviani, M., Lombes, A., Shanske, S., Miranda, A.F., Nakase, H., Bonilla, E., Werneck, L.C., Servidei, S*., et al.* (1989). Mitochondrial DNA deletions in progressive external ophthalmoplegia and Kearns-Sayre syndrome. The New England journal of medicine *320*, 1293-1299.

Moreno-Navarrete, J.M., Blasco, G., Xifra, G., Karczewska-Kupczewska, M., Stefanowicz, M., Matulewicz, N., Puig, J., Ortega, F., Ricart, W., Straczkowski, M*., et al.* (2016). Obesity Is Associated With Gene Expression and Imaging Markers of Iron Accumulation in Skeletal Muscle. J Clin Endocrinol Metab *101*, 1282-1289.

Moreno-Navarrete, J.M., Ortega, F., Moreno, M., Ricart, W., and Fernandez-Real, J.M. (2014). Fine-tuned iron availability is essential to achieve optimal adipocyte differentiation and mitochondrial biogenesis. Diabetologia *57*, 1957-1967.

Moreno, M., Ortega, F., Xifra, G., Ricart, W., Fernandez-Real, J.M., and Moreno-Navarrete, J.M. (2015). Cytosolic aconitase activity sustains adipogenic capacity of adipose tissue connecting iron metabolism and adipogenesis. FASEB journal : official publication of the Federation of American Societies for Experimental Biology *29*, 1529-1539.

Morley, J.E. (2008). Sarcopenia: diagnosis and treatment. The journal of nutrition, health & aging *12*, 452-456.

Mortiboys, H., Thomas, K.J., Koopman, W.J., Klaffke, S., Abou-Sleiman, P., Olpin, S., Wood, N.W., Willems, P.H., Smeitink, J.A., Cookson, M.R*., et al.* (2008). Mitochondrial function and morphology are impaired in parkin-mutant fibroblasts. Annals of neurology *64*, 555-565.

Motohashi, N., and Asakura, A. (2014). Muscle satellite cell heterogeneity and self-renewal. Frontiers in cell and developmental biology *2*, 1.

Navarro-Sastre, A., Tort, F., Stehling, O., Uzarska, M.A., Arranz, J.A., Del Toro, M., Labayru, M.T., Landa, J., Font, A., Garcia-Villoria, J*., et al.* (2011). A fatal mitochondrial disease is associated with defective NFU1 function in the maturation of a subset of mitochondrial Fe-S proteins. Am J Hum Genet *89*, 656-667.

Ngo, H.B., Lovely, G.A., Phillips, R., and Chan, D.C. (2014). Distinct structural features of TFAM drive mitochondrial DNA packaging versus transcriptional activation. Nature Communications *5*.

Nilsen, T.W., and Graveley, B.R. (2010). Expansion of the eukaryotic proteome by alternative splicing. Nature *463*, 457-463.

Olga Martins de Brito, L.S. (2008). Mitofusin 2 tethers endoplasmic reticulum to mitochondria. Nature *456*, 605-610.

Oliveira, R.L., Ueno, M., de Souza, C.T., Pereira-da-Silva, M., Gasparetti, A.L., Bezzera, R.M., Alberici, L.C., Vercesi, A.E., Saad, M.J., and Velloso, L.A. (2004). Cold-induced PGC-1alpha expression modulates muscle glucose uptake through an insulin receptor/Akt-independent, AMPK-dependent pathway. Am J Physiol Endocrinol Metab *287*, E686-695.

Pagliarini, D.J., Calvo, S.E., Chang, B., Sheth, S.A., Vafai, S.B., Ong, S.E., Walford, G.A., Sugiana, C., Boneh, A., Chen, W.K*., et al.* (2008). A mitochondrial protein compendium elucidates complex I disease biology. Cell *134*, 112-123.

Palacios, D., Mozzetta, C., Consalvi, S., Caretti, G., Saccone, V., Proserpio, V., Marquez, V.E., Valente, S., Mai, A., Forcales, S.V*., et al.* (2010). TNF/p38alpha/polycomb signaling to Pax7 locus in satellite cells links inflammation to the epigenetic control of muscle regeneration. Cell Stem Cell *7*, 455-469.

Paradkar, P.N., Zumbrennen, K.B., Paw, B.H., Ward, D.M., and Kaplan, J. (2008). Regulation of mitochondrial iron import through differential turnover of mitoferrin 1 and mitoferrin 2. Molecular and cellular biology *29*, 1007-1016.

Parihar, M.S., Parihar, A., Fujita, M., Hashimoto, M., and Ghafourifar, P. (2009). Alpha-synuclein overexpression and aggregation exacerbates impairment of mitochondrial functions by augmenting oxidative stress in human neuroblastoma cells. The international journal of biochemistry & cell biology *41*, 2015-2024.

Pasinelli, P., Belford, M.E., Lennon, N., Bacskai, B.J., Hyman, B.T., Trotti, D., and Brown, R.H., Jr. (2004). Amyotrophic lateral sclerosis-associated SOD1 mutant proteins bind and aggregate with Bcl-2 in spinal cord mitochondria. Neuron *43*, 19-30.

Pasinelli, P., Houseweart, M.K., Brown, R.H., Jr., and Cleveland, D.W. (2000). Caspase-1 and -3 are sequentially activated in motor neuron death in Cu,Zn superoxide dismutase-mediated familial amyotrophic lateral sclerosis. Proc Natl Acad Sci U S A *97*, 13901-13906.

Patananan, A.N., Wu, T.H., Chiou, P.Y., and Teitell, M.A. (2016). Modifying the Mitochondrial Genome. Cell Metab *23*, 785-796.

Patti, M.E., Butte, A.J., Crunkhorn, S., Cusi, K., Berria, R., Kashyap, S., Miyazaki, Y., Kohane, I., Costello, M., Saccone, R*., et al.* (2003). Coordinated reduction of genes of oxidative metabolism in humans with insulin resistance and diabetes: Potential role of PGC1 and NRF1. Proc Natl Acad Sci U S A *100*, 8466-8471.

Patti, M.E., and Corvera, S. (2010). The role of mitochondria in the pathogenesis of type 2 diabetes. Endocrine reviews *31*, 364-395.

Paul, V.D., and Lill, R. (2015). Biogenesis of cytosolic and nuclear iron-sulfur proteins and their role in genome stability. Biochim Biophys Acta *1853*, 1528-1539.

Pearson, H.A., Lobel, J.S., Kocoshis, S.A., Naiman, J.L., Windmiller, J., Lammi, A.T., Hoffman, R., and Marsh, J.C. (1979). A new syndrome of refractory sideroblastic anemia with vacuolization of marrow precursors and exocrine pancreatic dysfunction. The Journal of pediatrics *95*, 976-984.

Peault, B., Rudnicki, M., Torrente, Y., Cossu, G., Tremblay, J.P., Partridge, T., Gussoni, E., Kunkel, L.M., and Huard, J. (2007). Stem and progenitor cells in skeletal muscle development, maintenance, and therapy. Molecular therapy : the journal of the American Society of Gene Therapy *15*, 867-877.

Pedersen, B.K., and Febbraio, M.A. (2012). Muscles, exercise and obesity: skeletal muscle as a secretory organ. Nature reviews Endocrinology *8*, 457-465.

Pedro-Segura, E., Vergara, S.V., Rodriguez-Navarro, S., Parker, R., Thiele, D.J., and Puig, S. (2008). The Cth2 ARE-binding protein recruits the Dhh1 helicase to promote the decay of succinate dehydrogenase SDH4 mRNA in response to iron deficiency. J Biol Chem *283*, 28527-28535.

Peng, X., Zhao, Y., Cao, J., Zhang, W., Jiang, H., Li, X., Ma, Q., Zhu, S., and Cheng, B. (2012). CCCH-type zinc finger family in maize: genome-wide identification, classification and expression profiling under abscisic acid and drought treatments. PLoS One *7*, e40120.

Perrimon, F.D., Rosanna, P., Alfred, L.G., and Norbert (2013). Mechanisms of skeletal muscle aging: insights from Drosophila and mammalian models.

Petersen, K.F., Dufour, S., Befroy, D., Garcia, R., and Shulman, G.I. (2004). Impaired mitochondrial activity in the insulin-resistant offspring of patients with type 2 diabetes. The New England journal of medicine *350*, 664-671.

Price, F.D., von Maltzahn, J., Bentzinger, C.F., Dumont, N.A., Yin, H., Chang, N.C., Wilson, D.H., Frenette, J., and Rudnicki, M.A. (2014). Inhibition of JAK-STAT signaling stimulates adult satellite cell function. Nat Med *20*, 1174-1181.

Qiu, J., Wenz, L.S., Zerbes, R.M., Oeljeklaus, S., Bohnert, M., Stroud, D.A., Wirth, C., Ellenrieder, L., Thornton, N., Kutik, S*., et al.* (2013). Coupling of mitochondrial import and export translocases by receptor-mediated supercomplex formation. Cell *154*, 596-608.

Rabani, M., Levin, J.Z., Fan, L., Adiconis, X., Raychowdhury, R., Garber, M., Gnirke, A., Nusbaum, C., Hacohen, N., Friedman, N*., et al.* (2011). Metabolic labeling of RNA uncovers principles of RNA production and degradation dynamics in mammalian cells. Nat Biotechnol *29*, 436-442.

Rahn, J.J., Stackley, K.D., and Chan, S.S. (2013). Opa1 is required for proper mitochondrial metabolism in early development. PLoS One *8*, e59218.

Rajala, N., Gerhold, J.M., Martinsson, P., Klymov, A., and Spelbrink, J.N. (2014). Replication factors transiently associate with mtDNA at the mitochondrial inner membrane to facilitate replication. Nucleic Acids Res *42*, 952-967.

Rajpathak, S.N., Crandall, J.P., Wylie-Rosett, J., Kabat, G.C., Rohan, T.E., and Hu, F.B. (2008). The role of iron in type 2 diabetes in humans. Biochim Biophys Acta *1790*, 671-681.
Ramadasan-Nair, R., Gayathri, N., Mishra, S., Sunitha, B., Mythri, R.B., Nalini, A., Subbannayya, Y., Harsha, H.C., Kolthur-Seetharam, U., and Srinivas Bharath, M.M. (2013). Mitochondrial alterations and oxidative stress in an acute transient mouse model of muscle degeneration: implications for muscular dystrophy and related muscle pathologies. J Biol Chem *289*, 485-509.
Ravi, S., Schilder, R.J., and Kimball, S.R. (2015). Role of precursor mRNA splicing in nutrient-induced alterations in gene expression and metabolism. The Journal of nutrition *145*, 841-846.
Ray, D., Kazan, H., Cook, K.B., Weirauch, M.T., Najafabadi, H.S., Li, X., Gueroussov, S., Albu, M., Zheng, H., Yang, A.*, et al.* (2013). A compendium of RNA-binding motifs for decoding gene regulation. Nature *499*, 172-177.
Reardon, T.F., and Allen, D.G. (2009). Iron injections in mice increase skeletal muscle iron content, induce oxidative stress and reduce exercise performance. Experimental physiology *94*, 720-730.
Reja, R., Venkatakrishnan, A.J., Lee, J., Kim, B.C., Ryu, J.W., Gong, S., Bhak, J., and Park, D. (2009). MitoInteractome: mitochondrial protein interactome database, and its application in 'aging network' analysis. BMC Genomics *10 Suppl 3*, S20.
Richardson, D.R., Lane, D.J., Becker, E.M., Huang, M.L., Whitnall, M., Suryo Rahmanto, Y., Sheftel, A.D., and Ponka, P. (2010). Mitochondrial iron trafficking and the integration of iron metabolism between the mitochondrion and cytosol. Proc Natl Acad Sci U S A *107*, 10775-10782.
Richter, E.A., and Hargreaves, M. (2013). Exercise, GLUT4, and skeletal muscle glucose uptake. Physiological reviews *93*, 993-1017.
Riemer, J., Hoepken, H.H., Czerwinska, H., Robinson, S.R., and Dringen, R. (2004). Colorimetric ferrozine-based assay for the quantitation of iron in cultured cells. Anal Biochem *331*, 370-375.
Rimessi, A., Giorgi, C., Pinton, P., and Rizzuto, R. (2008). The versatility of mitochondrial calcium signals: from stimulation of cell metabolism to induction of cell death. Biochim Biophys Acta *1777*, 808-816.
Rinn, J.L., and Chang, H.Y. (2012). Genome regulation by long noncoding RNAs. Annual review of biochemistry *81*, 145-166.
Rosen, D.R. (1993). Mutations in Cu/Zn superoxide dismutase gene are associated with familial amyotrophic lateral sclerosis. Nature *364*, 362.
Rothfuss, O., Fischer, H., Hasegawa, T., Maisel, M., Leitner, P., Miesel, F., Sharma, M., Bornemann, A., Berg, D., Gasser, T.*, et al.* (2009). Parkin protects mitochondrial genome integrity and supports mitochondrial DNA repair. Hum Mol Genet *18*, 3832-3850.
Rouault, T.A., and Tong, W.H. (2005). Iron-sulphur cluster biogenesis and mitochondrial iron homeostasis. Nat Rev Mol Cell Biol *6*, 345-351.
Ryall, J.G. (2013). Metabolic reprogramming as a novel regulator of skeletal muscle development and regeneration. The FEBS journal *280*, 4004-4013.
Ryall, J.G., Dell'Orso, S., Derfoul, A., Juan, A., Zare, H., Feng, X., Clermont, D., Koulnis, M., Gutierrez-Cruz, G., Fulco, M.*, et al.* (2015). The NAD(+)-dependent SIRT1 deacetylase translates a metabolic switch into regulatory epigenetics in skeletal muscle stem cells. Cell Stem Cell *16*, 171-183.
Sachidanandan, C., Sambasivan, R., and Dhawan, J. (2002). Tristetraprolin and LPS-inducible CXC chemokine are rapidly induced in presumptive satellite cells in response to skeletal muscle injury. Journal of cell science *115*, 2701-2712.
Sakuma, K., Akiho, M., Nakashima, H., Akima, H., and Yasuhara, M. (2008). Age-related reductions in expression of serum response factor and myocardin-related transcription factor A in mouse skeletal muscles. Biochim Biophys Acta *1782*, 453-461.
Salisbury, E., Sakai, K., Schoser, B., Huichalaf, C., Schneider-Gold, C., Nguyen, H., Wang, G.L., Albrecht, J.H., and Timchenko, L.T. (2008). Ectopic expression of cyclin D3 corrects differentiation of DM1 myoblasts through activation of RNA CUG-binding protein, CUGBP1. Experimental cell research *314*, 2266-2278.

Scarpulla, R. (2008a). Transcriptional paradigms in mammalian mitochondrial biogenesis and function. Physiological reviews *88*, 611-638.
Scarpulla, R.C. (2008b). Transcriptional paradigms in mammalian mitochondrial biogenesis and function. Physiological reviews *88*, 611-638.
Scarpulla, R.C., Vega, R.B., and Kelly, D.P. (2012). Transcriptional integration of mitochondrial biogenesis. Trends Endocrinol Metab *23*, 459-466.
Schiaffino, S., and Reggiani, C. (2011). Fiber types in mammalian skeletal muscles. Physiological reviews *91*, 1447-1531.
Schon, E.A., DiMauro, S., and Hirano, M. (2012). Human mitochondrial DNA: roles of inherited and somatic mutations. Nature reviews Genetics *13*, 878-890.
Schonberg, D.L., Miller, T.E., Wu, Q., Flavahan, W.A., Das, N.K., Hale, J.S., Hubert, C.G., Mack, S.C., Jarrar, A.M., Karl, R.T.*, et al.* (2015). Preferential Iron Trafficking Characterizes Glioblastoma Stem-like Cells. Cancer Cell *28*, 441-455.
Schwanhausser, B., Busse, D., Li, N., Dittmar, G., Schuchhardt, J., Wolf, J., Chen, W., and Selbach, M. (2011). Global quantification of mammalian gene expression control. Nature *473*, 337-342.
Scotti, M.M., and Swanson, M.S. (2015). RNA mis-splicing in disease. Nature reviews Genetics *17*, 19-32.
Seale, P., Sabourin, L.A., Girgis-Gabardo, A., Mansouri, A., Gruss, P., and Rudnicki, M.A. (2000). Pax7 is required for the specification of myogenic satellite cells. Cell *102*, 777-786.
Severance, S., and Hamza, I. (2009). Trafficking of heme and porphyrins in metazoa. Chemical reviews *109*, 4596-4616.
Sheftel, A., Stehling, O., and Lill, R. (2010). Iron-sulfur proteins in health and disease. Trends Endocrinol Metab *21*, 302-314.
Shintaku, J., Peterson, J.M., Talbert, E.E., Gu, J.M., Ladner, K.J., Williams, D.R., Mousavi, K., Wang, R., Sartorelli, V., and Guttridge, D.C. (2016). MyoD Regulates Skeletal Muscle Oxidative Metabolism Cooperatively with Alternative NF-kappaB. Cell Rep *17*, 514-526.
Shutt, T.E., Bestwick, M., and Shadel, G.S. (2011). The core human mitochondrial transcription initiation complex: It only takes two to tango. Transcription *2*, 55-59.
Silva, J.P., Kohler, M., Graff, C., Oldfors, A., Magnuson, M.A., Berggren, P.O., and Larsson, N.G. (2000). Impaired insulin secretion and beta-cell loss in tissue-specific knockout mice with mitochondrial diabetes. Nat Genet *26*, 336-340.
Song, D.D., Shults, C.W., Sisk, A., Rockenstein, E., and Masliah, E. (2004). Enhanced substantia nigra mitochondrial pathology in human alpha-synuclein transgenic mice after treatment with MPTP. Experimental neurology *186*, 158-172.
Sousa-Victor, P., Gutarra, S., Garcia-Prat, L., Rodriguez-Ubreva, J., Ortet, L., Ruiz-Bonilla, V., Jardi, M., Ballestar, E., Gonzalez, S., Serrano, A.L.*, et al.* (2014). Geriatric muscle stem cells switch reversible quiescence into senescence. Nature *506*, 316-321.
Sun, H., and Chasin, L.A. (2000). Multiple splicing defects in an intronic false exon. Molecular and cellular biology *20*, 6414-6425.
Suomalainen, A., and Isohanni, P. (2010). Mitochondrial DNA depletion syndromes--many genes, common mechanisms. Neuromuscular disorders : NMD *20*, 429-437.
Suzuki, T., and Nagao, A. (2011). Human mitochondrial tRNAs: biogenesis, function, structural aspects, and diseases. Annual review of genetics *45*, 299-329.
Tabrizi, S.J., Orth, M., Wilkinson, J.M., Taanman, J.W., Warner, T.T., Cooper, J.M., and Schapira, A.H. (2000). Expression of mutant alpha-synuclein causes increased susceptibility to dopamine toxicity. Hum Mol Genet *9*, 2683-2689.
Tay, S.H., Nordli, D.R., Jr., Bonilla, E., Null, E., Monaco, S., Hirano, M., and DiMauro, S. (2006). Aortic rupture in mitochondrial encephalopathy, lactic acidosis, and stroke-like episodes. Arch Neurol *63*, 281-283.

Thornton, X.L., Jill, W.M., Ami, M., Rahul, N.K., Yuan, Y., Richard, T.M., Maurice, S.S., and Charles, A. (2006). Failure of MBNL1-dependent post-natal splicing transitions in myotonic dystrophy.
Tierney, M.T., Aydogdu, T., Sala, D., Malecova, B., Gatto, S., Puri, P.L., Latella, L., and Sacco, A. (2014). STAT3 signaling controls satellite cell expansion and skeletal muscle repair. Nat Med *20*, 1182-1186.
Tierney, M.T., and Sacco, A. (2016). Satellite Cell Heterogeneity in Skeletal Muscle Homeostasis. Trends in cell biology *26*, 434-444.
Troy, A., Cadwallader, A.B., Fedorov, Y., Tyner, K., Tanaka, K.K., and Olwin, B.B. (2012). Coordination of satellite cell activation and self-renewal by Par-complex-dependent asymmetric activation of p38alpha/beta MAPK. Cell Stem Cell *11*, 541-553.
Turrina, A., Martinez-Gonzalez, M.A., and Stecco, C. (2013). The muscular force transmission system: role of the intramuscular connective tissue. Journal of bodywork and movement therapies *17*, 95-102.
Uehata, T., and Akira, S. (2013). mRNA degradation by the endoribonuclease Regnase-1/ZC3H12a/MCPIP-1. Biochim Biophys Acta *1829*, 708-713.
Valencia-Sanchez, M.A., Liu, J., Hannon, G.J., and Parker, R. (2006). Control of translation and mRNA degradation by miRNAs and siRNAs. Genes Dev *20*, 515-524.
Van Dusen, C.M., Yee, L., McNally, L.M., and McNally, M.T. (2010). A Glycine-Rich Domain of hnRNP H/F Promotes Nucleocytoplasmic Shuttling and Nuclear Import through an Interaction with Transportin 1▽†. In Molecular and cellular biology, pp. 2552-2562.
Veatch, J.R., McMurray, M.A., Nelson, Z.W., and Gottschling, D.E. (2009). Mitochondrial dysfunction leads to nuclear genome instability via an iron-sulfur cluster defect. Cell *137*, 1247-1258.
Vernochet, C., Mourier, A., Bezy, O., Macotela, Y., Boucher, J., Rardin, M.J., An, D., Lee, K.Y., Ilkayeva, O.R., Zingaretti, C.M.*, et al.* (2012). Adipose-specific deletion of TFAM increases mitochondrial oxidation and protects mice against obesity and insulin resistance. Cell Metab *16*, 765-776.
Visconte, V., Avishai, N., Mahfouz, R., Tabarroki, A., Cowen, J., Sharghi-Moshtaghin, R., Hitomi, M., Rogers, H.J., Hasrouni, E., Phillips, J.*, et al.* (2014). Distinct iron architecture in SF3B1-mutant myelodysplastic syndrome patients is linked to an SLC25A37 splice variant with a retained intron. Leukemia *29*, 188-195.
von Moeller, H., Basquin, C., and Conti, E. (2009). The mRNA export protein DBP5 binds RNA and the cytoplasmic nucleoporin NUP214 in a mutually exclusive manner. Nature structural & molecular biology *16*, 247-254.
Vondra, K., Rath, R., Bass, A., Slabochova, Z., Teisinger, J., and Vitek, V. (1977). Enzyme activities in quadriceps femoris muscle of obese diabetic male patients. Diabetologia *13*, 527-529.
Wai, T., and Langer, T. (2016). Mitochondrial Dynamics and Metabolic Regulation. Trends Endocrinol Metab *27*, 105-117.
Wallace, D. (2005). A mitochondrial paradigm of metabolic and degenerative diseases, aging, and cancer: a dawn for evolutionary medicine. Annual review of genetics *39*, 359-407.
Wanet, A., Arnould, T., Najimi, M., and Renard, P. (2015). Connecting Mitochondria, Metabolism, and Stem Cell Fate. In Stem Cells Dev, pp. 1957-1971.
Wang, J., and Pantopoulos, K. (2011). Regulation of cellular iron metabolism. The Biochemical journal *434*, 365-381.
Wang, L., Miao, Y.L., Zheng, X., Lackford, B., Zhou, B., Han, L., Yao, C., Ward, J.M., Burkholder, A., Lipchina, I.*, et al.* (2013). The THO complex regulates pluripotency gene mRNA export and controls embryonic stem cell self-renewal and somatic cell reprogramming. Cell Stem Cell *13*, 676-690.
Wang, W., Esbensen, Y., Kunke, D., Suganthan, R., Rachek, L., Bjoras, M., and Eide, L. (2011). Mitochondrial DNA damage level determines neural stem cell differentiation fate. The Journal of neuroscience : the official journal of the Society for Neuroscience *31*, 9746-9751.
Wang, Z., and Burge, C.B. (2008). Splicing regulation: from a parts list of regulatory elements to an integrated splicing code. RNA (New York, NY) *14*, 802-813.

Wei, N., Cheng, Y., Wang, Z., Liu, Y., Luo, C., Liu, L., Chen, L., Xie, Z., Lu, Y., and Feng, Y. (2015). SRSF10 Plays a Role in Myoblast Differentiation and Glucose Production via Regulation of Alternative Splicing. Cell Rep *13*, 1647-1657.

Weirich, C.S., Erzberger, J.P., Flick, J.S., Berger, J.M., Thorner, J., and Weis, K. (2006). Activation of the DExD/H-box protein Dbp5 by the nuclear-pore protein Gle1 and its coactivator InsP6 is required for mRNA export. Nature cell biology *8*, 668-676.

Wenz, L.S., Opalinski, L., Schuler, M.H., Ellenrieder, L., Ieva, R., Bottinger, L., Qiu, J., van der Laan, M., Wiedemann, N., Guiard, B.*, et al.* (2014). The presequence pathway is involved in protein sorting to the mitochondrial outer membrane. EMBO Rep *15*, 678-685.

Wickramasinghe, V.O., Andrews, R., Ellis, P., Langford, C., Gurdon, J.B., Stewart, M., Venkitaraman, A.R., and Laskey, R.A. (2014). Selective nuclear export of specific classes of mRNA from mammalian nuclei is promoted by GANP. Nucleic Acids Res *42*, 5059-5071.

Wickramasinghe, V.O., and Laskey, R.A. (2015). Control of mammalian gene expression by selective mRNA export. Nat Rev Mol Cell Biol *16*, 431-442.

Wickramasinghe, V.O., McMurtrie, P.I., Mills, A.D., Takei, Y., Penrhyn-Lowe, S., Amagase, Y., Main, S., Marr, J., Stewart, M., and Laskey, R.A. (2009). mRNA export from mammalian cell nuclei is dependent on GANP. Current biology : CB *20*, 25-31.

Winklhofer, K.F., and Haass, C. (2009). Mitochondrial dysfunction in Parkinson's disease. Biochim Biophys Acta *1802*, 29-44.

Wolf, A.R., and Mootha, V.K. (2014). Functional genomic analysis of human mitochondrial RNA processing. Cell Rep *7*, 918-931.

Wolff, N.A., Ghio, A.J., Garrick, L.M., Garrick, M.D., Zhao, L., Fenton, R.A., and Thevenod, F. (2014). Evidence for mitochondrial localization of divalent metal transporter 1 (DMT1). FASEB journal : official publication of the Federation of American Societies for Experimental Biology *28*, 2134-2145.

Wood-Kaczmar, A., Gandhi, S., Yao, Z., Abramov, A.Y., Miljan, E.A., Keen, G., Stanyer, L., Hargreaves, I., Klupsch, K., Deas, E.*, et al.* (2008). PINK1 is necessary for long term survival and mitochondrial function in human dopaminergic neurons. PLoS One *3*, e2455.

Wu, Z., Puigserver, P., Andersson, U., Zhang, C., Adelmant, G., Mootha, V., Troy, A., Cinti, S., Lowell, B., Scarpulla, R.C.*, et al.* (1999). Mechanisms controlling mitochondrial biogenesis and respiration through the thermogenic coactivator PGC-1. Cell *98*, 115-124.

Xia, J., Sinelnikov, I.V., Han, B., and Wishart, D.S. (2015). MetaboAnalyst 3.0--making metabolomics more meaningful. Nucleic Acids Res *43*, W251-257.

Xia, J., and Wishart, D.S. (2011). Web-based inference of biological patterns, functions and pathways from metabolomic data using MetaboAnalyst. Nature protocols *6*, 743-760.

Xu, W., Barrientos, T., and Andrews, N.C. (2013a). Iron and copper in mitochondrial diseases. Cell Metab *17*, 319-328.

Xu, X., Duan, S., Yi, F., Ocampo, A., Liu, G.H., and Izpisua Belmonte, J.C. (2013b). Mitochondrial regulation in pluripotent stem cells. Cell Metab *18*, 325-332.

Yakubovskaya, E., Guja, K.E., Eng, E.T., Choi, W.S., Mejia, E., Beglov, D., Lukin, M., Kozakov, D., and Garcia-Diaz, M. (2014). Organization of the human mitochondrial transcription initiation complex. Nucleic Acids Res *42*, 4100-4112.

Yang, J., Hung, L.H., Licht, T., Kostin, S., Looso, M., Khrameeva, E., Bindereif, A., Schneider, A., and Braun, T. (2014). RBM24 is a major regulator of muscle-specific alternative splicing. Developmental cell *31*, 87-99.

Yang, J.S., Kim, J., Park, S., Jeon, J., Shin, Y.E., and Kim, S. (2013). Spatial and functional organization of mitochondrial protein network. Scientific reports *3*, 1403.

Yin, H., Price, F., and Rudnicki, M.A. (2013). Satellite cells and the muscle stem cell niche. In Physiological reviews (United States), pp. 23-67.

Youle, R.J., and Karbowski, M. (2005). Mitochondrial fission in apoptosis. Nat Rev Mol Cell Biol *6*, 657-663.

Zhang, H., Ryu, D., Wu, Y., Gariani, K., Wang, X., Luan, P., D'Amico, D., Ropelle, E.R., Lutolf, M.P., Aebersold, R.*, et al.* (2016a). NAD(+) repletion improves mitochondrial and stem cell function and enhances life span in mice. Science *352*, 1436-1443.

Zhang, J., Ratanasirintrawoot, S., Chandrasekaran, S., Wu, Z., Ficarro, S.B., Yu, C., Ross, C.A., Cacchiarelli, D., Xia, Q., Seligson, M.*, et al.* (2016b). LIN28 Regulates Stem Cell Metabolism and Conversion to Primed Pluripotency. Cell Stem Cell *19*, 66-80.

Zhang, L., Li, X., and Zhao, R. (2013). Structural analyses of the pre-mRNA splicing machinery. Protein science : a publication of the Protein Society *22*, 677-692.

Zhou, B., Westaway, S.K., Levinson, B., Johnson, M.A., Gitschier, J., and Hayflick, S.J. (2001). A novel pantothenate kinase gene (PANK2) is defective in Hallervorden-Spatz syndrome. Nat Genet *28*, 345-349.

Zurlo, F., Larson, K., Bogardus, C., and Ravussin, E. (1990). Skeletal muscle metabolism is a major determinant of resting energy expenditure. J Clin Invest *86*, 1423-1427.

Ringraziamenti

Ringrazio innanzitutto il professor Mitro per avermi dato la possibilità di effettuare il dottorato in scienze biochimiche sotto la sua supervisione. Farò sempre tesoro dei preziosi insegnamenti e consigli di questi tre anni. Un grazie sincero anche alla professoressa De Fabiani per l'aiuto nel lavoro quotidiano e nella stesura della tesi. Ringrazio i miei genitori e mia sorella per avermi accompagnato in questo percorso con interesse e passione.

Grazie a tutti i ragazzi del laboratorio, Raffa, Rui, Ale, Silvia, Enrico, Marco e Gaia per l'amicizia e l'aiuto che riuscite a darmi quotidianamente. Infine, un ringraziamento speciale va a mia moglie, amica paziente e compagna di vita sempre presente, per avermi sostenuto, incoraggiato e guidato nelle scelte di questi anni. Il tuo coraggio, la tua forza e la tua perseveranza saranno sempre il mio riferimento.